BTU Syngas Mechanism Version 1.0 as of 11-2017

Comparison of chosen reaction rates and validation against experiments

Krishna P. Shrestha[1], Lars Seidel[1], Anders Borg[2], Fabian Mauss[1,] Thomas Zeuch[3]

1) Thermodynamics and Thermal Process Engineering, Brandenburg University of Technology, Siemens-Halske-Ring 8, D-03046 Cottbus, Germany

2) Lund Combustion Engineering, LOGE AB, Adress

3) Institut für Physikalische Chemie,Georg-August-Universität, Tammannstr. 6, D-37077 Göttingen

1. Arrhenius Plots of Rate constant

The rate constant comparison of elementary reactions involved in H_2/CO system from different authors are shown below. The solid blue line represents the proposed rate constant by Baulch et.al. [1] whereas the blue dash line represents the lower uncertainty limit and blue dot line represents the upper uncertainty limit suggested by [1]. In the plots where Baulch et.al.[1] rate constant are not presented are the reactions that are not reviewed by them. The solid red line is the rate constant that is used in our work. Symbols represents the rate constant from other authors : Warnatz et.al.[2] (2006), cyan filled circle; Kéromnès et.al.[3] (2013), red filled triangle; Peters et.al.[4] (1993), pink filled square; NIST[5] , yellow filled square; San Diego (2014) [6], green filled square; Starik et.al.(2010) [7], black open square; Konnov (2008)[8], black half-filled circle; Vagra et.al. (2016) [9], dark green open up triangle; Hong et.al. (2010, 2011, 2013)[10–12] dark red half-filled diamond, Mueller et.al. (1999) [13], dark yellow open down triangle; Burke et.al. (2012, 2013) [14,15], dark pink open star; Li et.al. (2015)[16], blue open star; Sun et.al. (2007) [17], red open up triangle; Li et.al. (2007) [18], dark red crossed square; Davis et.al. (2005) [19], blue open circle;

Troe (2011) [20], red plus. Reaction rate constant from different authors which are presented in Arrhenius plots can be found in kinetic scheme.

Table S1: Detailed H_2 / CO Kinetic scheme

	Reaction		**A**	**n**	**Ea**	**Reference**
R1	$H+O_2=OH+O$		2.065E+14	-0.097	1.503E+04	[1]*0.87
R2	$O+H_2=H+OH$		3.817E+12	0.000	7.963E+03	[1]*0.79
	DUPLICATE					
	$O+H_2=H+OH$		8.792E+14	0.000	1.918E+04	[1]*0.91
	DUPLICATE					
R3	$OH+H_2=H+H_2O$		2.167E+08	1.520	3.460E+03	[1]
R4	$OH+OH=H_2O+O$		3.348E+04	2.420	-1.928E+03	[1]*1.19
R5	$H+H+M=H_2+M$		7.453E+17	-1.000	0.000E+00	[1]*3
	H_2/1.0/H_2O/6.40/CO_2/1.50/O_2/0.45/N_2/0.40/Ar/0.35/He/0.35/CO/0.75/					
R6	$O+O+M=O_2+M$		2.900E+17	-1.000	0.000E+00	[4]
	H_2/1.0/H_2O/6.40/CO_2/1.50/O_2/0.45/N_2/0.40/Ar/0.35/He/0.35/CO/0.75/					
R7	O+H+M=OH+M		9.436E+18	-1.000	0.000E+00	[16]
	H_2/1.0/H_2O/6.40/CO_2/1.50/O_2/0.45/N_2/0.40/Ar/0.35/He/0.35/CO/0.75/					
R8	$H+OH+M=H_2O+M$		2.212E+22	-2.000	0.000E+00	[1]*1.81
	H_2/1.0/H_2O/6.40/CO_2/1.50/O_2/0.45/N_2/0.40/Ar/0.35/He/0.35/CO/0.75/					
R9	$H+O_2(+M)=HO_2(+M)$		5.590E+13	0.200	0.000E+00	[11]
	Low pressure limit		2.650E+19	-1.300	0.000E+00	[11]*1.32
	F_{cent} = 0.70					
	H_2/2.5/ H_2O/0.00/ H_2O_2/12.0/ Ar/0.00/ O_2/0.00/					
	$H+O_2(+Ar)=HO_2(+Ar)$		5.590E+13	0.200	0.000E+00	
	Low pressure limit		6.810E+18	-1.200	0.000E+00	
	F_{cent} = 0.70					
	$H+O_2(+O_2)=HO_2(+O_2)$		5.590E+13	0.200	0.000E+00	
	Low pressure limit		5.690E+18	-1.100	0.000E+00	
	F_{cent} = 0.70					
	$H+O_2(+H_2O)=HO_2(+H_2O)$		5.590E+13	0.200	0.000E+00	
	Low pressure limit		3.700E+19	-1.200	0.000E+00	
	F_{cent} = 0.80					
R10	$H+HO_2=H_2+O_2$		3.660E+06	2.087	-1.450E+03	[21]*1.27
R11	$H+HO_2=OH+OH$		7.080E+13	0.000	3.000E+02	[22]
R12	$O+HO_2=OH+O_2$		1.630E+13	0.000	-4.452E+02	[1]
R13	$HO_2+OH=H_2O+O_2$		7.000E+12	0.000	-1.093E+03	[12]
	DUPLICATE					
	$HO_2+OH=H_2O+O_2$		4.500E+14	0.000	1.093E+04	

	DUPLICATE					
R14	$HO_2+HO_2= H_2O_2+O_2$		4.220E+14	0.000	1.198E+04	[1]
	DUPLICATE					
	$HO_2+HO_2= H_2O_2+O_2$		1.320E+11	0.000	-1.630E+03	
	DUPLICATE					
R15	H_2O_2 (+M)=OH+OH(+M)		2.000E+12	0.900	4.877E+04	[20]
	Low pressure limit		3.660E+24	-2.300	4.877E+04	
	F_{cent} = 0.43					
	H_2O/5.1/H_2O_2/5.2/H_2/2.5/O_2/0.79/N_2/1.0/Ar/0.68/He/0.44/CO_2/1.06/CO/0.53/					[20]
R16	$H_2O_2+H=H_2O+OH$		1.023E+13	0.000	3.586E+03	[1]
R17	$H_2O_2+H=HO_2+H_2$		1.210E+07	2.000	5.200E+03	[23]
R18	$H_2O_2+O=OH+HO_2$		9.630E+06	2.000	3.993E+03	[24]
R19	$H_2O_2+OH=H_2O+HO_2$		1.740E+12	0.000	3.180E+02	[25]
	DUPLICATE					
	$H_2O_2+OH=H_2O+HO_2$		7.590E+13	0.000	7.269E+03	
	DUPLICATE					
R20	$CO+O(+M)=CO_2(+M)$		1.800E+10	0.000	2.384E+03	[13]
	Low pressure limit		1.550E+24	-2.790	4.185E+03	
	H_2/1.0/H_2O/6.40/CO_2/1.50/O_2/0.45/N_2/0.40/Ar/0.35/He/0.35/CO/0.75/					
R21	$CO+O_2= CO_2+O$		2.500E+12	0.000	4.782E+04	[24]
R22	$CO+OH= CO_2+H$		1.000E+13	0.000	1.600E+04	[1]
	DUPLICATE					
	$CO+OH= CO_2+H$		1.010E+11	0.000	5.978E+01	[1]*0.89
	DUPLICATE					
	$CO+OH= CO_2+H$		9.030E+11	0.000	4.567E+03	
	DUPLICATE					
R23	$CO+ HO_2=CO_2+OH$		1.570E+05	2.180	1.794E+04	[26]
R24	HCO(+M)=H+CO(+M)		4.930E+16	-0.93	1.973E+04	[9]
	Low pressure limit		4.942E+10	0.959	1.467E+04	
	TROE /8.52E-01 5.14E+01 3.57E+03 3.42E+03 /					
	H2/2/ O2/1/ AR/0.55/ HE/0.786/ H2O/12/ CO/1.5/ CO2/2/					
R25	$HCO+O_2=CO+HO_2$		2.710E+10	0.680	-4.691E+02	[1]*1.11
R26	$HCO+H=CO+H_2$		9.030E+13	0.000	0.000E+00	[1]
R27	HCO+O=CO+OH		3.010E+13	0.000	0.000E+00	[1]
R28	$HCO+O=CO_2+H$		3.010E+13	0.000	0.000E+00	[1]
R29	$HCO+OH=CO+H_2O$		1.080E+14	0.000	0.000E+00	[1]
R30	$HCO+HO_2=>CO_2+H+OH$		3.000E+13	0.000	0.000E+00	[24]
R31	$HCO+HCO=>H_2+CO+CO$		3.000E+12	0.000	0.000E+00	[1]
R32	$HCO+HO_2=H_2O_2+CO$		3.000E+12	0.000	0.000E+00	[24]
A1	$O+OH+M=HO_2$ +M		8.000E+15	0.000	0.000E+00	[6]*2
	H_2/1.0/H_2O/6.40/CO_2/1.50/O_2/0.45/N_2/0.40/Ar/0.35/He/0.35/CO/0.75/					

A2	$H+HO_2=H_2O+O$		1.450E+12	0.000	0.000E+00	[1]
A3	$H_2+O_2=OH+OH$		1.700E+13	0.000	4.780E+04	[27]
A4	$H_2O_2+O=H_2O+O_2$		8.430E+11	0.000	3.980E+03	[1]
A5	$H_2O+O=H_2+O_2$		1.070E+10	0.970	6.870E+04	[28]
	OH* Chemiluminescence mechanism					
B1	$H+O+M=OH^*+M$		1.500E+13	0.000	5.975E+03	[29]
	H_2/1.0/H_2O/6.40/CO_2/1.50/O_2/0.45/N_2/0.40/Ar/0.35/He/0.35/CO/0.75/					
B2	$HCO+O=OH^*+CO$		2.890E+11	0.000	4.609E+02	[30]
B3	$OH^*=OH$		1.450E+06	0.000	0.000E+00	[31]
B4	$OH^*+O_2=OH+O_2$		2.100E+12	0.500	-4.824E+02	[31]
B5	$OH^*+H_2=OH+H_2$		2.950E+12	0.500	-4.543E+02	[31]
B6	$OH^*+N_2=OH+N_2$		1.080E+11	0.500	-1.243E+02	[32]
B7	$OH^*+Ar=OH+Ar$		1.690E+12	0.000	4.137E+03	[31]
B8	$OH^*+H_2O=OH+H_2O$		5.930E+12	0.500	-8.608E+02	[31]
B9	$OH^*+CO_2=OH+CO_2$		2.750E+12	0.500	-9.680E+02	[31]
B10	$OH^*+CO=OH+CO$		3.230E+12	0.500	-7.881E+02	[31]
B11	$OH^*+OH=OH+OH$		6.010E+12	0.500	-7.652E+02	[31]
B12	$OH^*+H=OH+H$		1.310E+12	0.500	-1.674E+02	[31]

Units are cm^3 - mol - s - cal - K; $k = AT^n \exp(-Ea/RT)$.

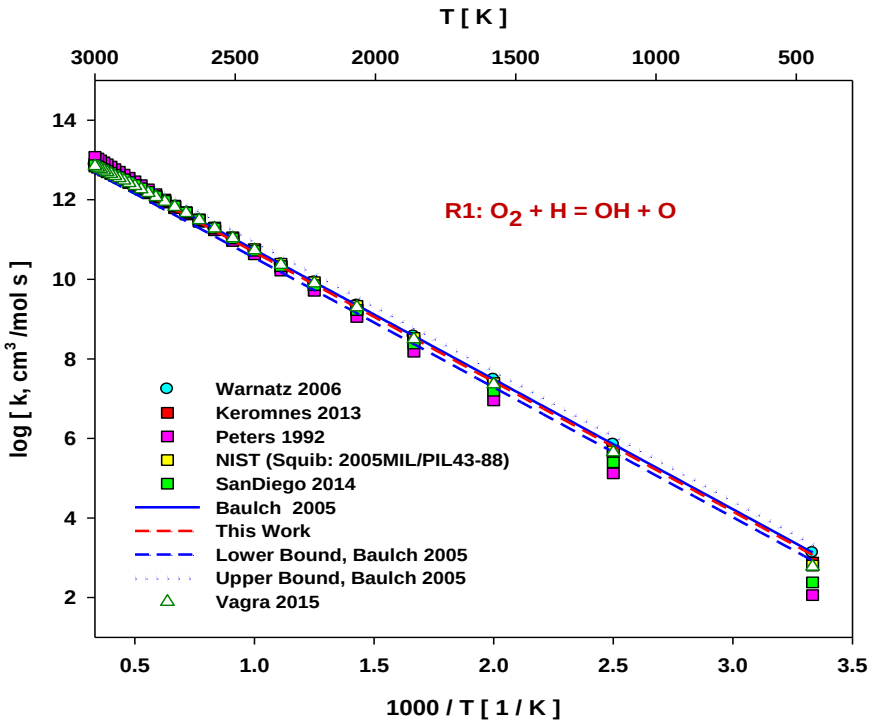

Figure S1.1: Rate constant comparison of reaction R1: $O_2+H=OH+O$ from different authors.

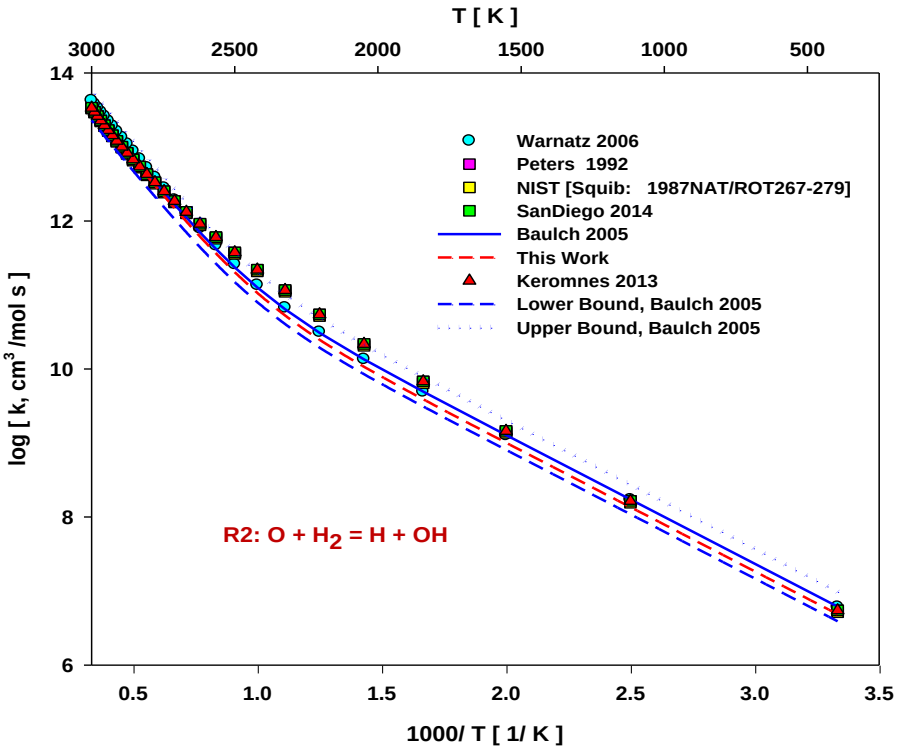

Figure S1.2: Rate constant comparison of reaction R2: O+H_2=H+OH from different authors.

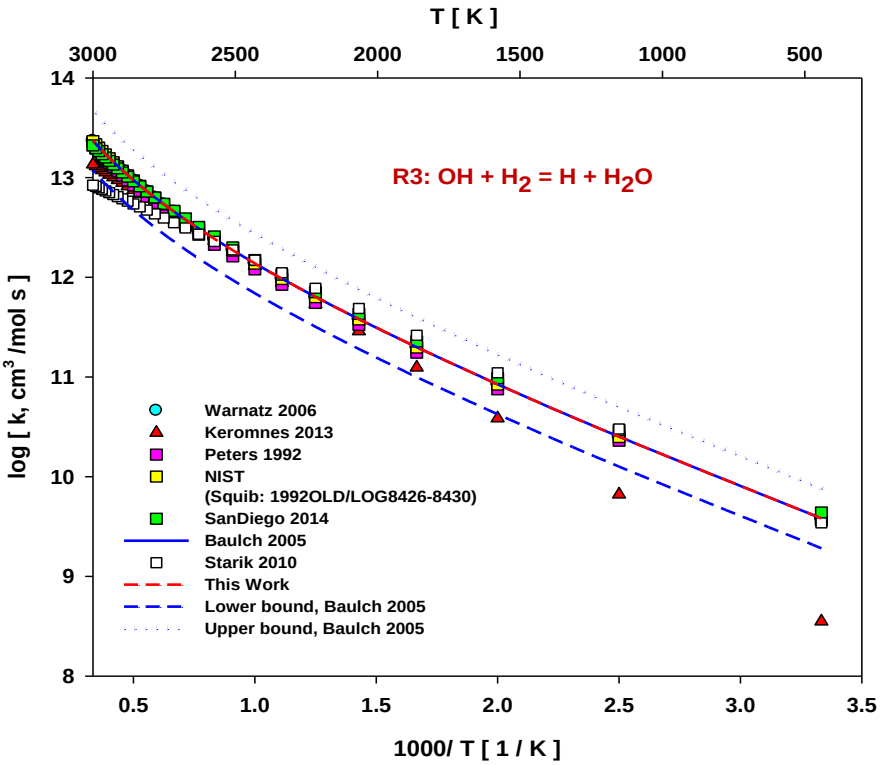

Figure S1.3: Rate constant comparison of reaction R3: OH+H_2=H+H_2O from different authors.

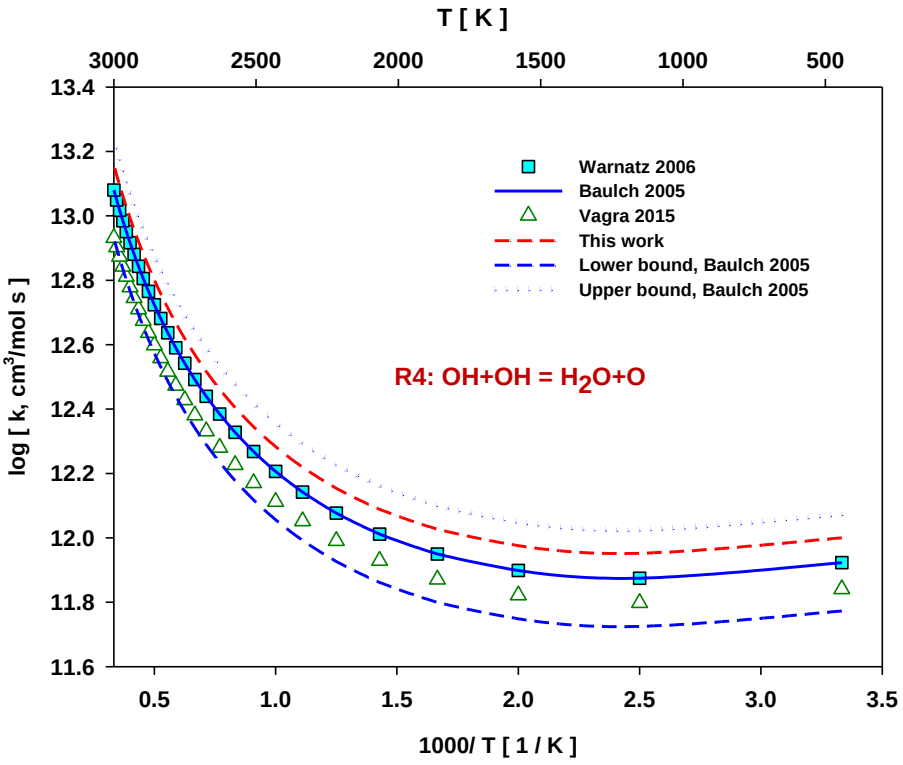

Figure S1.4: Rate constant comparison of reaction R4: OH+OH=H_2O+O from different authors.

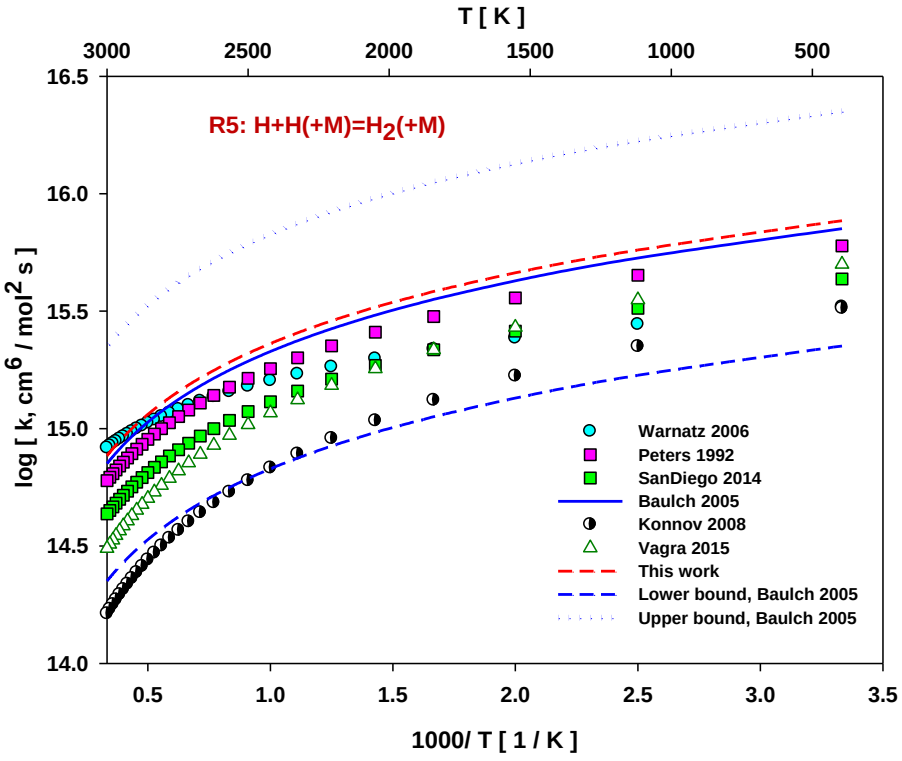

Figure S1.5: Rate constant comparison of reaction R5: H+H +M =H_2+M from different authors.

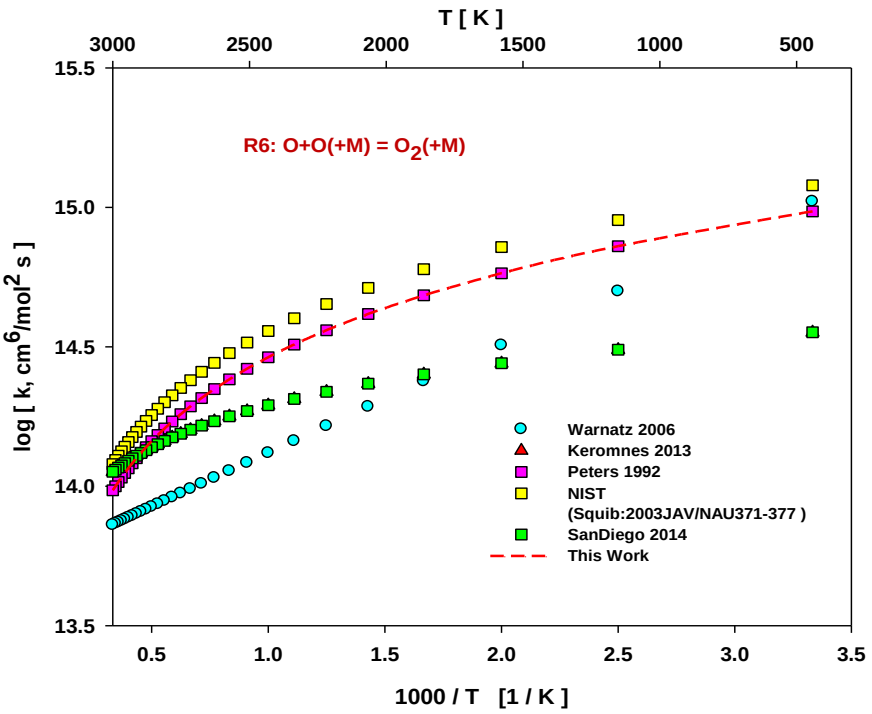

Figure S1.6: Rate constant comparison of reaction R6: O+O +M =O_2 +M from different authors.

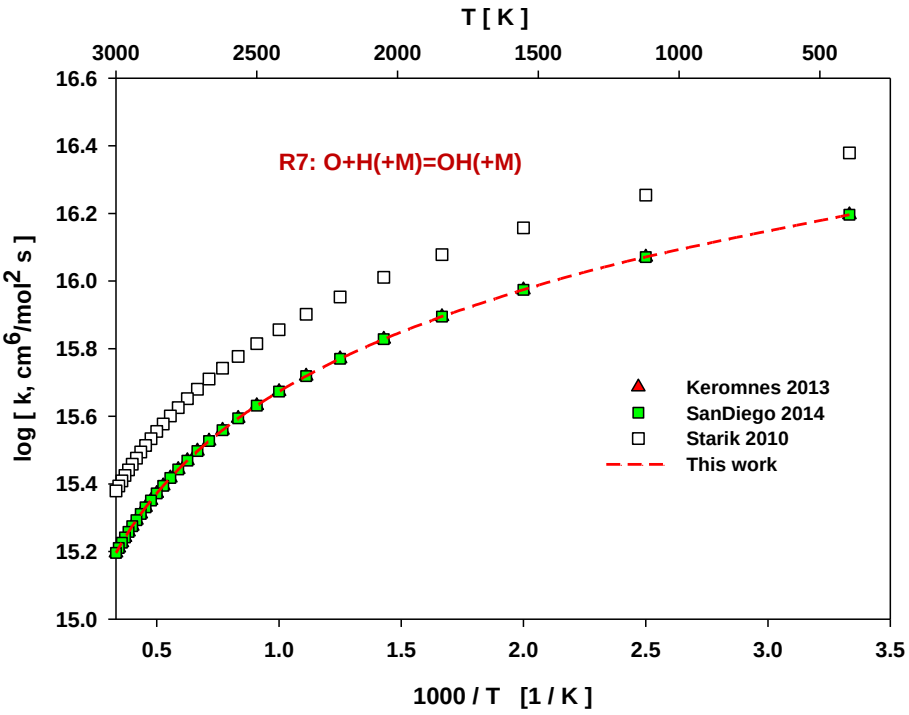

Figure S1.7: Rate constant comparison of reaction R7: O+H +M =OH +M from different authors.

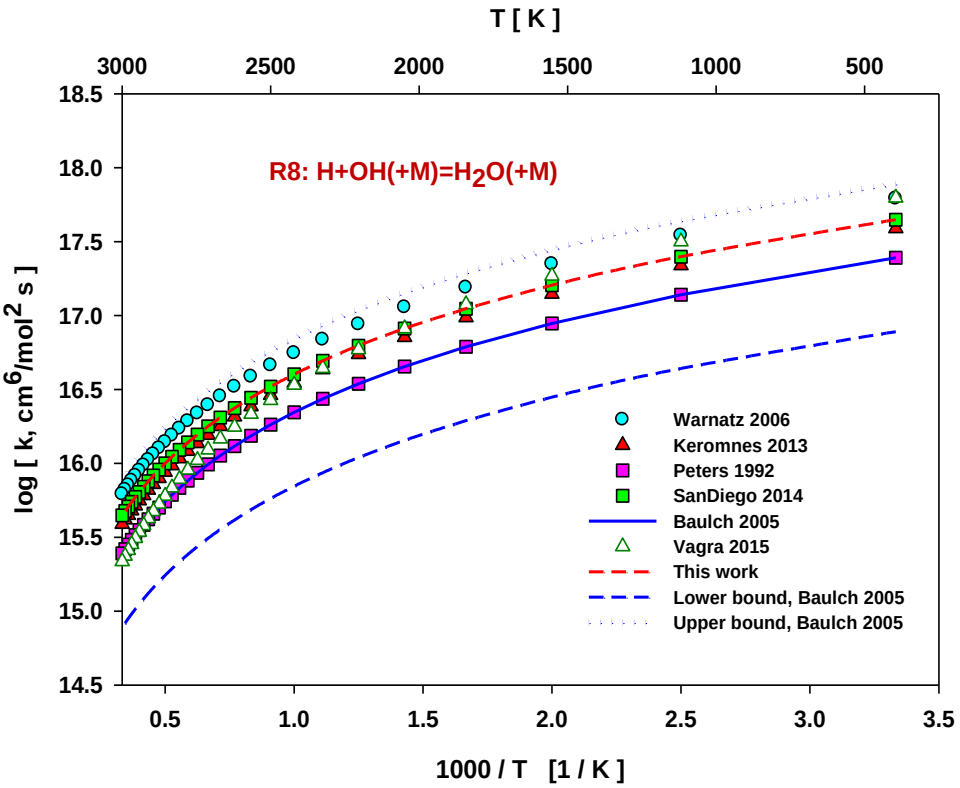

Figure S1.8: Rate constant comparison of reaction R8: H+OH +M =H_2O+M from different authors.

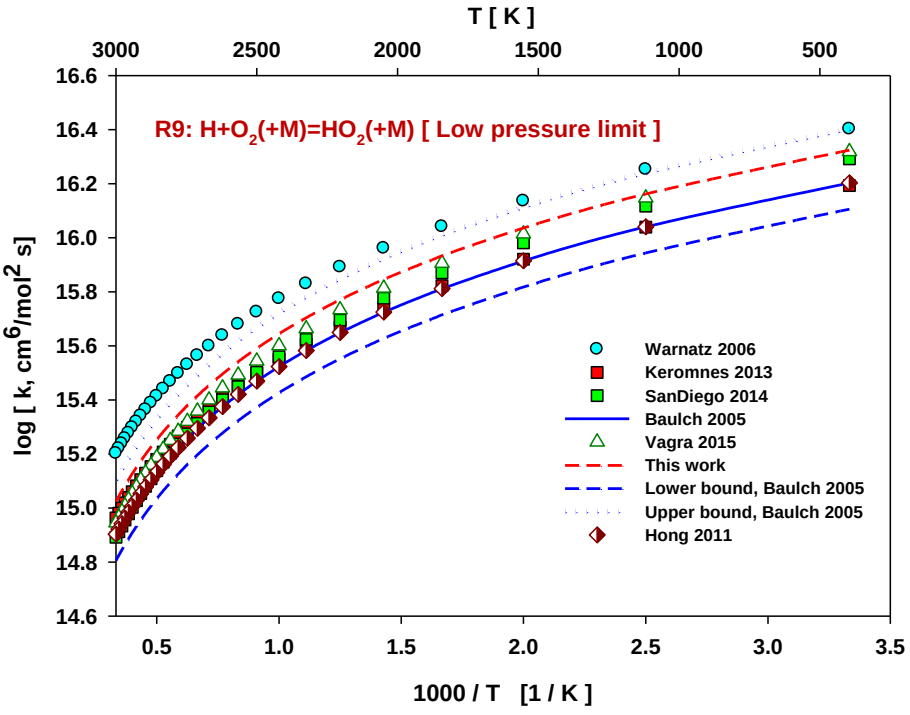

Figure S1.9: Rate constant comparison of reaction R9: H+O_2 (+M) =HO_2 (+M) from different authors.

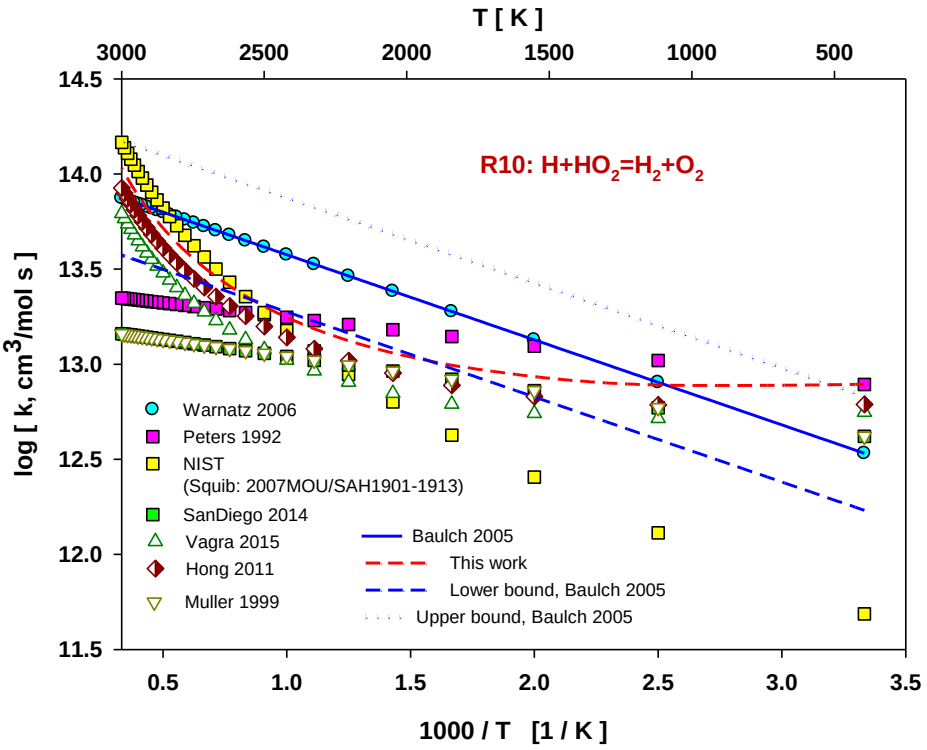

Figure S1.10: Rate constant comparison of reaction R10: $H+HO_2 = H_2+O_2$ from different authors.

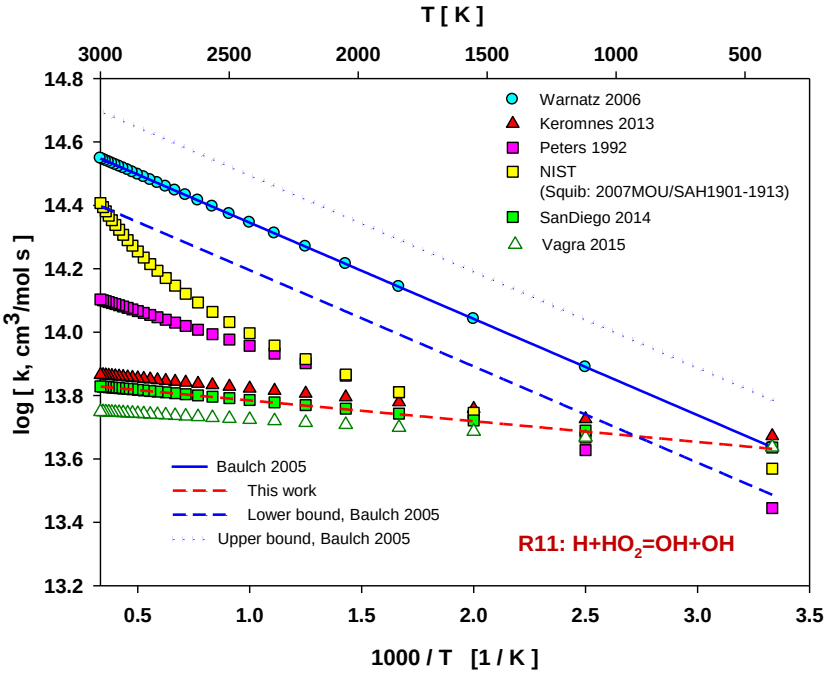

Figure S1.11: Rate constant comparison of reaction R11: $H+HO_2 = OH+OH$ from different authors.

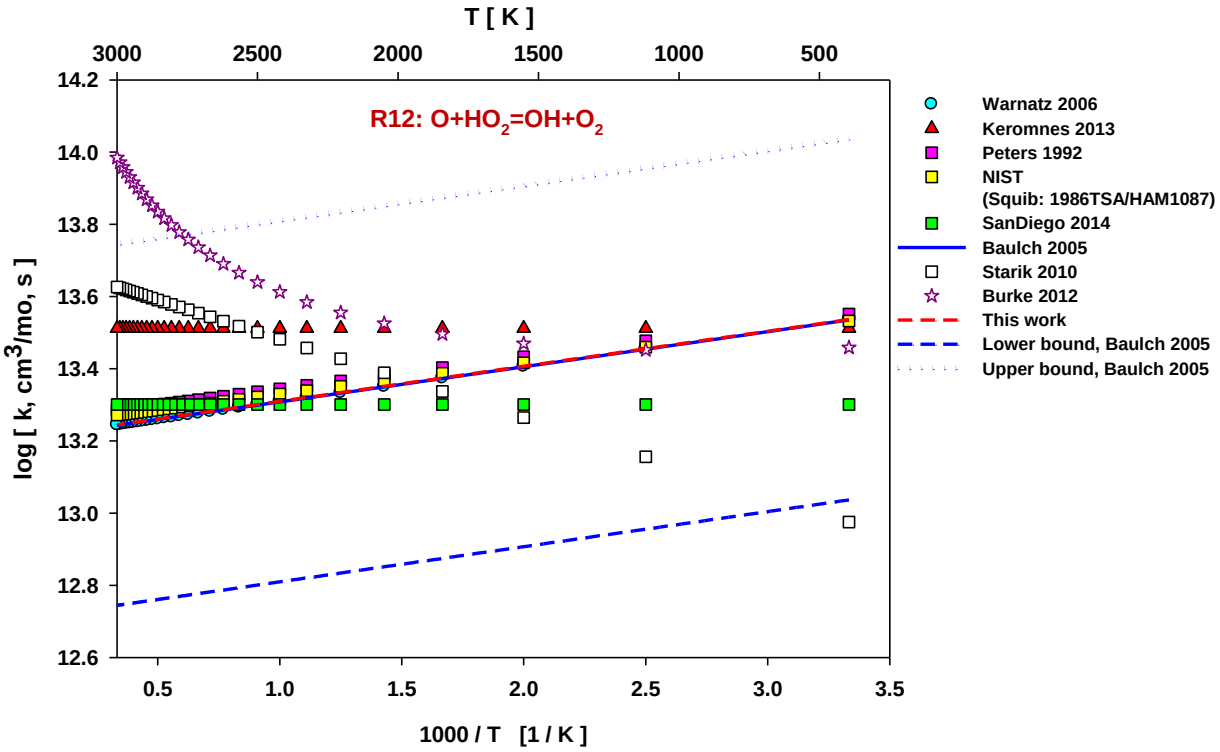

Figure S1.12: Rate constant comparison of reaction R12: $O+HO_2 =OH+O_2$ from different authors.

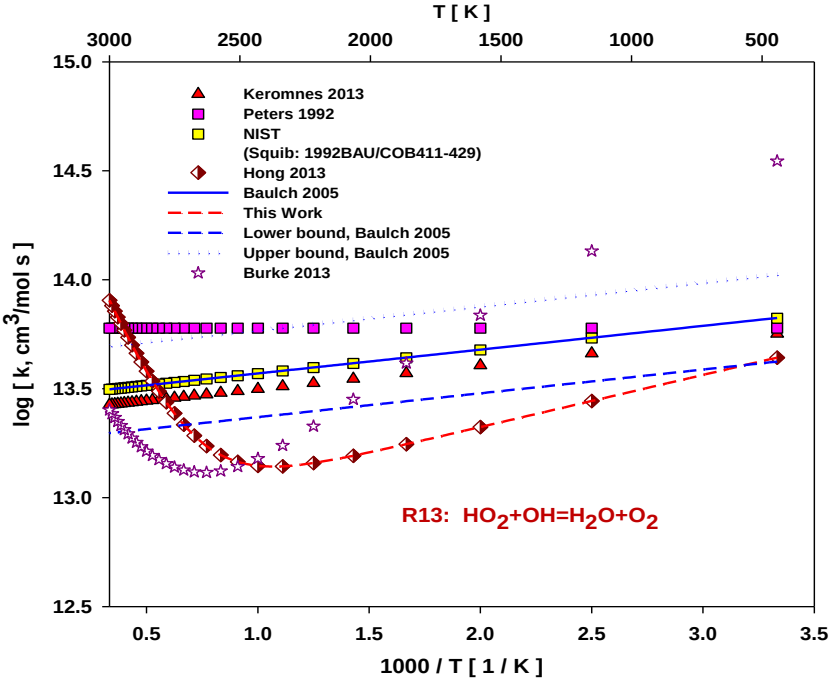

Figure S1.13: Rate constant comparison of reaction R13: $HO_2+OH=H_2O+O_2$ from different authors.

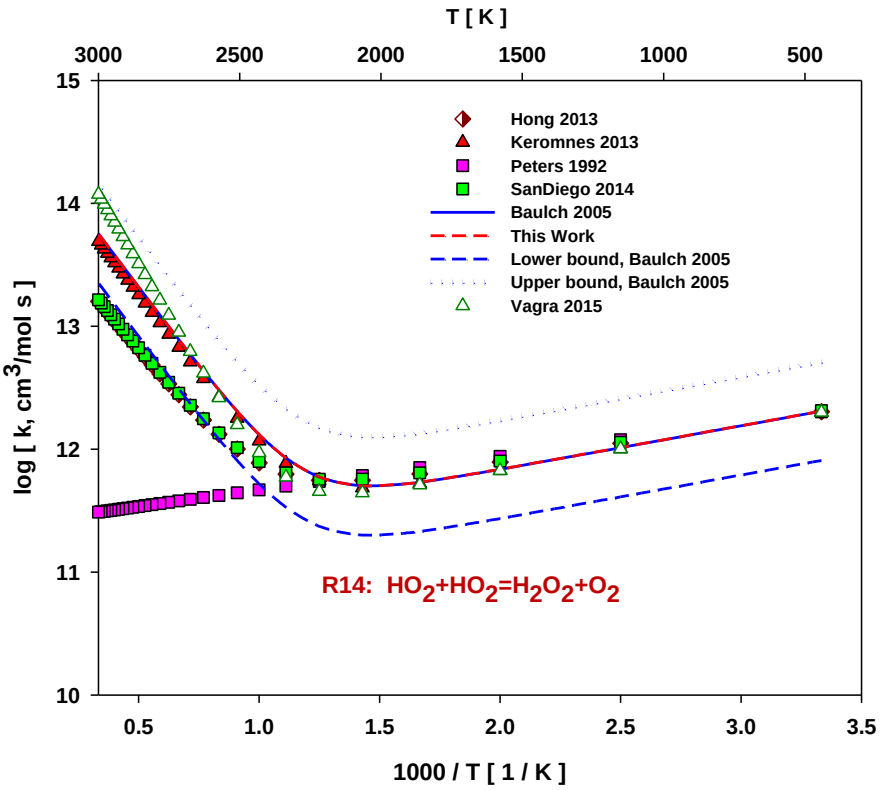

Figure S1.14: Rate constant comparison of reaction R14: HO_2+ HO_2=H_2O_2+O_2 from different authors.

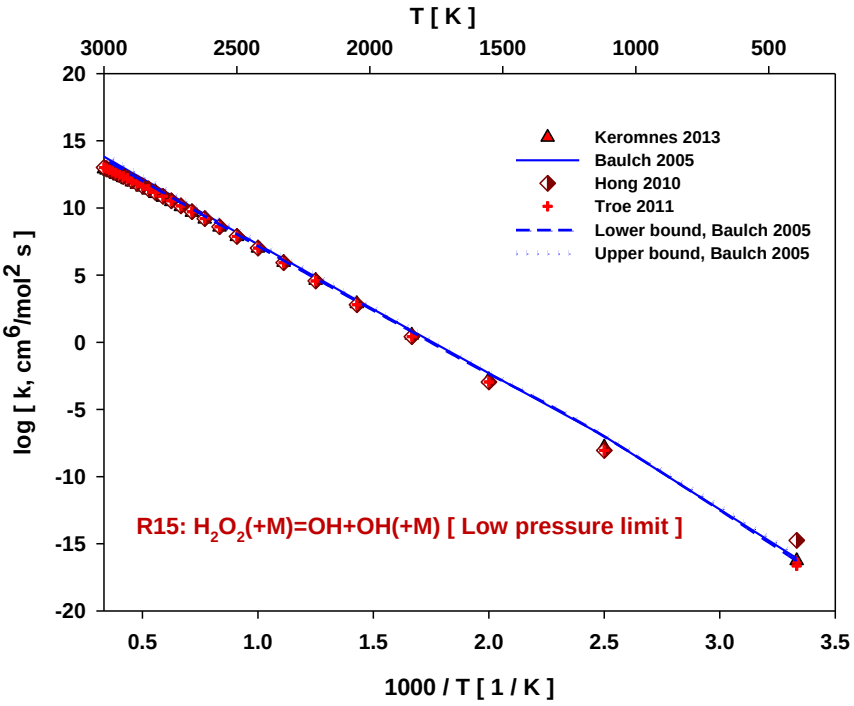

Figure S15: Rate constant comparison of reaction R15: H_2O_2 (+M) =OH+OH from different authors.

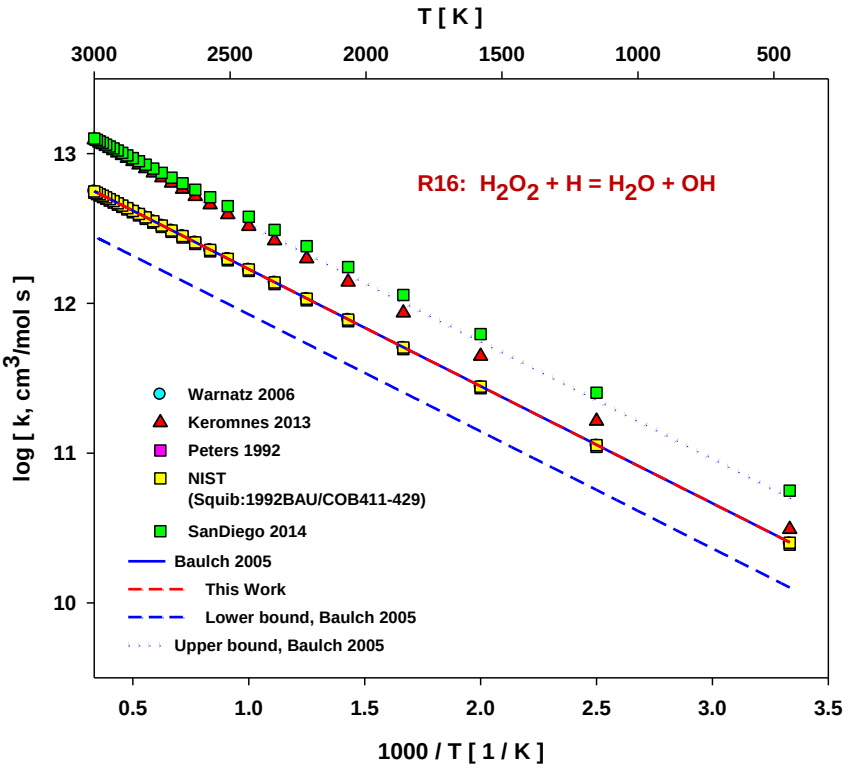

Figure S1.16: Rate constant comparison of reaction R16: H_2O_2+H =H_2O+OH from different authors.

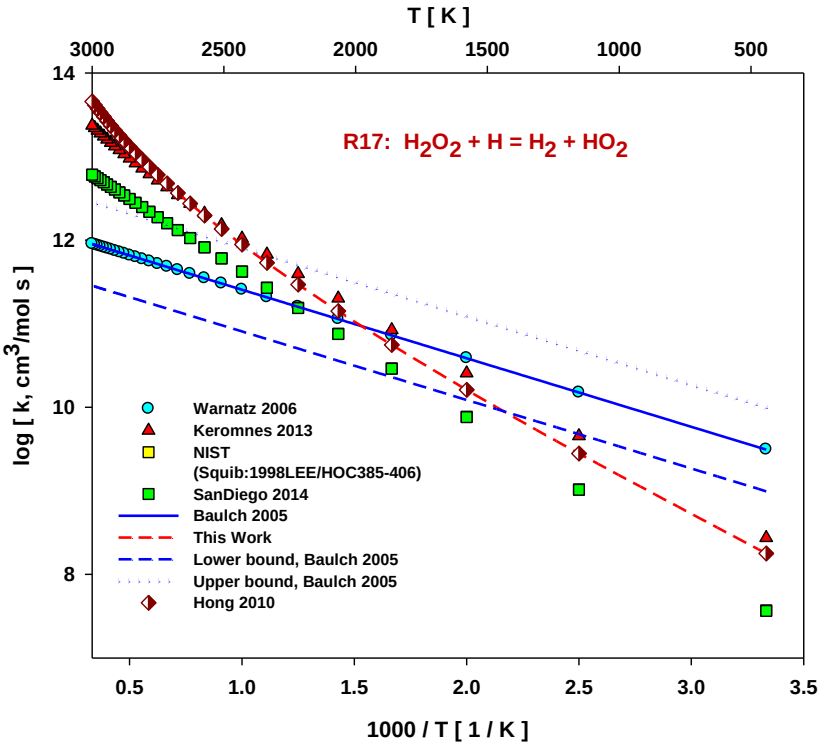

Figure S1.17: Rate constant comparison of reaction R17: H_2O_2+H =H_2+HO_2 from different authors.

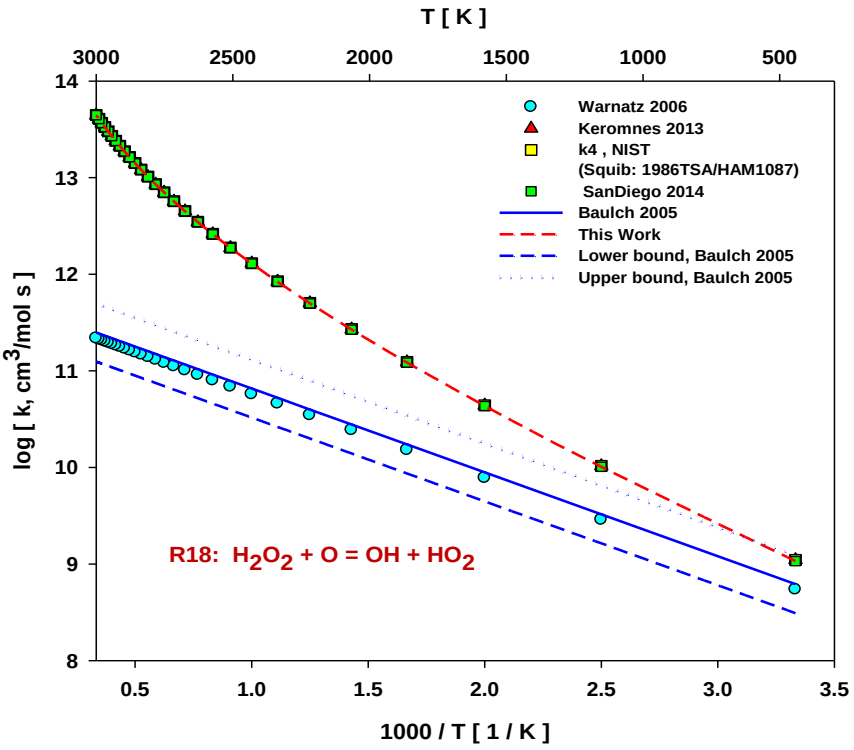

Figure S18: Rate constant comparison of reaction R18: H_2O_2+O =OH+HO_2 from different authors.

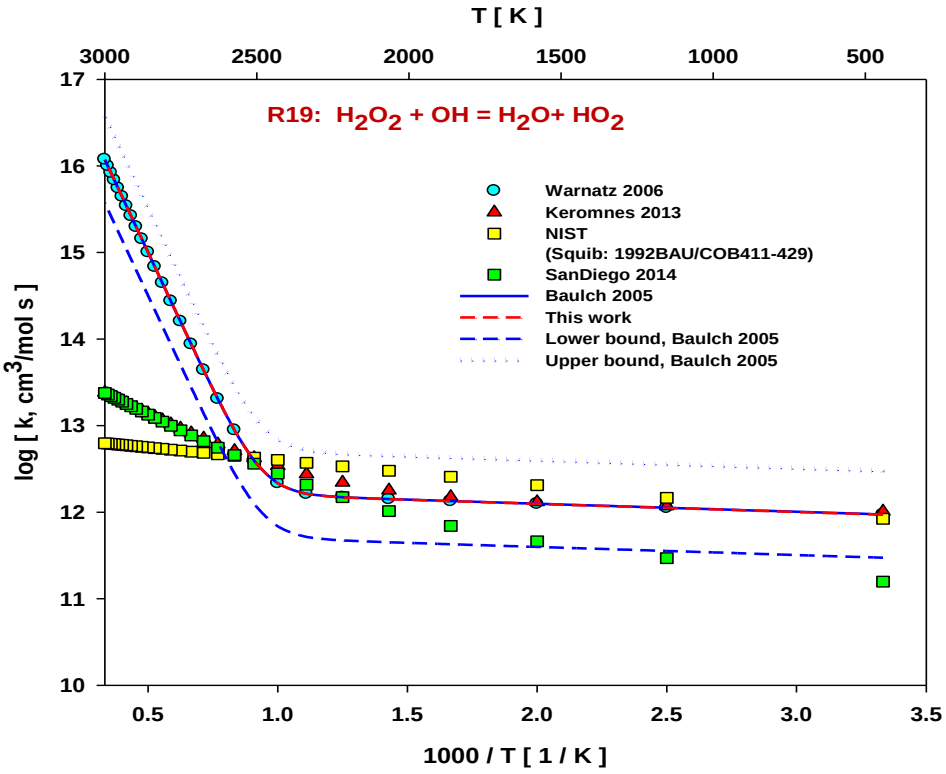

Figure S1.19: Rate constant comparison of reaction R19: H_2O_2+OH =H_2O+HO_2 from different authors.

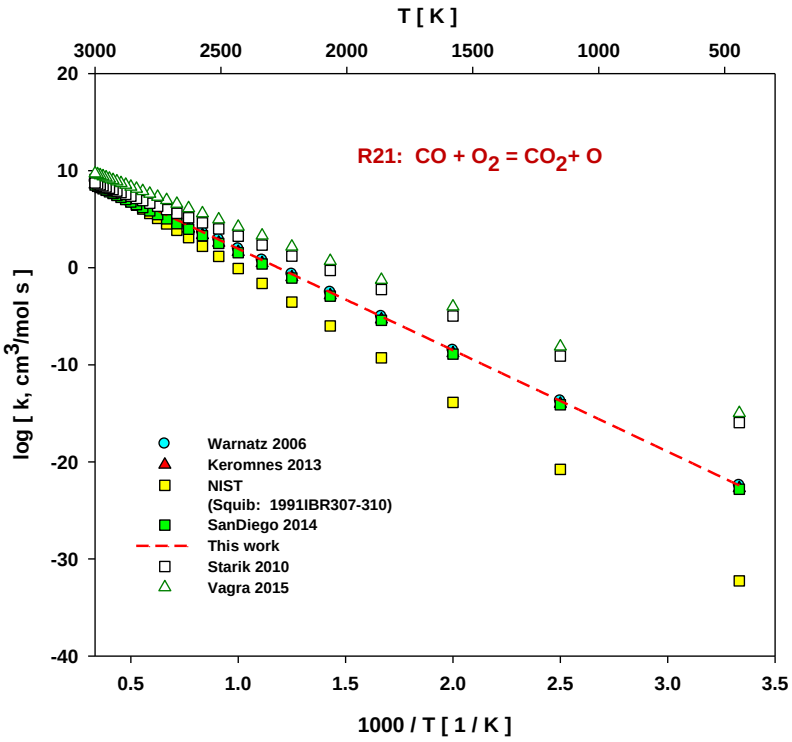

Figure S1.20: Rate constant comparison of reaction R21: $CO+O_2 = CO_2+O$ from different authors.

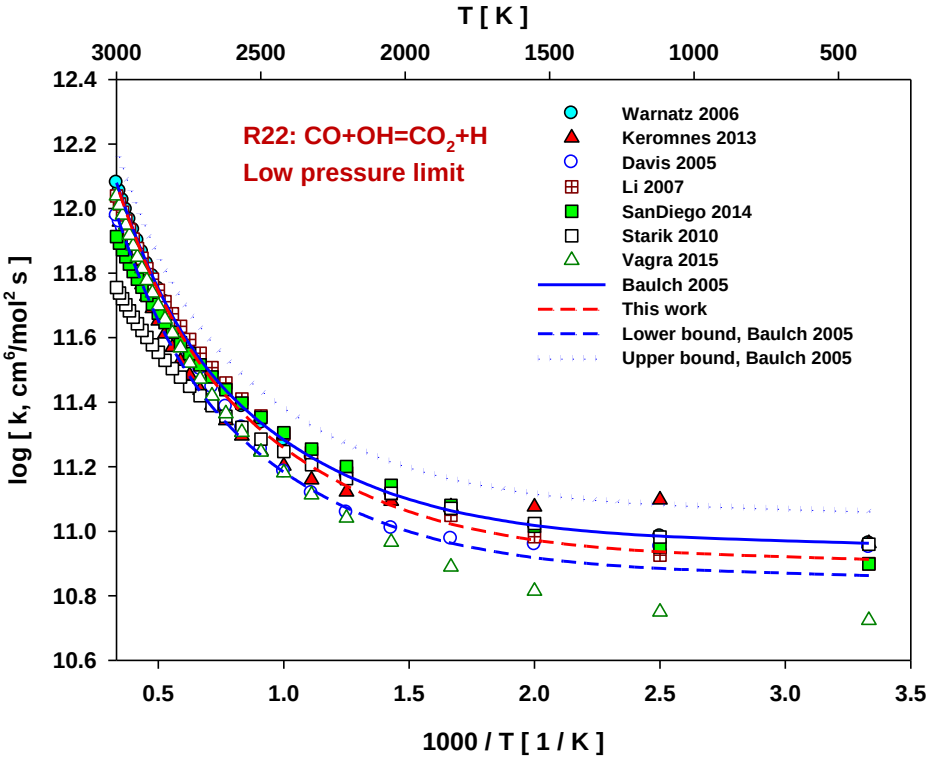

Figure S1.21: Rate constant comparison of reaction R22: $CO+OH = CO_2+H$ from different authors.

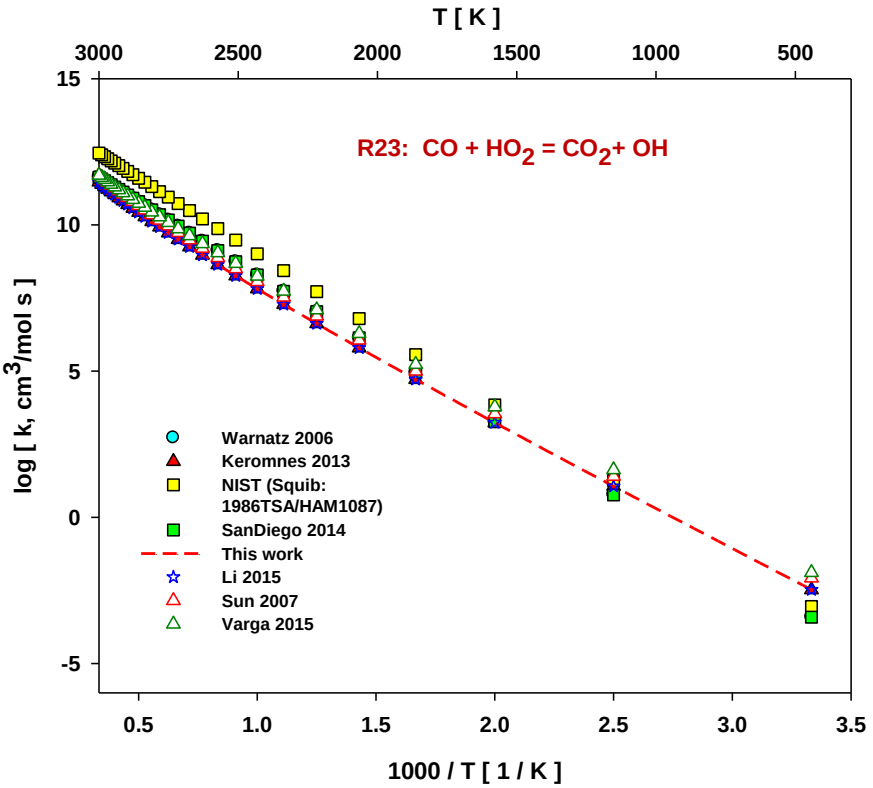

Figure S1.22: Rate constant comparison of reaction R23: $CO+HO_2=CO_2+OH$ from different authors.

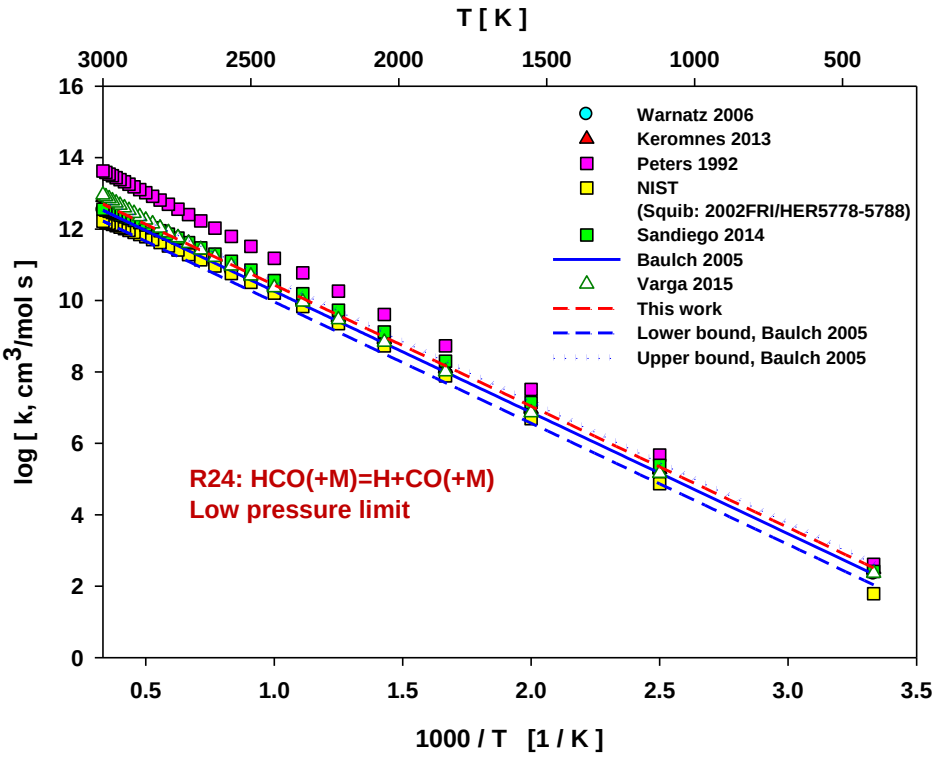

Figure S1.23: Rate constant comparison of reaction R24: HCO (+M) =H+CO (+M) from different authors.

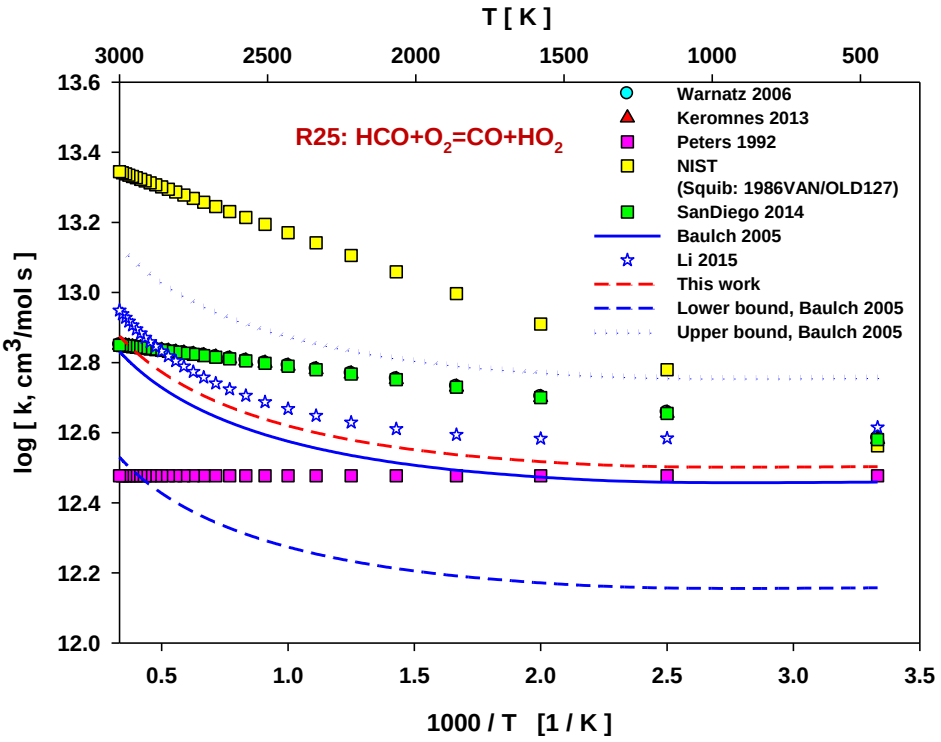

Figure S1.24: Rate constant comparison of reaction R25: $HCO+O_2 = CO+HO_2$ from different authors.

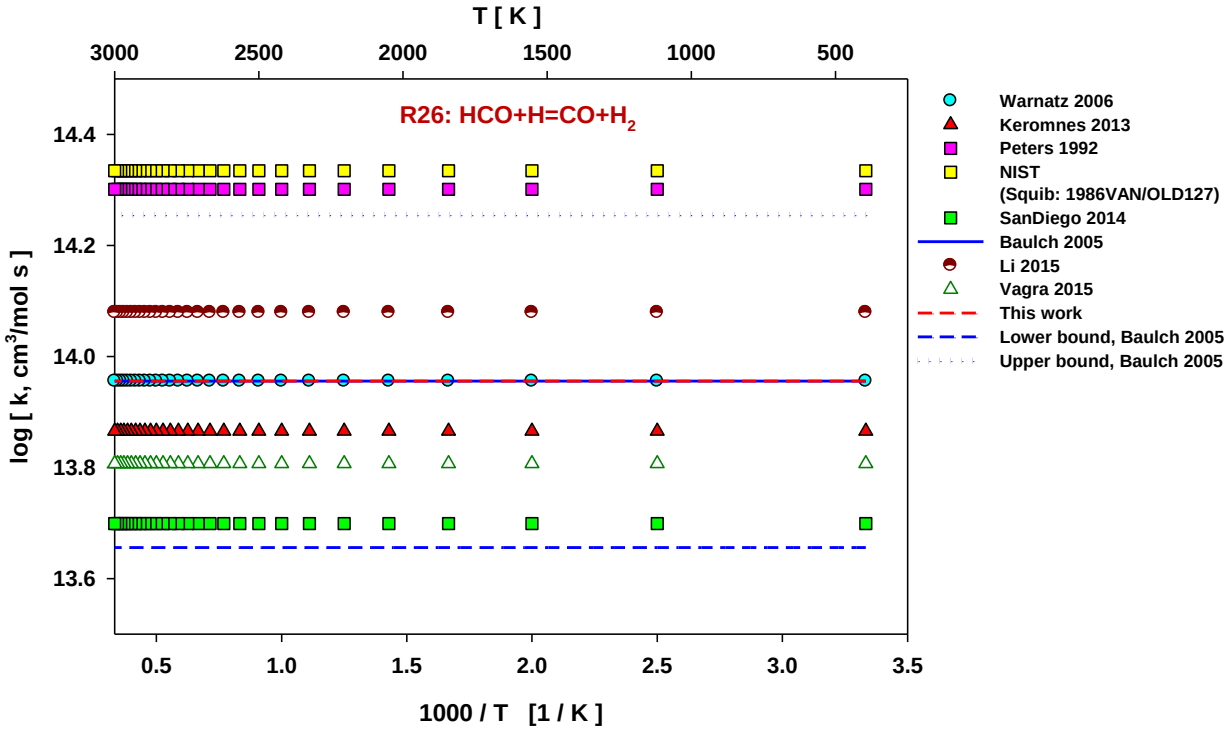

Figure S1.25: Rate constant comparison of reaction R26: $HCO+H = CO+H_2$ from different authors.

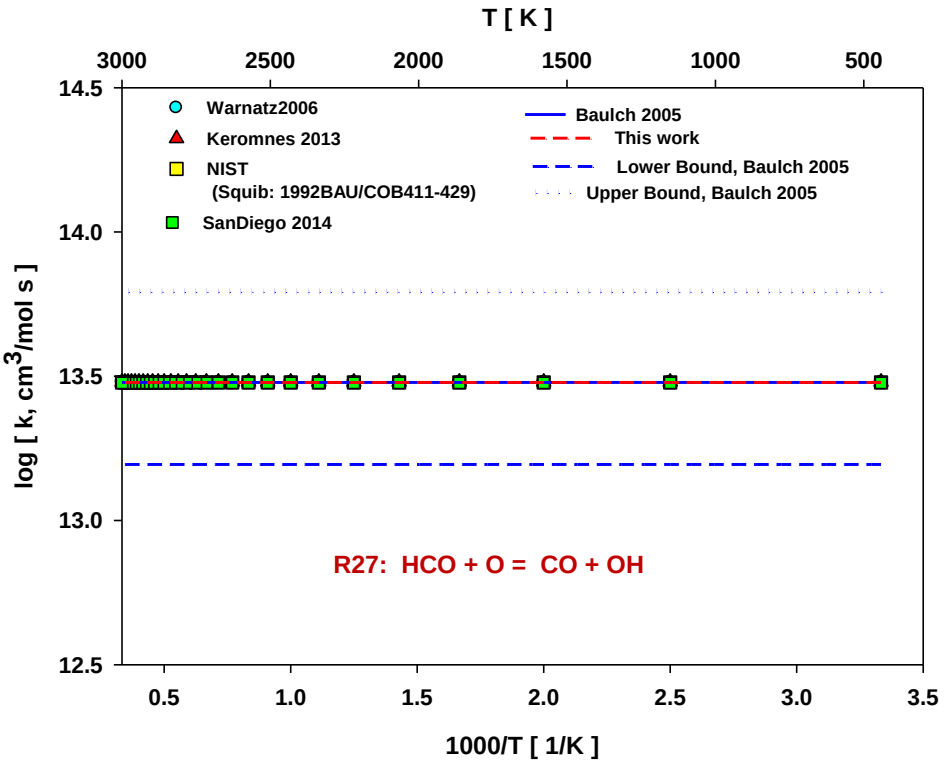

Figure S1.26: Rate constant comparison of reaction R27: HCO+O =CO+OH from different authors.

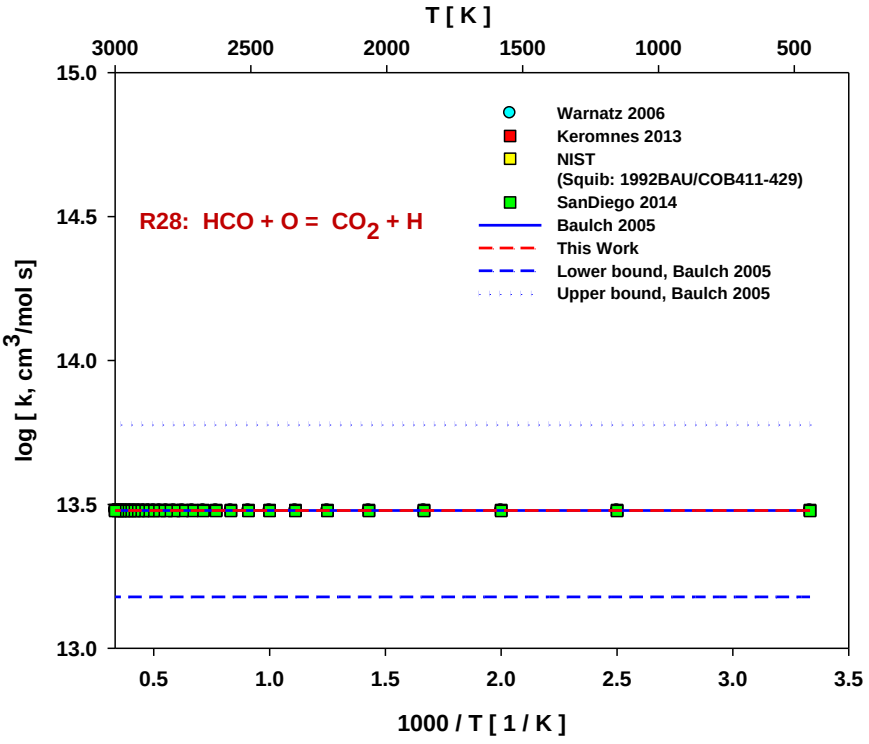

Figure S1.27: Rate constant comparison of reaction R28: HCO+O =CO_2+H from different authors.

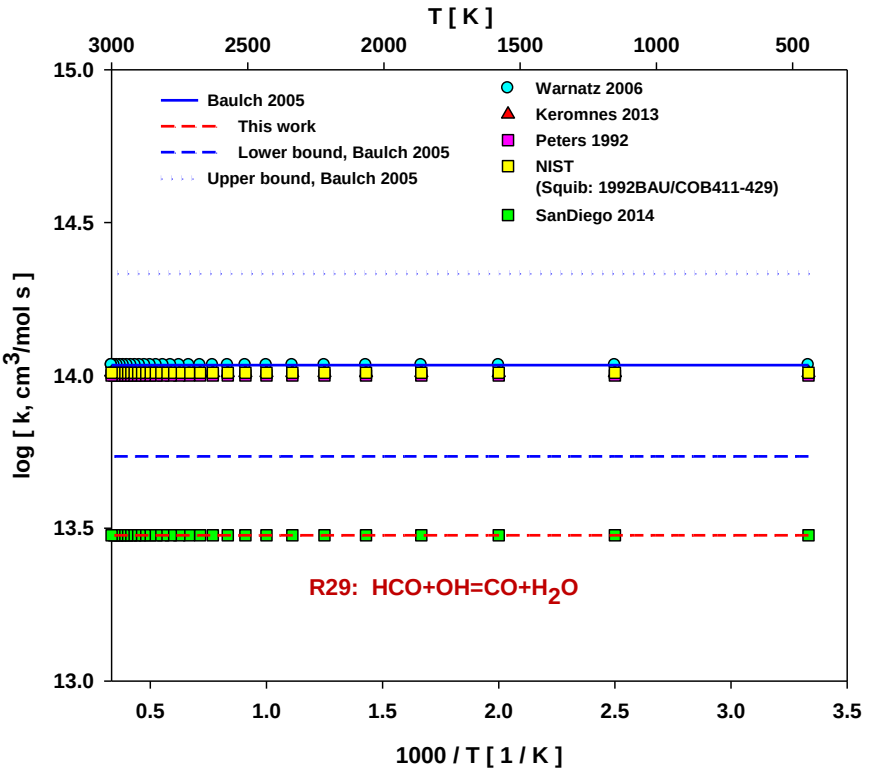

Figure S1.28: Rate constant comparison of reaction R29: HCO+OH =CO+H_2O from different authors.

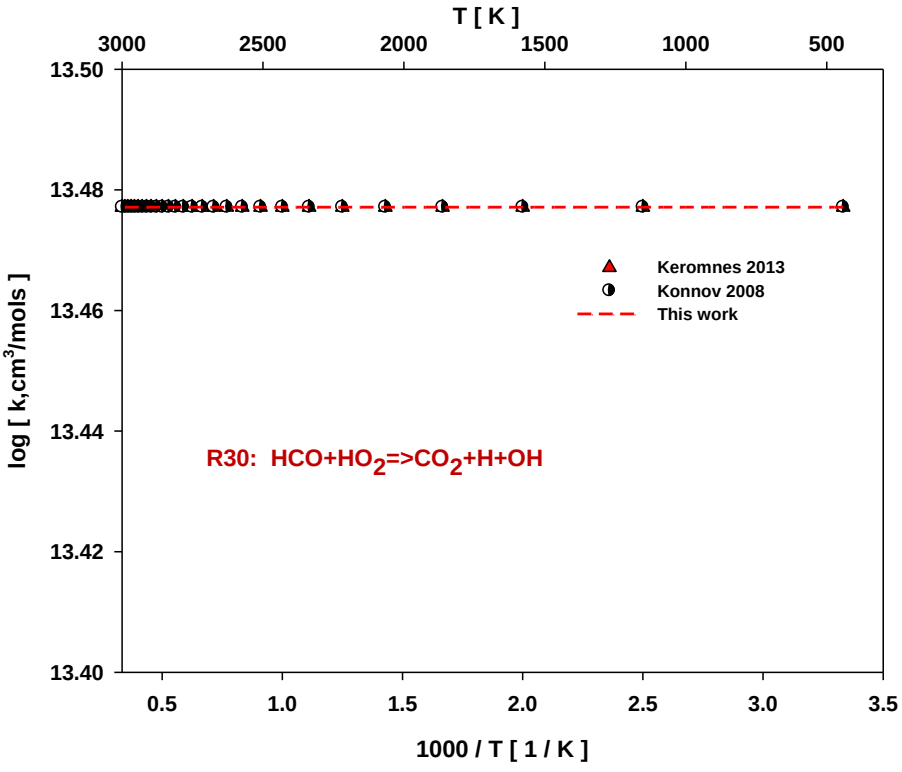

Figure S1.29: Rate constant comparison of reaction R30: HCO+HO_2 =>CO_2+H+OH from different authors.

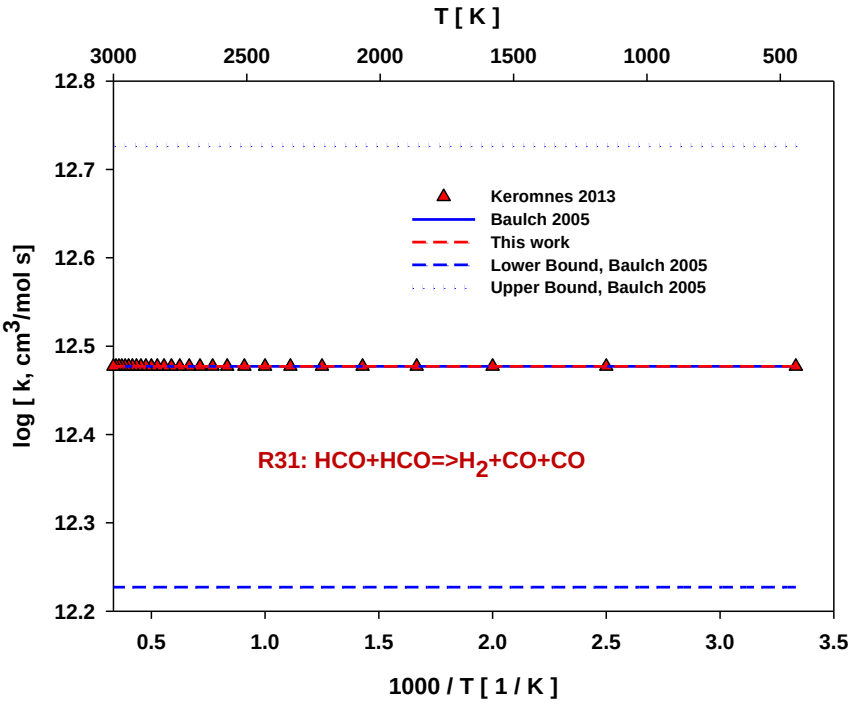

Figure S1.30: Rate constant comparison of reaction R31: HCO+HCO =>H_2+CO+CO from different authors.

2. Mechanism Validation

This section deals with the kinetic model validation. The mechanism is validated against laminar flame speed, ignition delay time, species prediction in burner stabilized flame, Jest stirred reactor and flow reactor.

For the laminar lame speed and burner stabilized flame solid line represents prediction implying the mixture average transport model and dash line represents the prediction implying the multi component transport model with current kinetic scheme unless stated. The solid or dash in the ignition delay, JSR and flow reactor plots represents prediction from the current kinetic model. All Symbols in the plots represents the experimental data from the published literature. Colors of lines and symbols are assigned to match each other for particular experimental condition or specific species.

2.1 Laminar Flame Speed

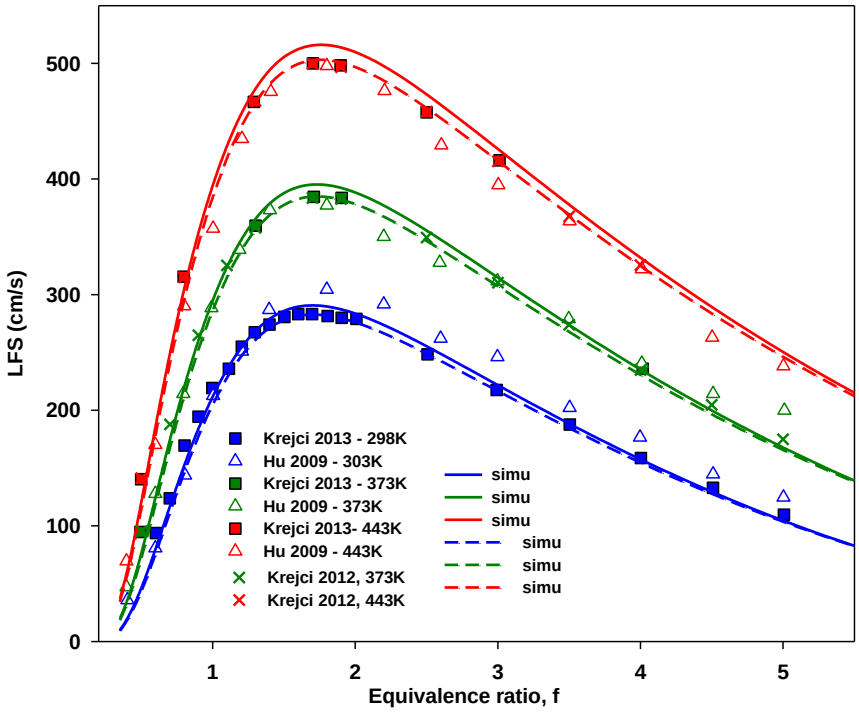

Figure S2.1: Comparison of Laminar flame speed of H_2 –air mixture at 1 atm and 303, 373 and 443 K. Filled square [33], open triangle [34] and crosses [35].

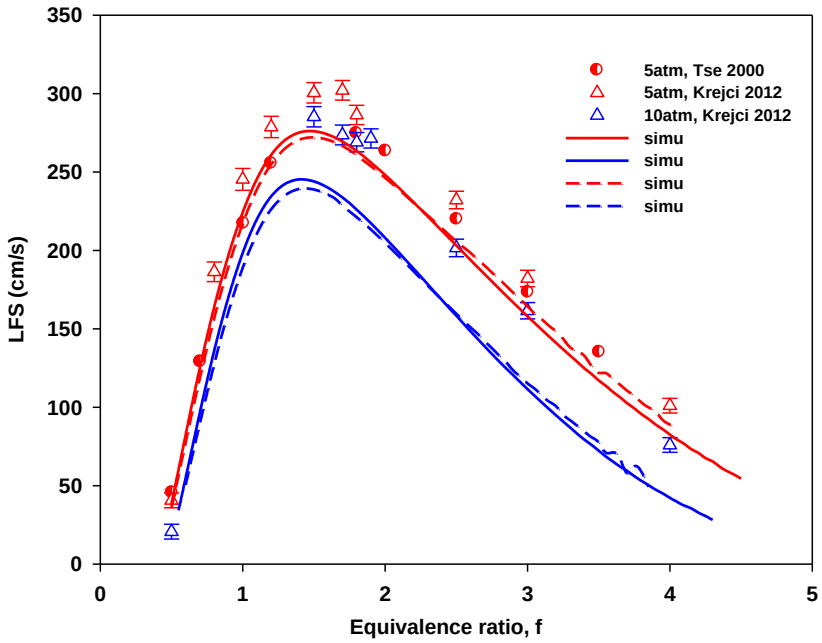

Figure S2.2: Comparison of laminar flame speed of H_2-O_2-He [O_2/He: 1/7] at 298 K and 5,s 10 atm. Open triangle [35], half-filled circle [36].

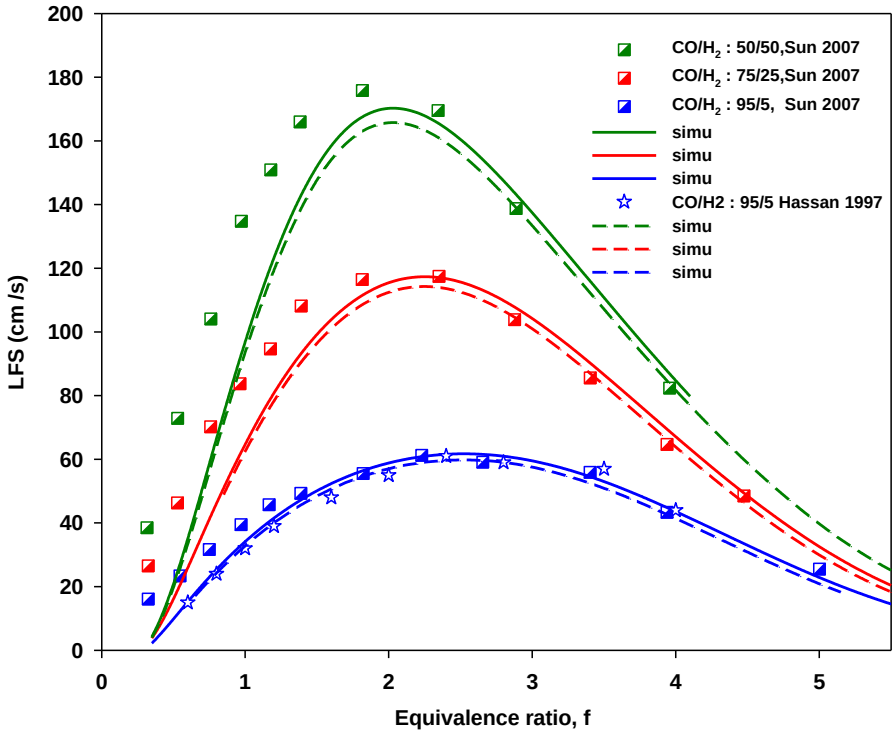

Figure S2.3: Laminar flame speed comparison of CO/H_2-air at 298 K and 2 atm. Half-filled square [17], open star [37].

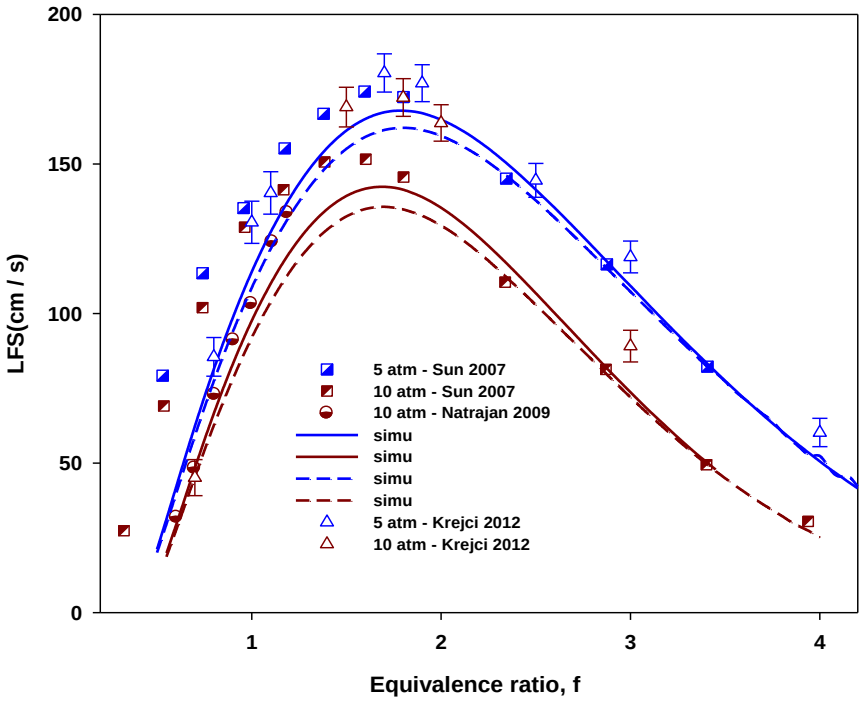

Figure S2.4: Laminar flame speed comparison of CO/H_2 (50/50) $-O_2$ /He (1/7) at 298 K and 5, 10 atm. Half-filled square [17], half-filled circle [38], open triangle [35] with uncertainty bars.

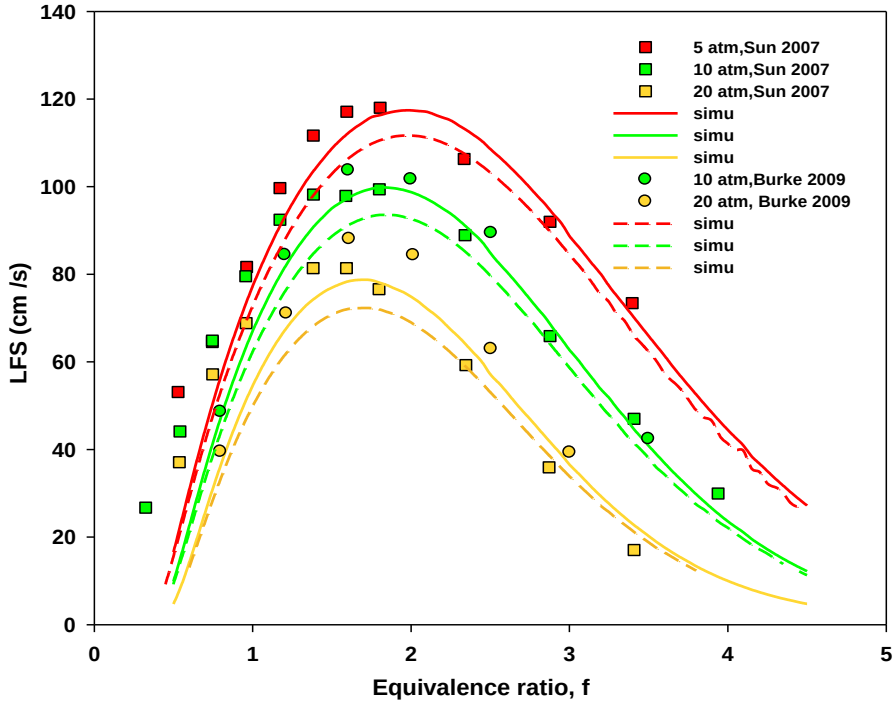

Fig S2.5: Laminar flame speed comparison of H_2/CO (25/75) –O_2 /He (1/7) at 298 K and 5, 10, 20 atm. Filled square [17] and filled circle [39].

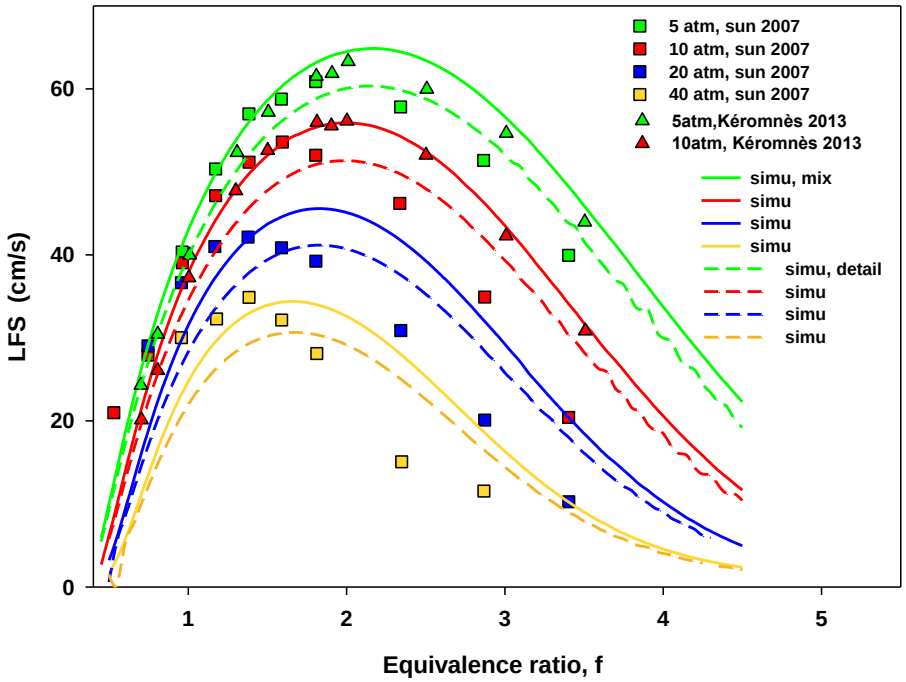

Fig S2.6: Laminar flame speed comparison of H_2/CO (5/95) –O_2 /He (1/7) at 298 K and 5, 10, 20, 40atm. Filled squares [17], filled triangles [3].

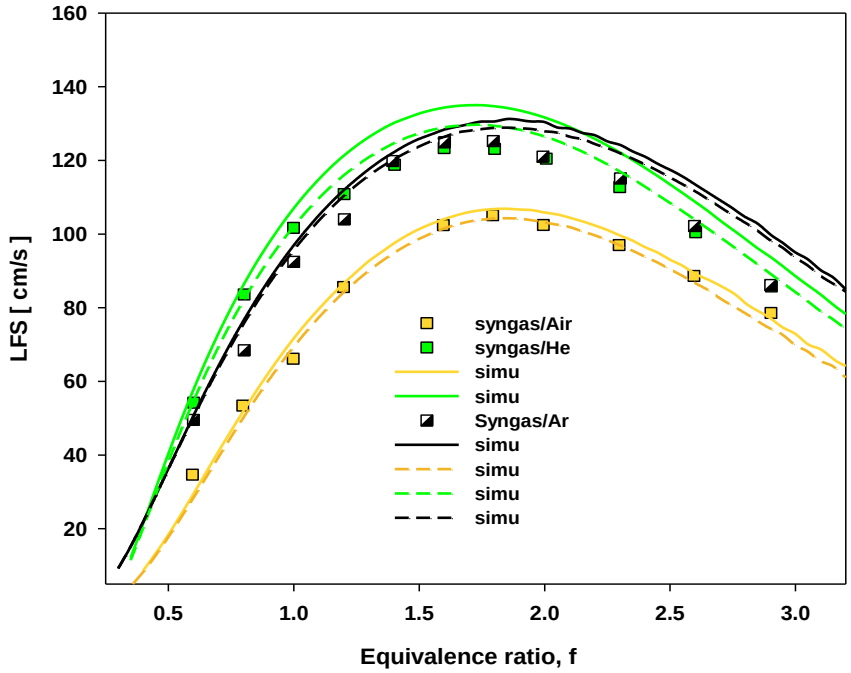

Figure S2.7: Laminar flame speed comparison of syngas / air, syngas /O_2/Ar and syngas /O_2/He at 1 bar and 298 K. syngas composition: H_2/CO/N_2/CO_2(33.55/40.26/13.20/12.99) %, O_2/ Ar ratio: 1/3.76, O_2/He ratio: 1/6. Symbols measurements from [40].

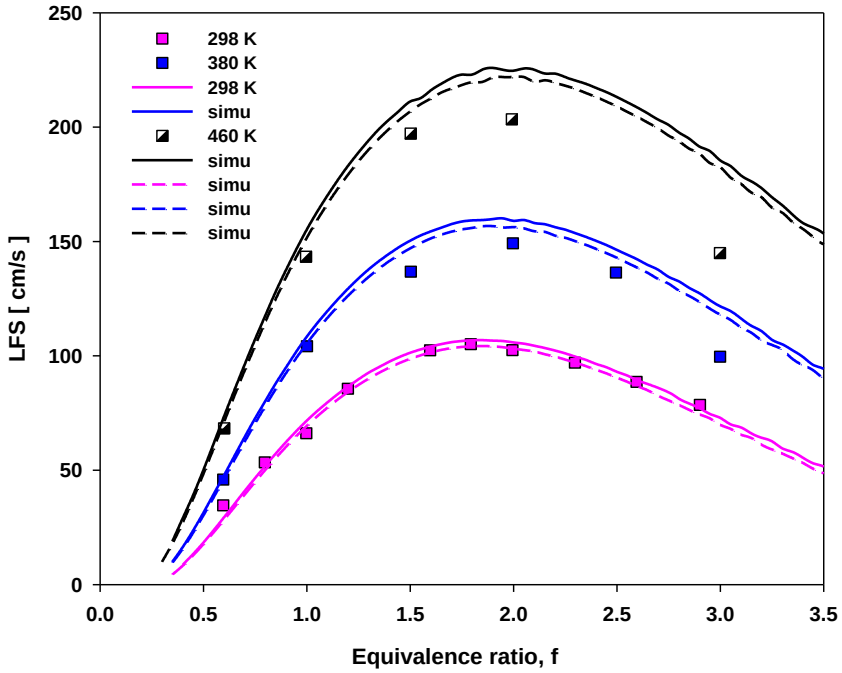

Figure S2.8: Laminar flame speed comparison of syngas / air at 1 bar and 298, 380, 460 K. Syngas composition: H_2/CO/N_2/CO_2 (33.55/40.26/13.20/12.99) %. Symbols measurements from [40].

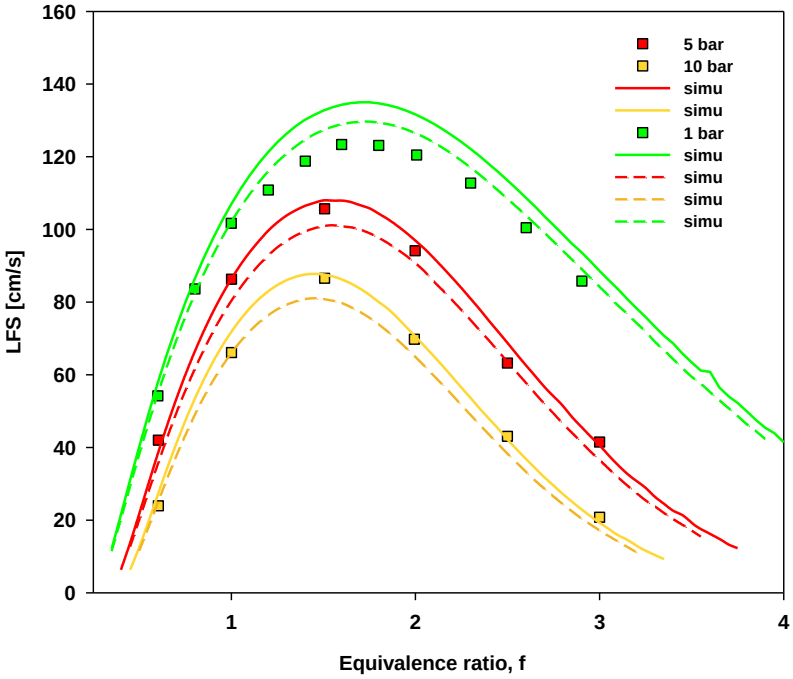

Figure S2.9: Laminar flame speed comparison of syngas/O_2/He at 298 K and 1, 5, 10 bar. Syngas composition: H_2/CO/N_2/CO_2 (33.55/40.26/13.20/12.99) %. O_2/He ratio: 1/6. Symbols measurements from [40].

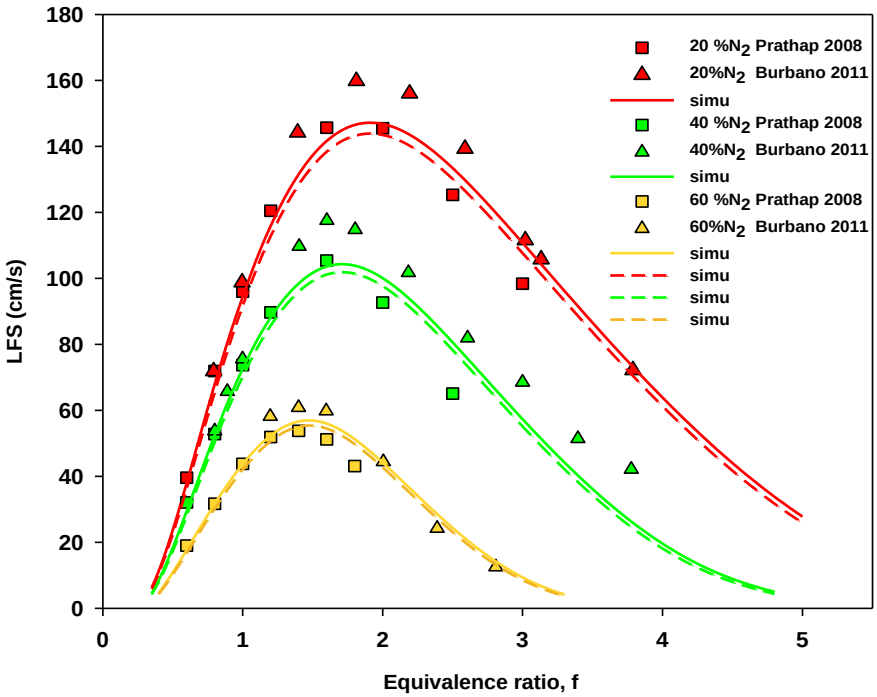

Figure S2.10: Laminar flame speed comparison of equimolar H_2/CO at different N_2 dilution at 1 bar and 302 K with air. Symbols measurements: filled squares [41] and filled triangles [42].

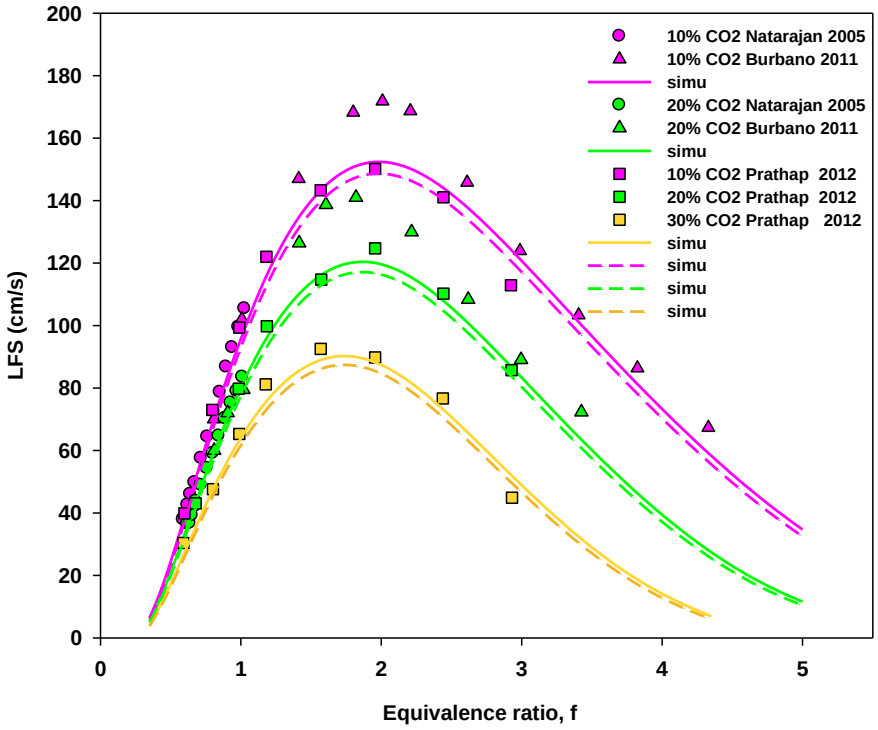

Figure S2.11: Laminar flame speed comparison of equimolar H_2/CO at different CO_2 dilution at 1 bar and 302 K with air. Symbols measurements: filled circles [43], filled triangles [42] and filled squares [44].

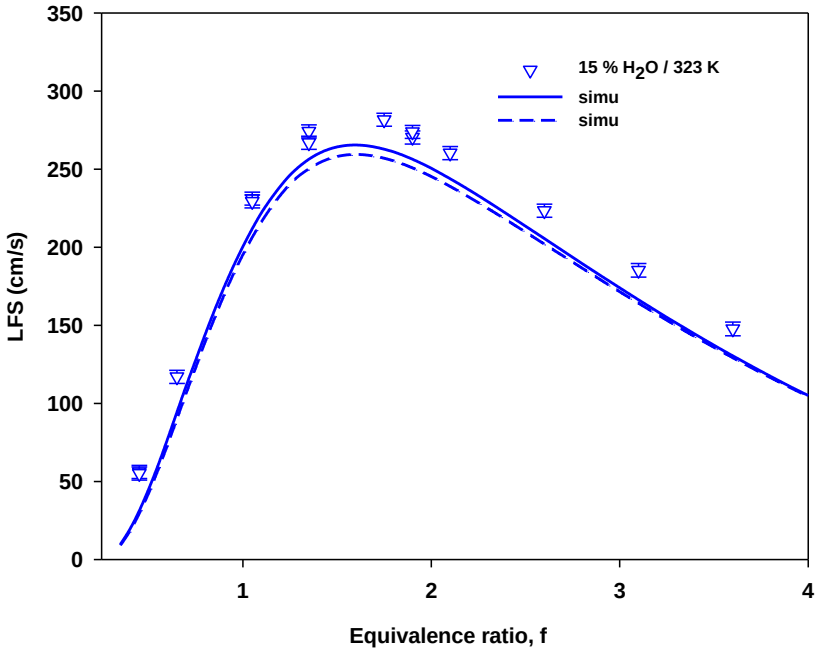

Figure S2.12: Laminar flame speed comparison of H_2 /H_2O –air mixture with 15 % H_2O dilution at 1 atm and 323 K. Symbols measurements from [35].

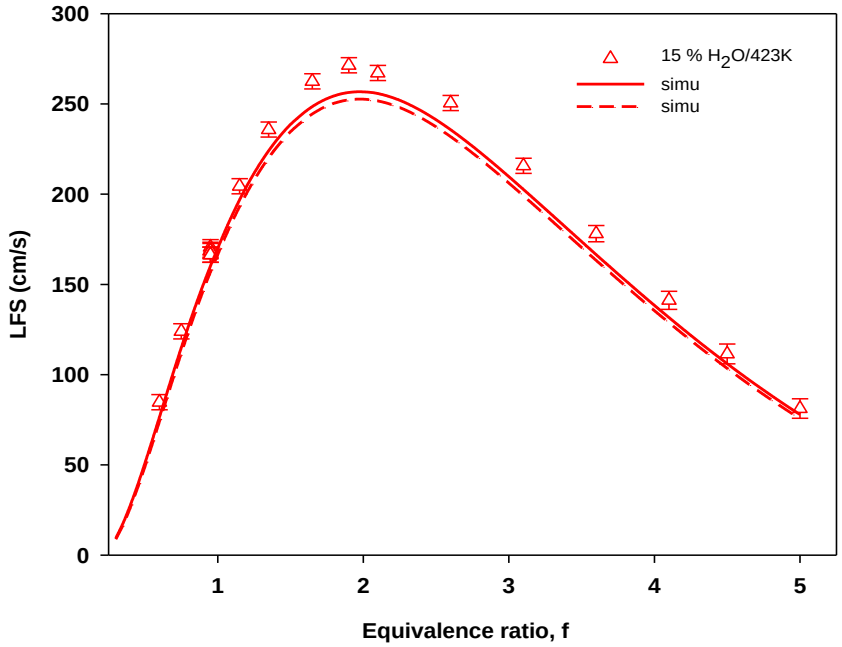

Figure S2.13: Laminar flame speed comparison of H_2 /CO(50/50)/H_2O –air mixture with 15 % H_2O dilution at 1 atm and 423 K. Symbols measurements from [35].

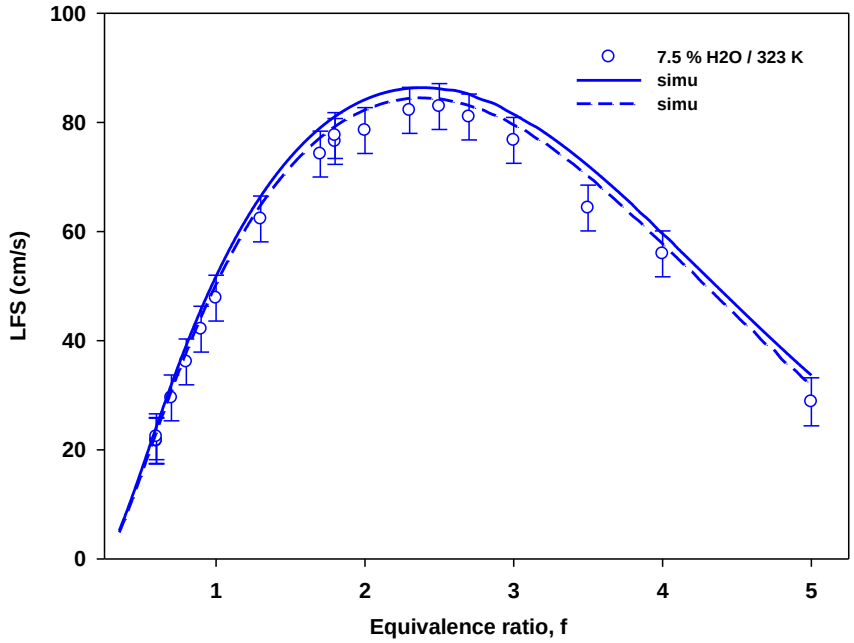

Figure S2.14: Laminar flame speed comparison of H_2 / CO(5/95) /H_2O – air mixture with 7.5 % H_2O dilution at 1 atm and 323 K. Symbols measurements from [35].

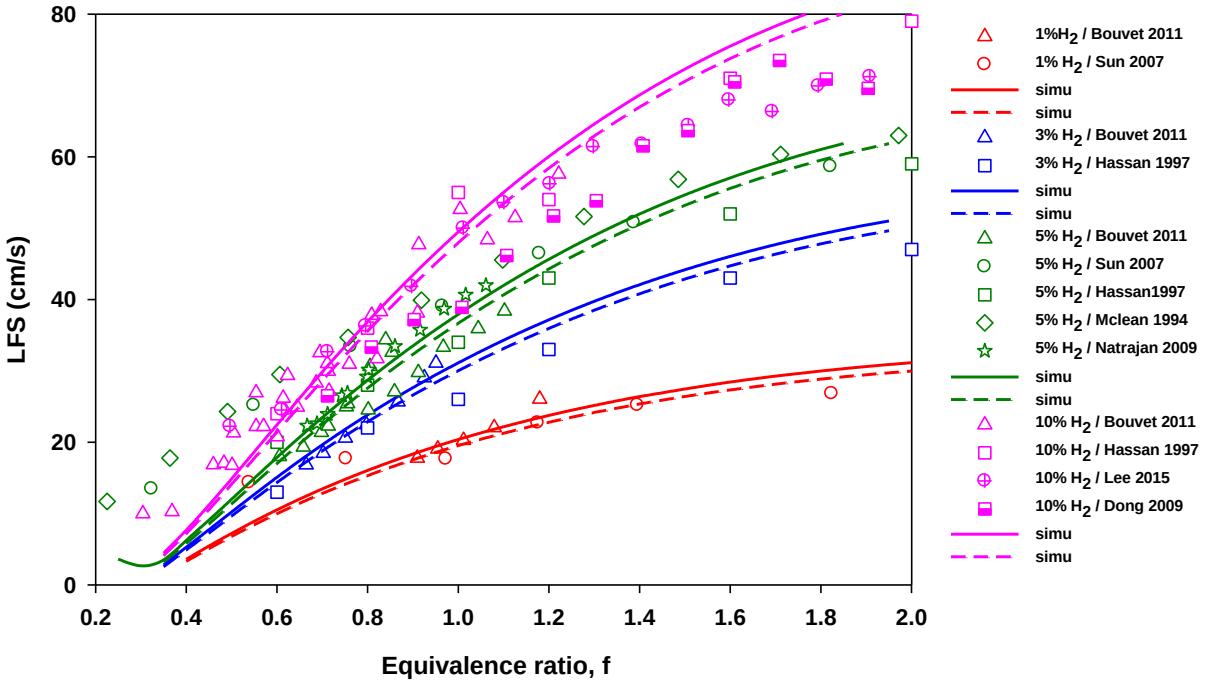

Figure S2.15: Laminar flame speed comparison of H_2 /CO-air mixture at 1 atm and 298 K for H_2 composition 1, 3, 5 and 10 % in fuel mixture. Symbols measurements: open circle [17], open triangle [45], open square [37], open diamond [46], open star [38] , crossed circle [47] and half-filled square [48].

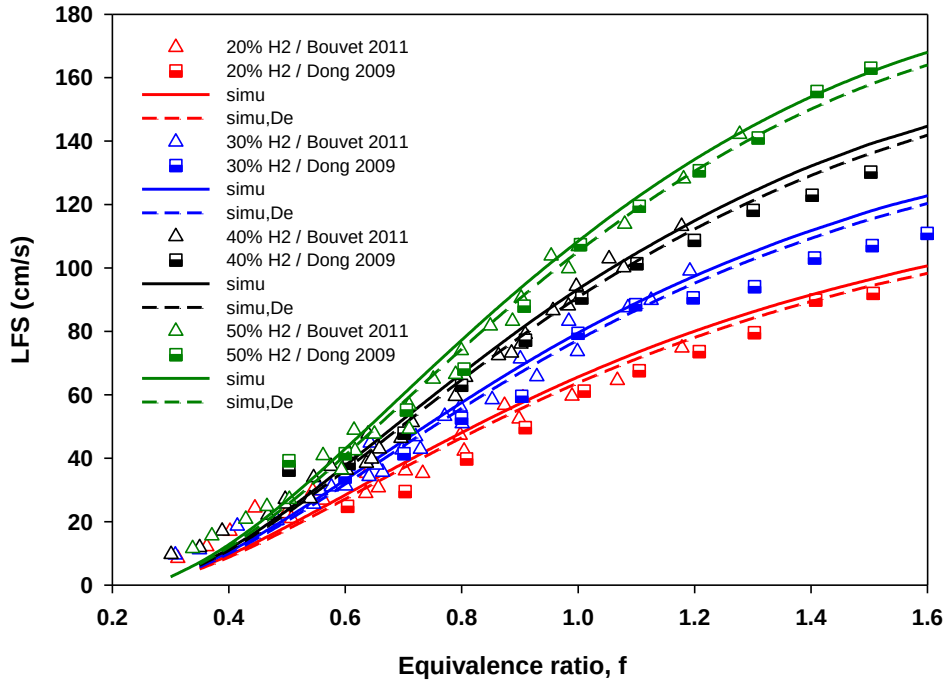

Figure S2.16: Laminar flame speed comparison of H_2 /CO-air mixture at 1 atm and 298 K for H_2 composition 20, 30, 40 and 50 % in fuel mixture. Symbols measurements: open triangle [45] and half-filled square [48].

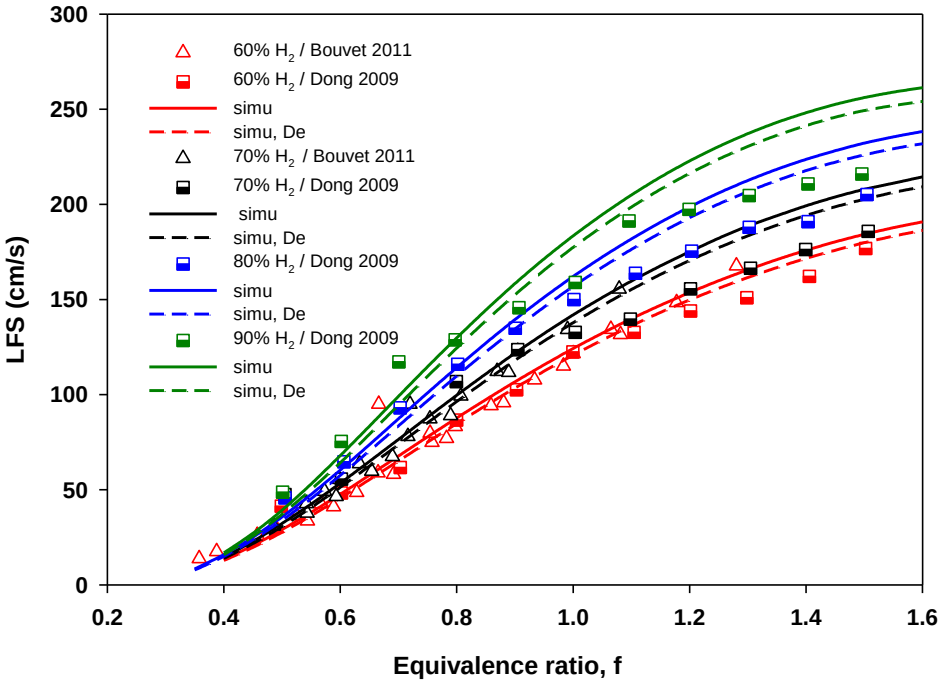

Figure S2.17: Laminar flame speed comparison of H_2 /CO-air mixture at 1 atm and 298 K for H_2 composition 60, 70, 80 and 90 % in fuel mixture. Symbols measurements: open triangle [45] and half-filled circle [48].

2.2 Burner Stabilized Flame

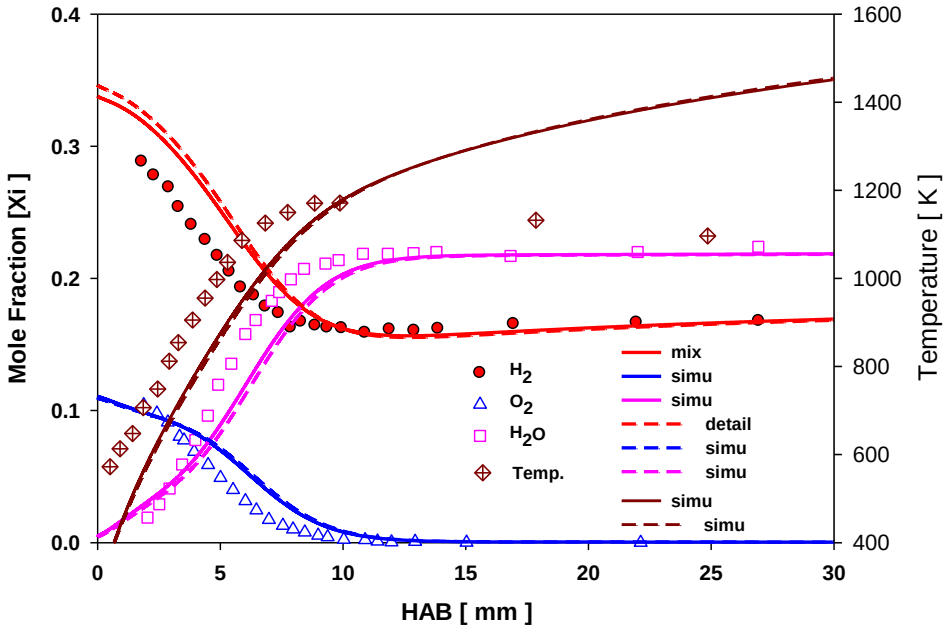

Figure S2.18: Comparison between model prediction and measurements for $H_2/O_2/Ar$ flame at 4.75kpa and 298 K. Symbols :measurements from [49] see Table III mixture 1 for initial condition and mixture composition. Lines: prediction without using the experimental temperature profile. Same condition and legend information applies to figure S2.19 to S2.21.

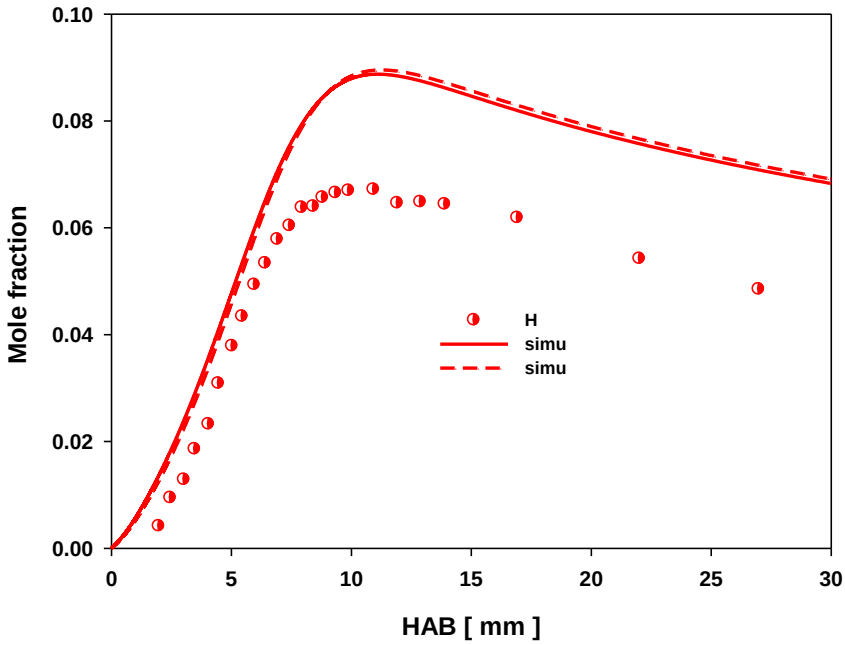

Figure S2.19: Comparison between model prediction and measurements for H radical. Symbols measurements from [49]. See Figure S2.18 for initial condition.

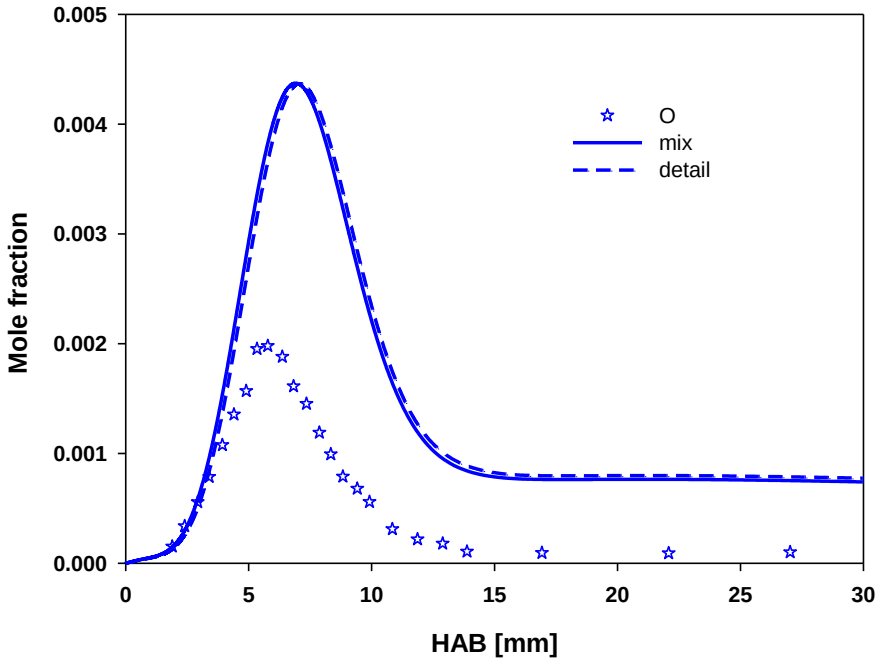

Figure S2.20: Comparison between model prediction and measurements for O radical. Symbols measurements from [49]. See Figure S2.18 for initial condition.

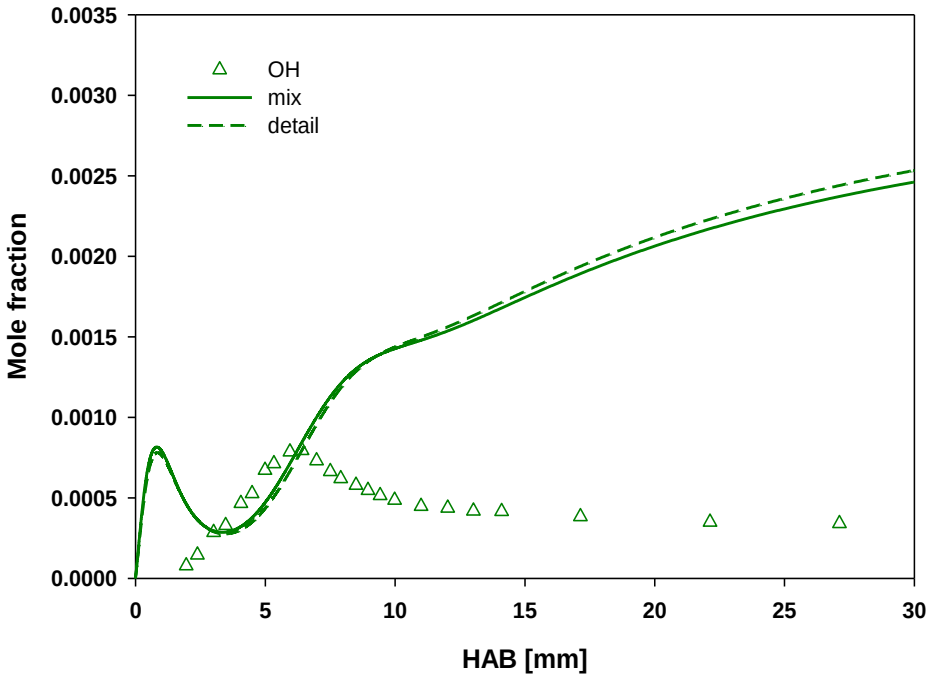

Figure S2.21: Comparison between model prediction and measurements for OH radical. Symbols measurements from [49]. See Figure S2.18 for initial condition.

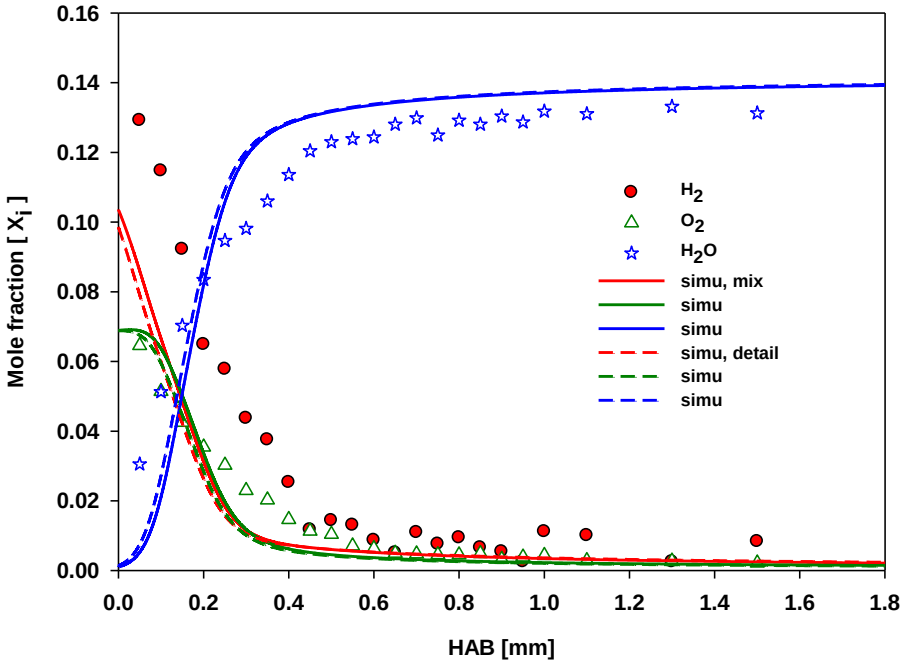

Figure S2.22: Comparison between model prediction and measurements for H_2/O_2/Ar flame at 3 atm and 333 K. Symbols :measurements from [50] see Table III mixture 5 for initial condition and mixture composition. Lines: prediction without using the experimental temperature profile. Same condition and legend information applies to figure S2.23 to S2.26.

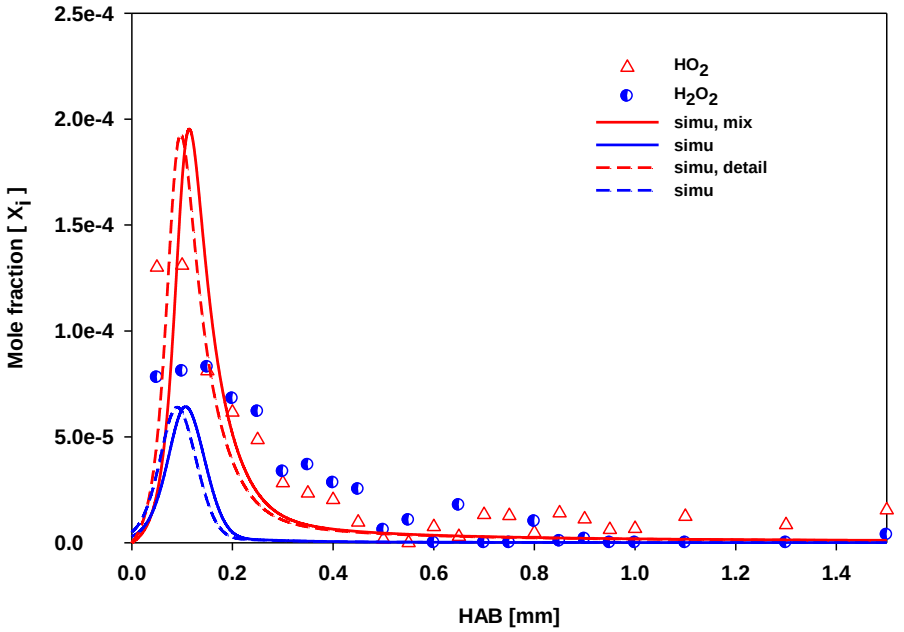

Figure S2.23: Comparison between model prediction and measurements for HO_2 and H_2O_2. Symbols measurements from [50]. See Figure S2.22 for initial condition.

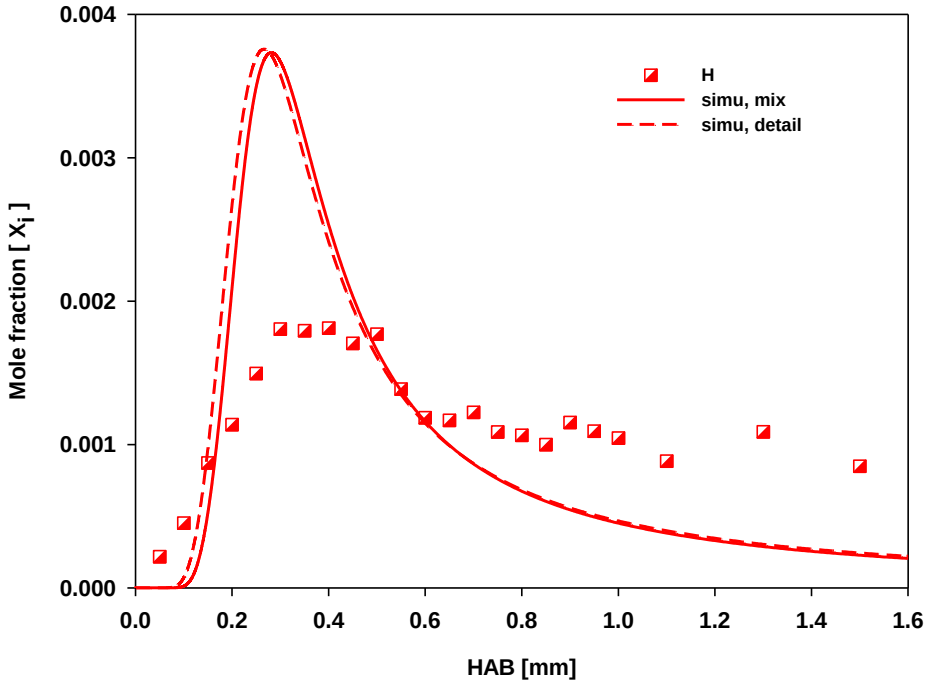

Figure S2.24: Comparison between model prediction and measurements for H radical. Symbols measurements from [50]. See Figure S2.22 for initial condition.

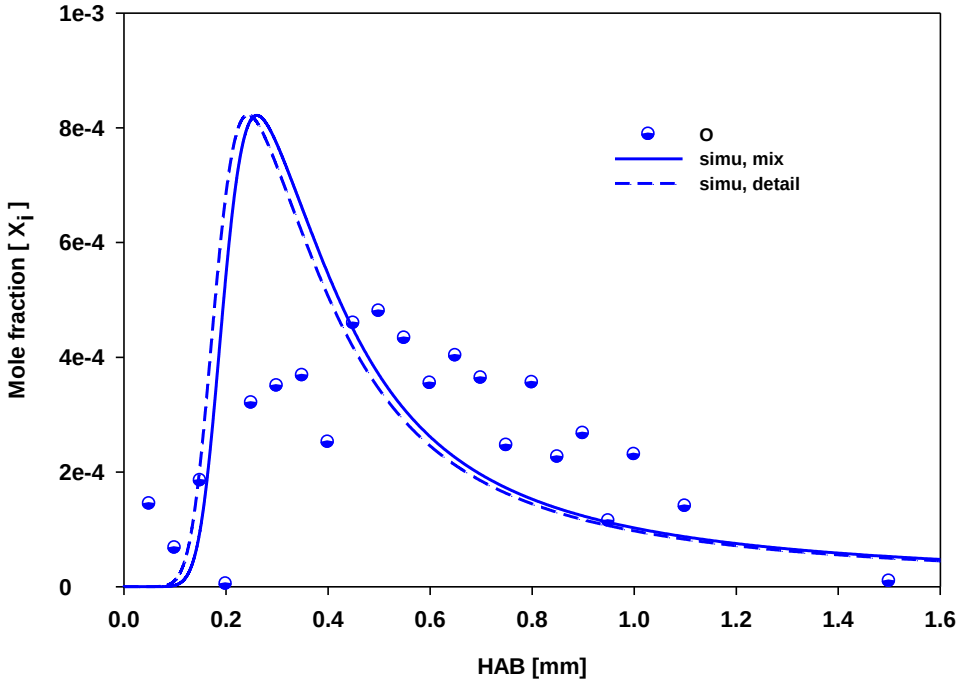

Figure S2.25: Comparison between model prediction and measurements for O radical. Symbols measurements from [50]. See Figure S2.22 for initial condition.

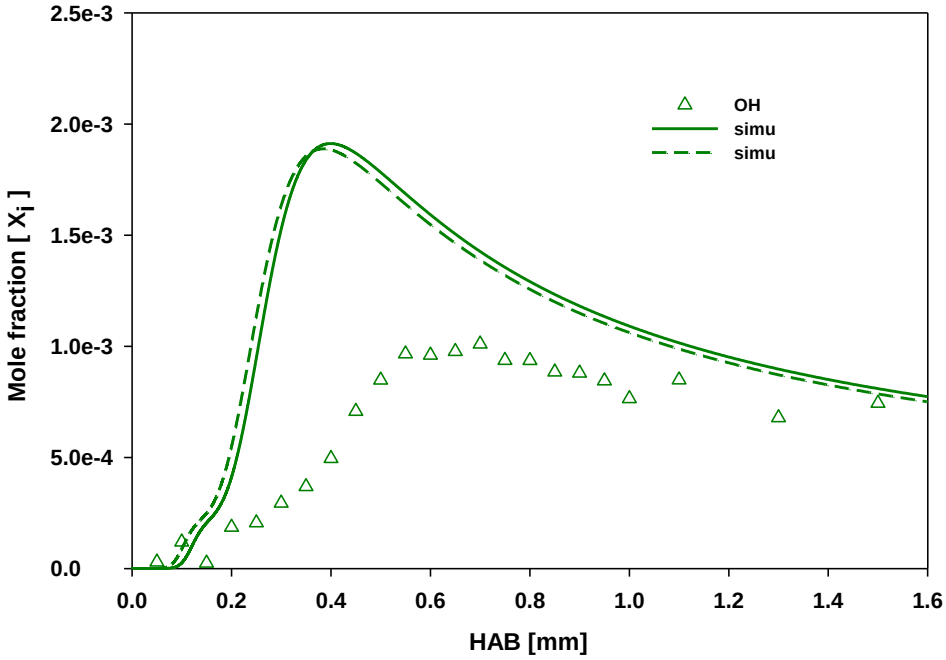

Figure S2.26: Comparison between model prediction and measurements for OH radical. Symbols measurements from [50]. See Figure S2.22 for initial condition.

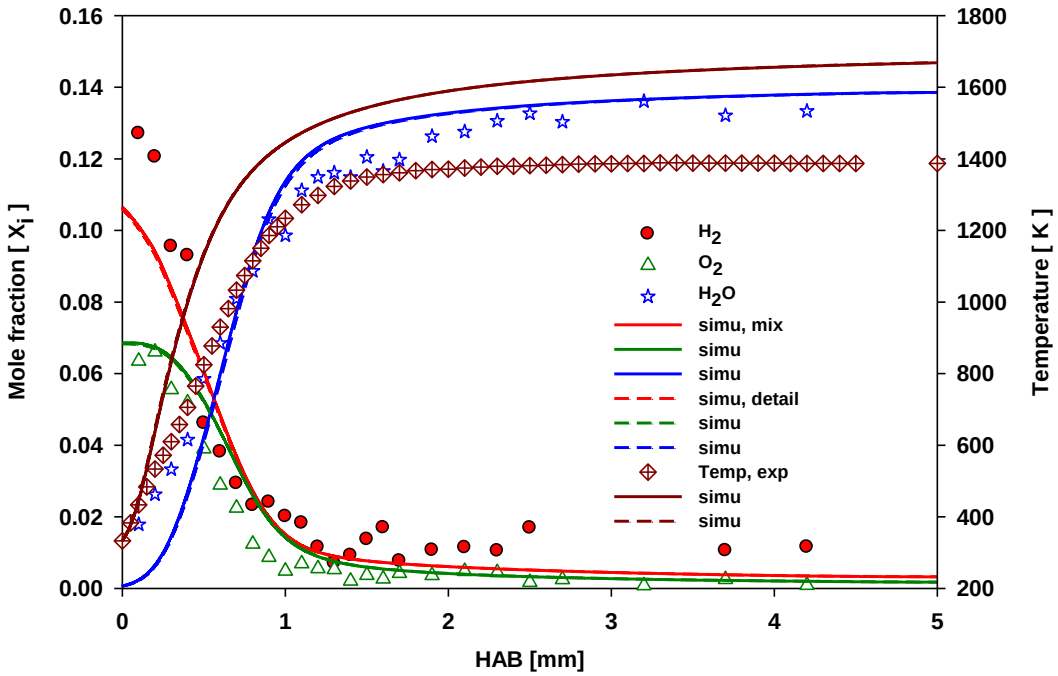

Figure S2.27: Comparison between model prediction and measurements for H_2/O_2/Ar flame at 1 atm and 333 K. Symbols :measurements from [50] see Table III, mixture 5 for initial condition and mixture composition. Lines: prediction using the experimental temperature profile. Same initial condition and legend information applies to figure S2.28 to S2.31.

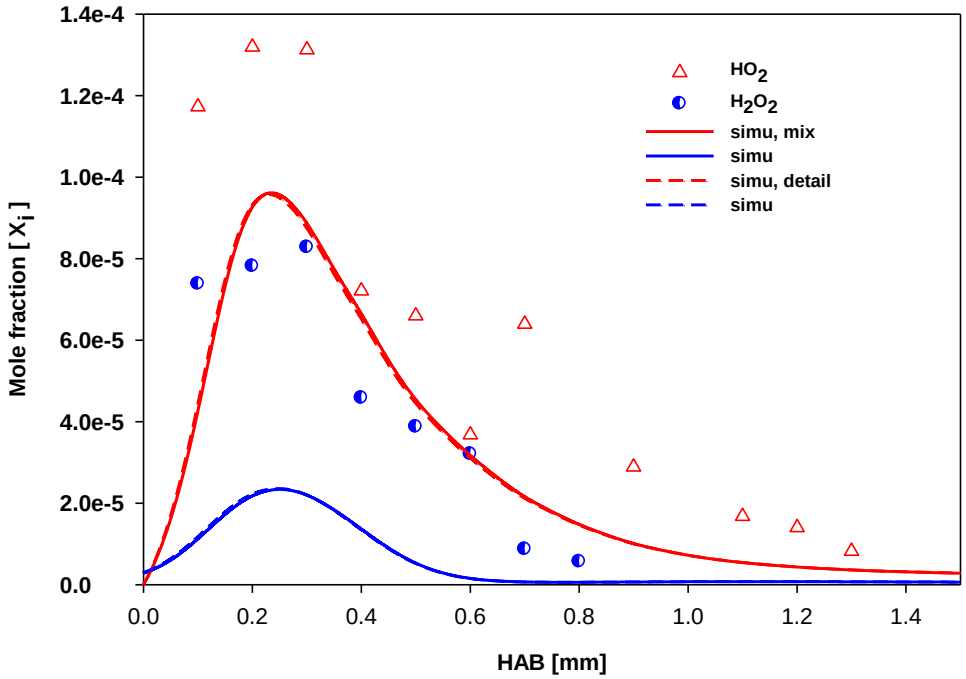

Figure S2.28: Comparison between model prediction and measurements for HO_2 and H_2O_2. Symbols measurements from [50]. See Figure S2.27 for initial condition.

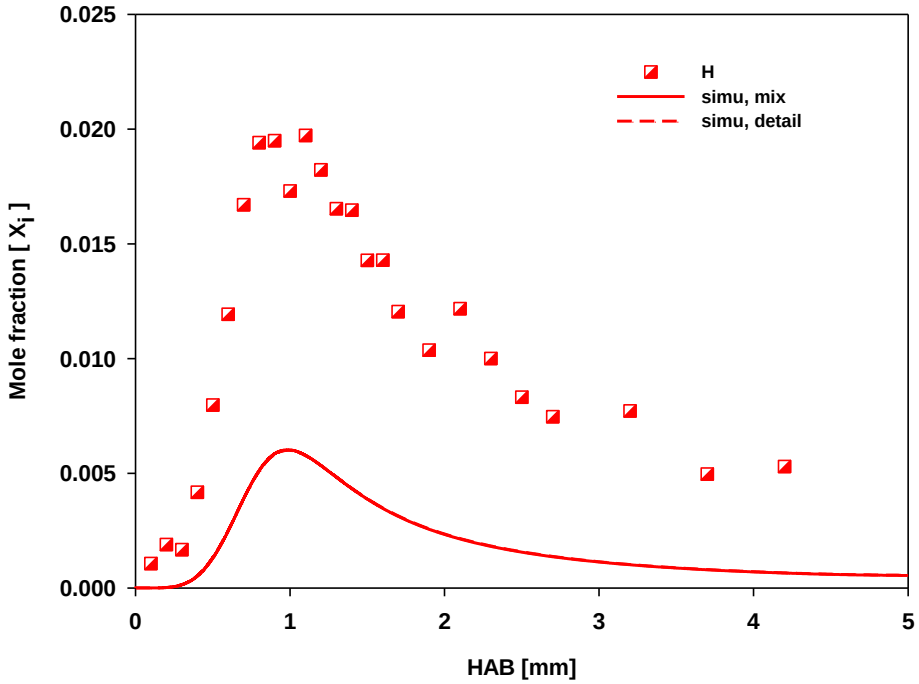

Figure S2.29: Comparison between model prediction and measurements for H radical. Symbols measurements from [50]. See Figure S2.27 for initial condition.

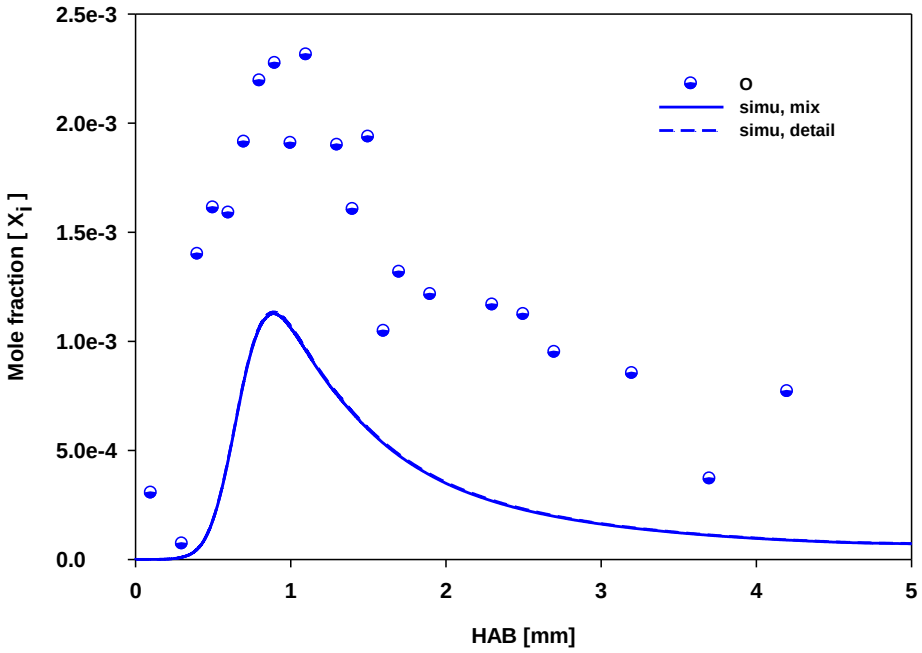

Figure S2.30: Comparison between model prediction and measurements for O radical. Symbols measurements from [50]. See Figure S2.27 for initial condition.

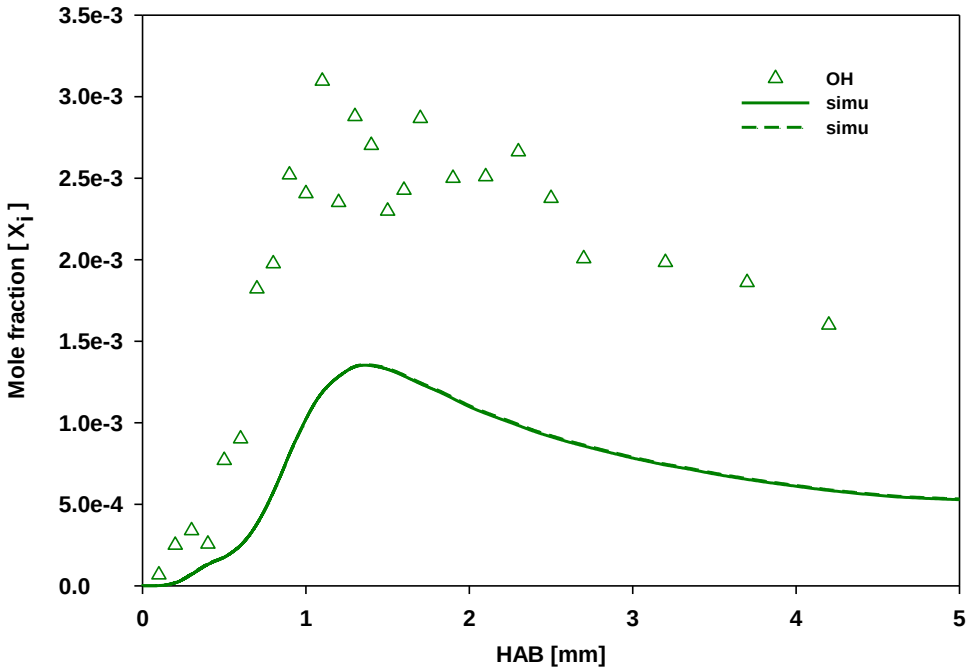

Figure S2.31: Comparison between model prediction and measurements for OH radical. Symbols measurements from [50]. See Figure S2.27 for initial condition.

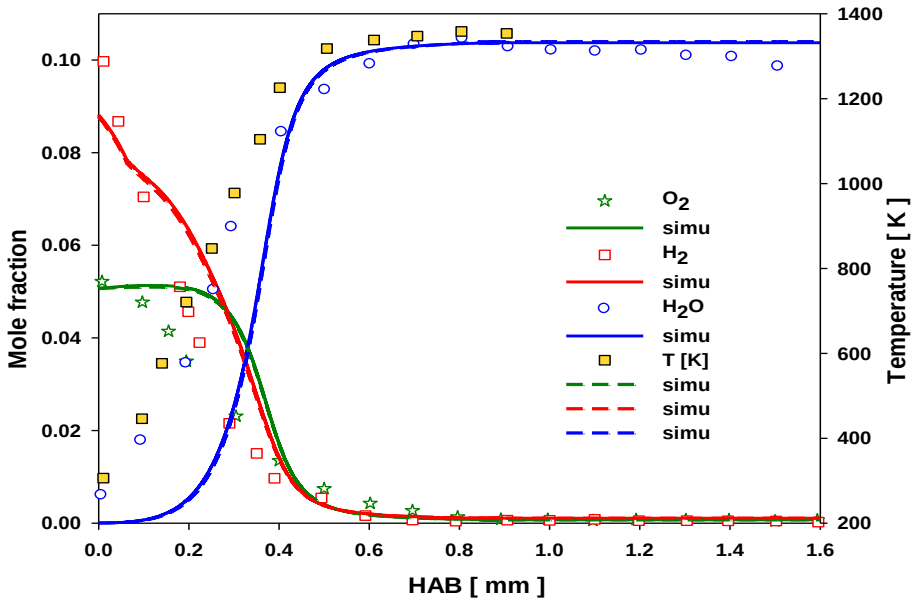

Figure 2.32: Comparison between model prediction and measurements for $H_2/O_2/Ar$ flame at 10 atm and 363 K. Symbols: measurements from [51] see Table III, mixture 4 for initial condition and mixture composition. Lines: prediction using the experimental temperature profile.

2.3 Ignition Delay (Shock Tube)

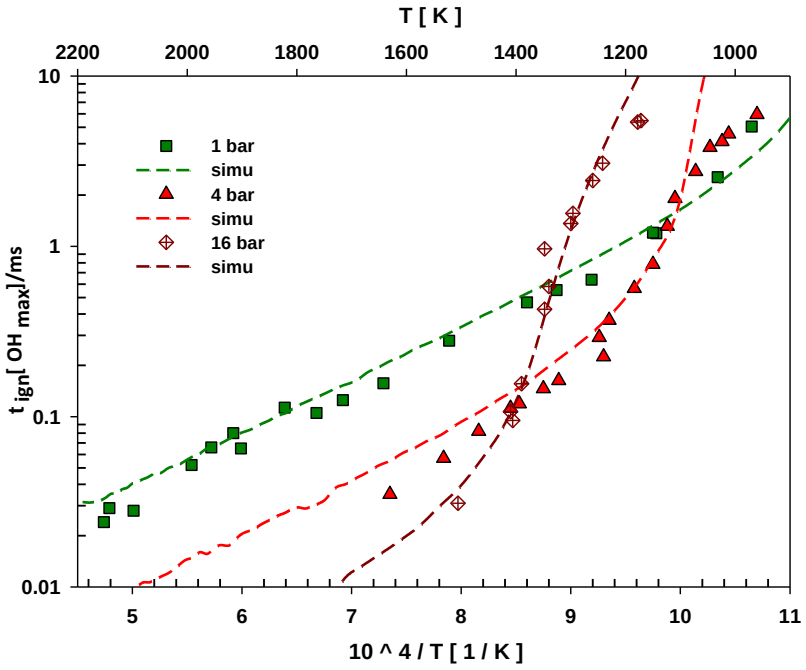

Figure S2.33: Comparison between model prediction and measurements for $H_2/O_2/Ar$ ignition delay time. Lines : model prediction; Symbols meaurments from [3] , see Table IV , mixture 1 for experimental condition.

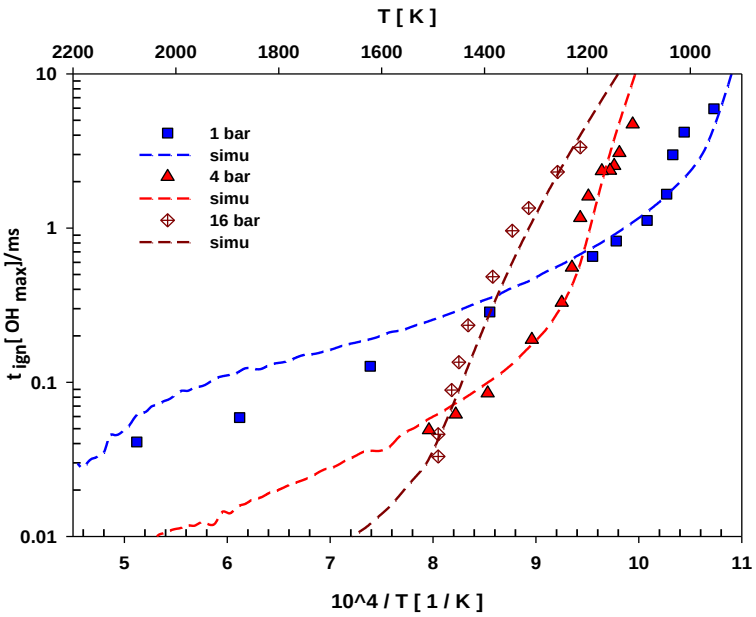

Figure S2.34: Comparison between model prediction and measurements for $H_2/O_2/N_2$ ignition delay time. Lines : model prediction; Symbols meaurments from [3] , see Table IV , mixture 2 for experimental condition.

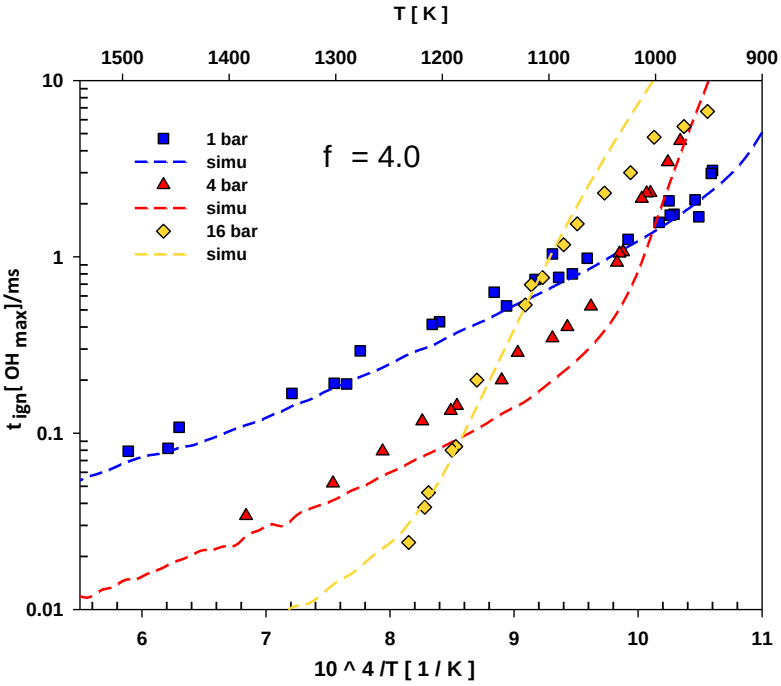

Figure S2.35: Comparison between model prediction and measurements for $H_2/O_2/Ar$ ignition delay time. Lines : model prediction; Symbols meaurments from [3] , see Table IV , mixture 3 for experimental condition.

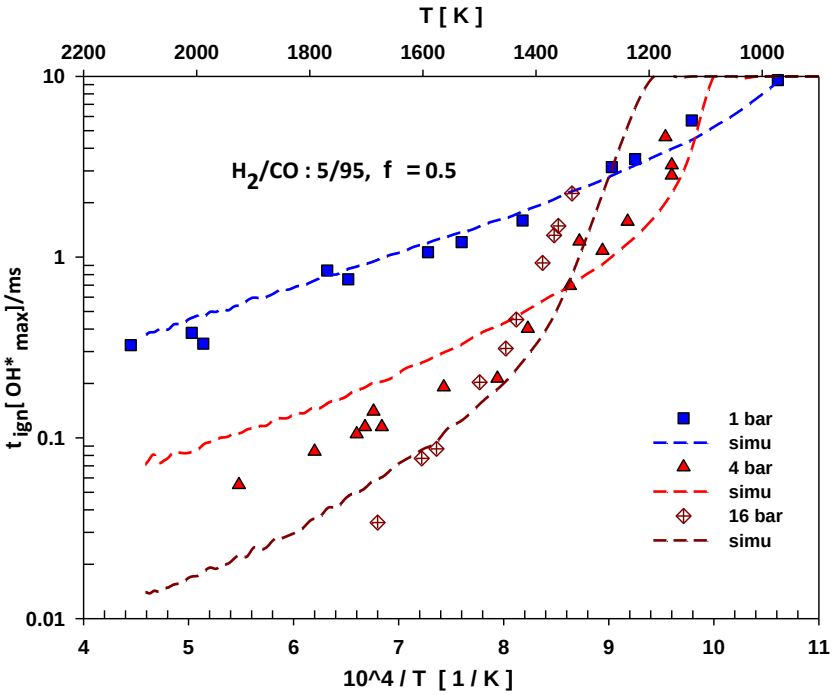

Figure S2.36: Comparison between model prediction and measurements for H_2/CO (5/95)-O_2/Ar ignition delay time. Lines : model prediction; Symbols meaurments from [3] , see Table IV , mixture 12 for experimental condition.

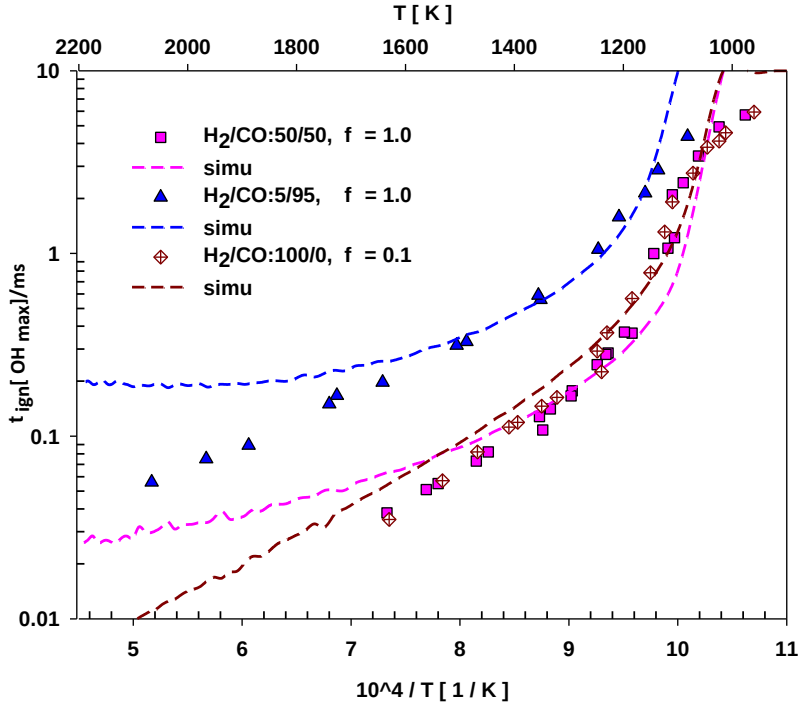

Figure S2.37: Comparison between model prediction and measurements for H_2/CO -O_2/Ar ignition delay time at 4 bar. Lines : model prediction; Symbols meaurments from [3] , see Table IV , mixture 13(H_2/CO:50/50), mixture 14 (H_2/CO:5/95) and mixture 1(H_2) for experimental condition

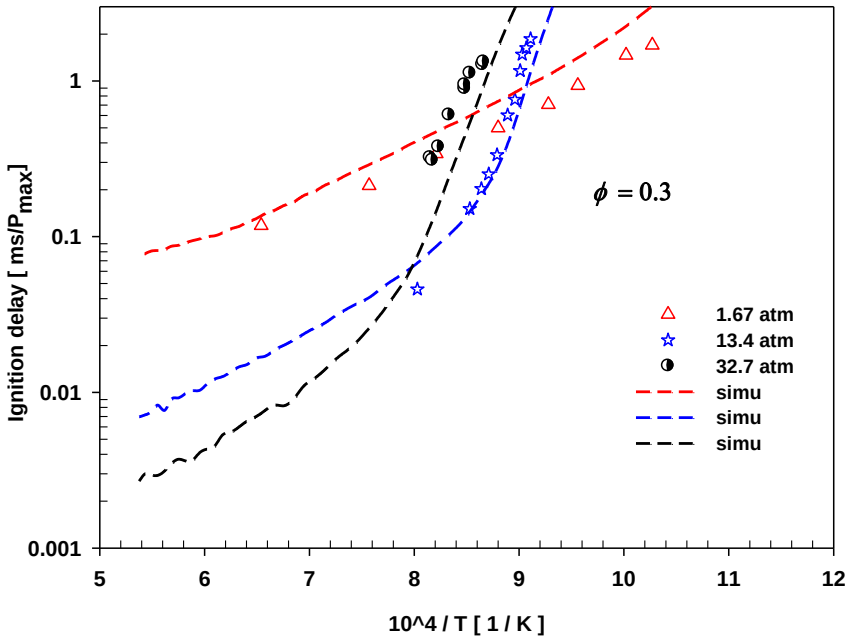

Figure S2.38: Comparison between model prediction and measurements for $H_2/O_2/Ar$ ignition delay time. Lines : model prediction; Symbols meaurments from [3], see Table IV , mixture 15 for experimental condition.

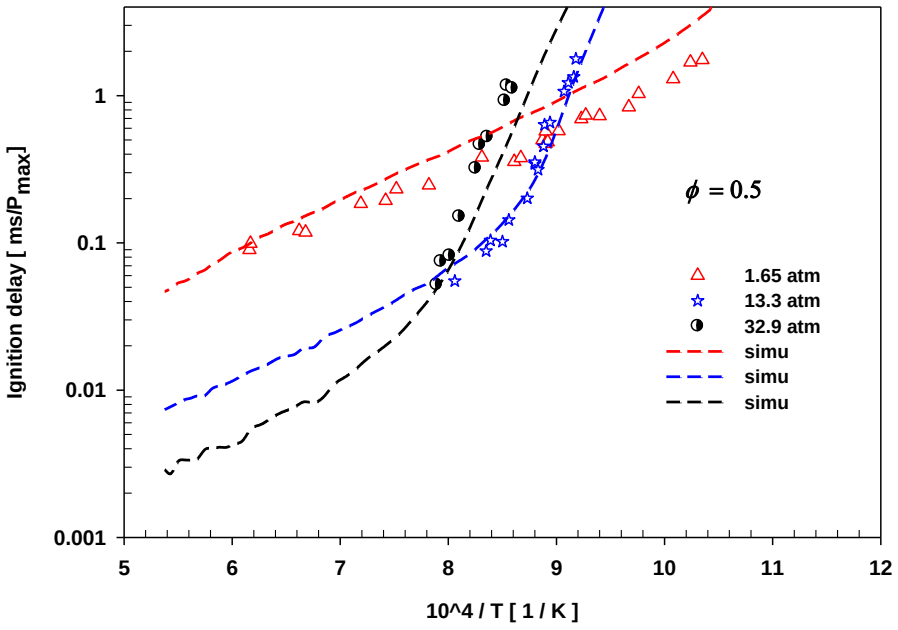

Figure S2.39: Comparison between model prediction and measurements for $H_2/O_2/Ar$ ignition delay time. Lines : model prediction; Symbols meaurments from [3], see Table IV , mixture 16 for experimental condition.

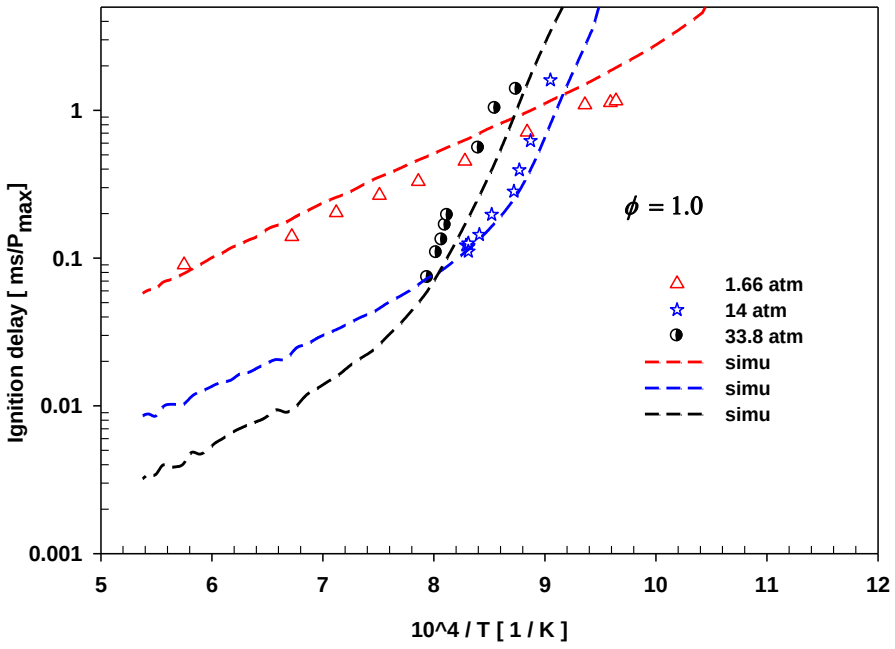

Figure S2.40: Comparison between model prediction and measurements for $H_2/O_2/Ar$ ignition delay time. Lines : model prediction; Symbols meaurments from [3], see Table IV , mixture 17 for experimental condition.

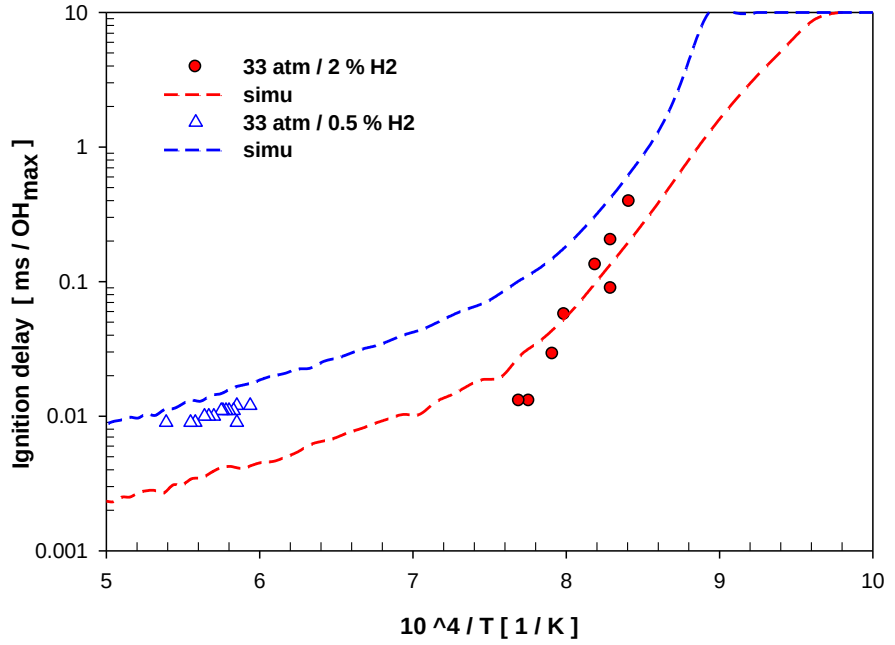

Figure S2.41: Comparison between model prediction and measurements of $H_2/O_2/Ar$ ignition delay at 33 atm. Lines: model prediction; Symbols: measurements from [52]. See Table IV, mixture 4 and 5 for initial condition.

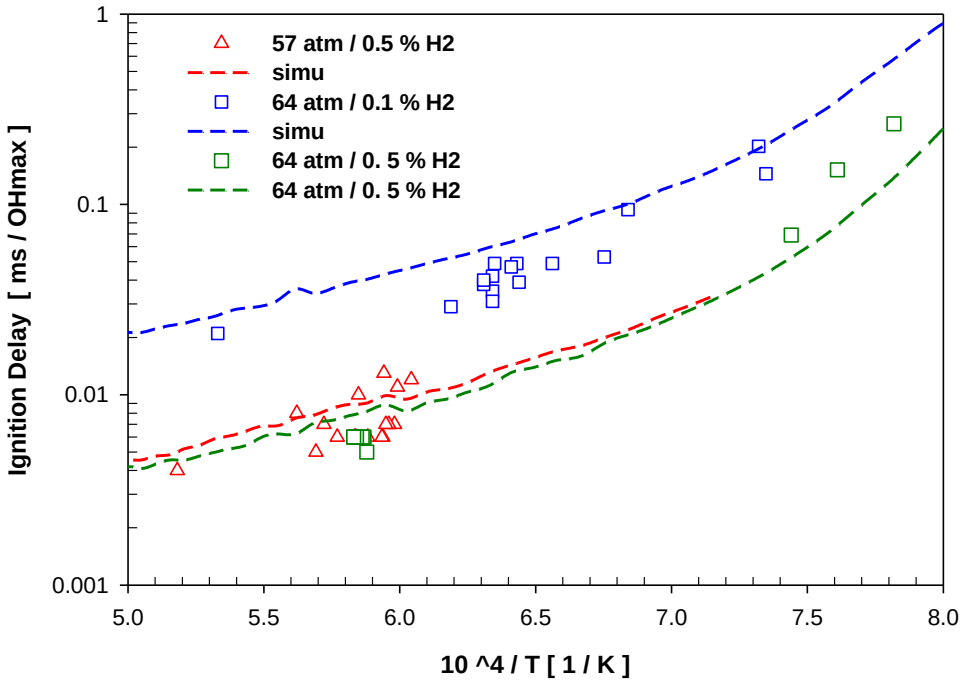

Figure S2.42: Comparison between model prediction and measurements of $H_2/O_2/Ar$ ignition delay at 57 and 64 atm. Lines: model prediction; Symbols: measurements from [52]. See Table IV, mixture 6, 7 and 8 for initial condition.

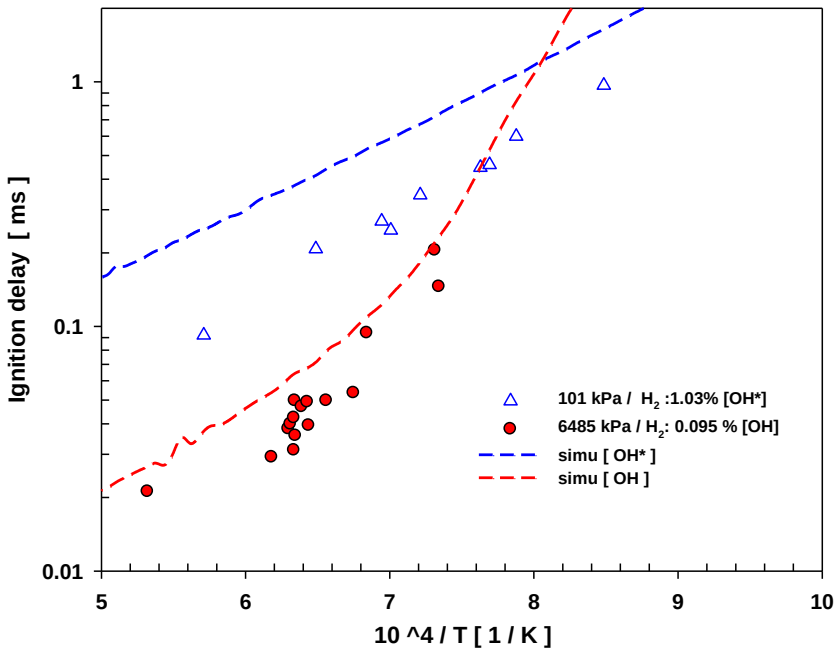

Figure S2.43: Comparison between model prediction and measurements of $H_2/O_2/Ar$ ignition delay at 101 kPa and 6485 kPa. Lines : model prediction; Symbols: measurements from [53]. See Table IV, Mixture 9 for initial condition.

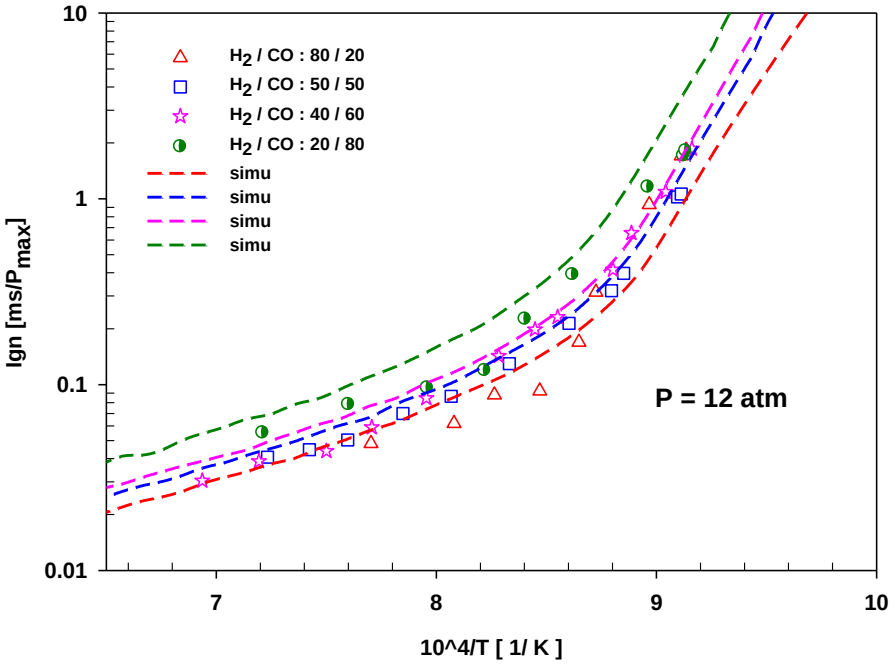

Figure S2.44: Comparison between model prediction and measurements for H_2/CO-O_2/Ar ignition delay time at different H_2/CO ratio, in 1 % O_2 and 98 % Ar at 12 atm. Lines : model prediction; Symbols meaurments from [33].

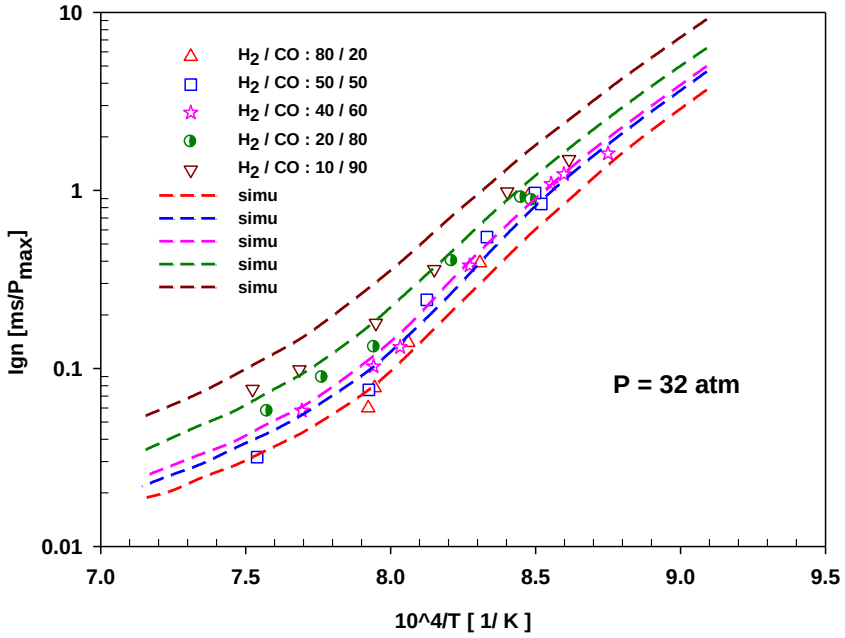

Figure S2.45: Comparison between model prediction and measurements for H_2/CO-O_2/Ar ignition delay time at different H_2/CO ratio, in 1 % O_2 and 98 % Ar at 32 atm. Lines : model prediction; Symbols: meaurments from [33].

2.4 Jet Stirred Reactor

Lines represents the model prediction from this work. Symbols represents the published experimental measurements. All the experimental data for JSR are extracted from the plots from the original paper. The initial mole fraction of the mixture are also taken from the graph to match the experimental work of respective group.

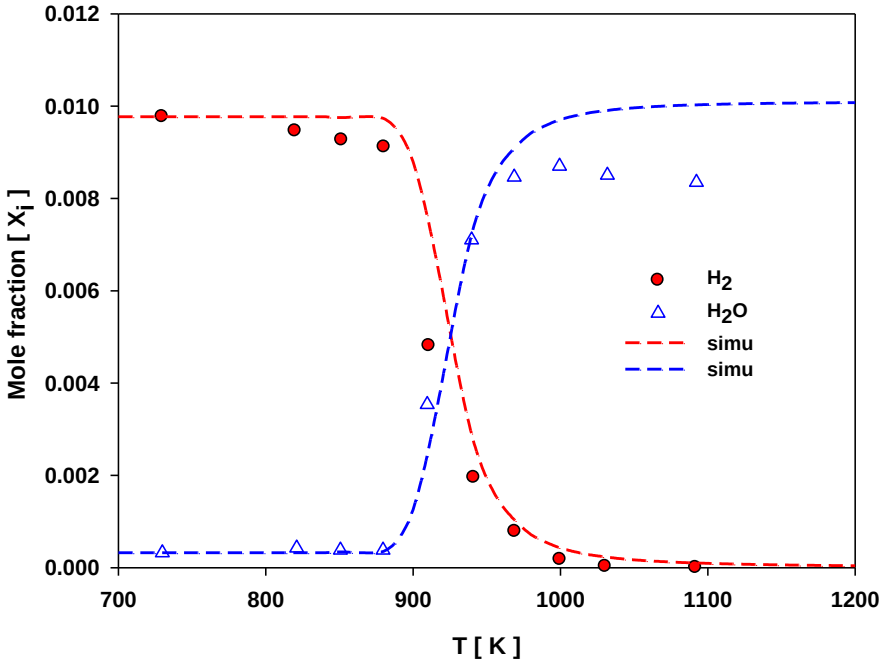

Figure S2.46: Comparison between model prediction and measurements for $H_2/O_2/N_2$ oxidation at 1atm, τ= 0.24 s and Ø=0.2. Symbols: measurements from [54]. See table V, Mixture 2 for initial condition and mixture composition.

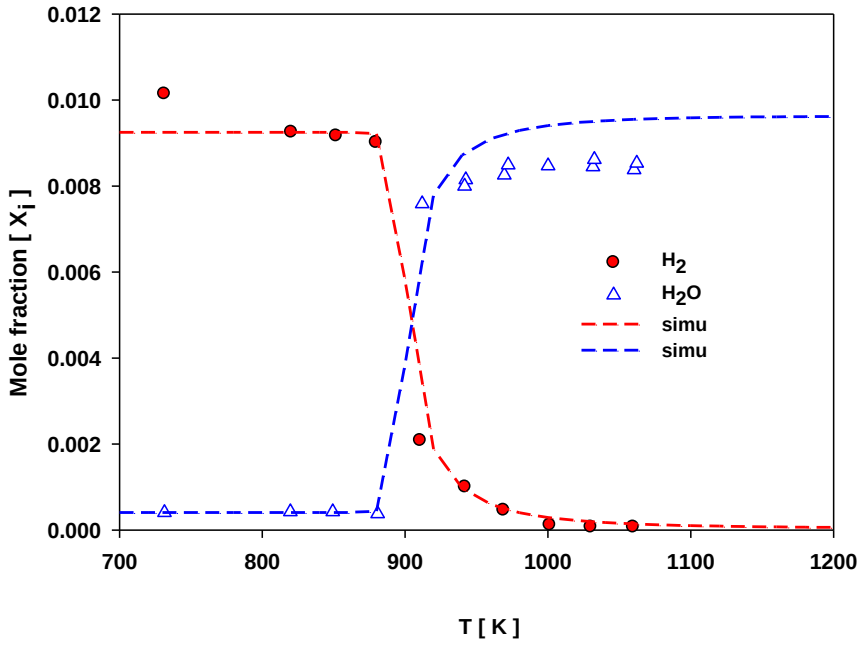

Figure S2.47: Comparison between model prediction and measurements for $H_2/O_2/N_2$ oxidation at 1atm, τ= 0.24 s and Ø=0.5. Symbols: measurements from [54]. See table V, Mixture 2 for initial condition and mixture composition.

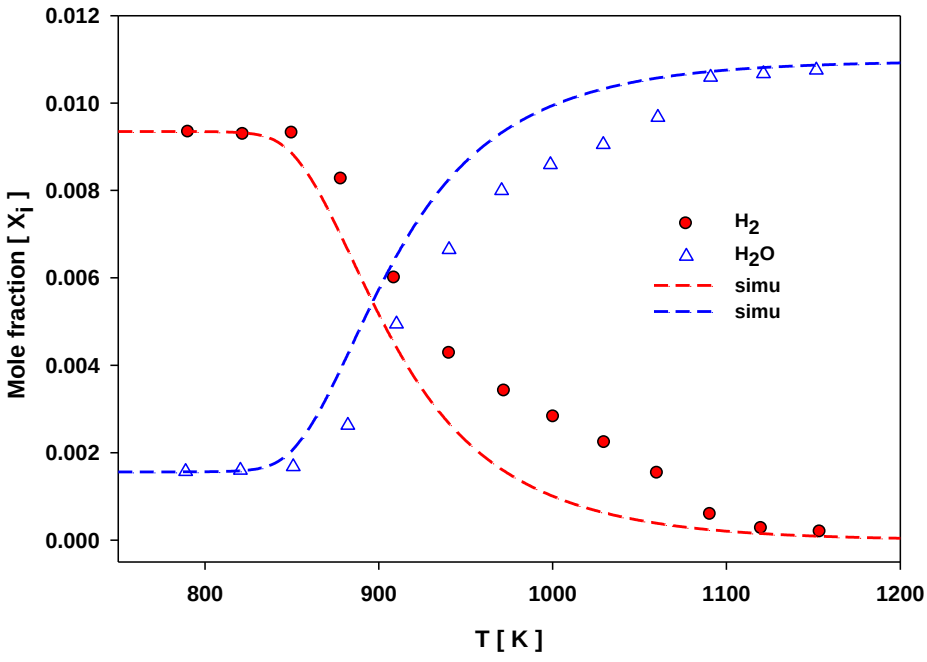

Figure S2.48: Comparison between model prediction and measurements for $H_2/O_2/N_2$ oxidation at 10atm, τ= 1.0 s and Ø=0.1. Symbols: measurements from [54]. See table V, Mixture 1 for initial condition and mixture composition.

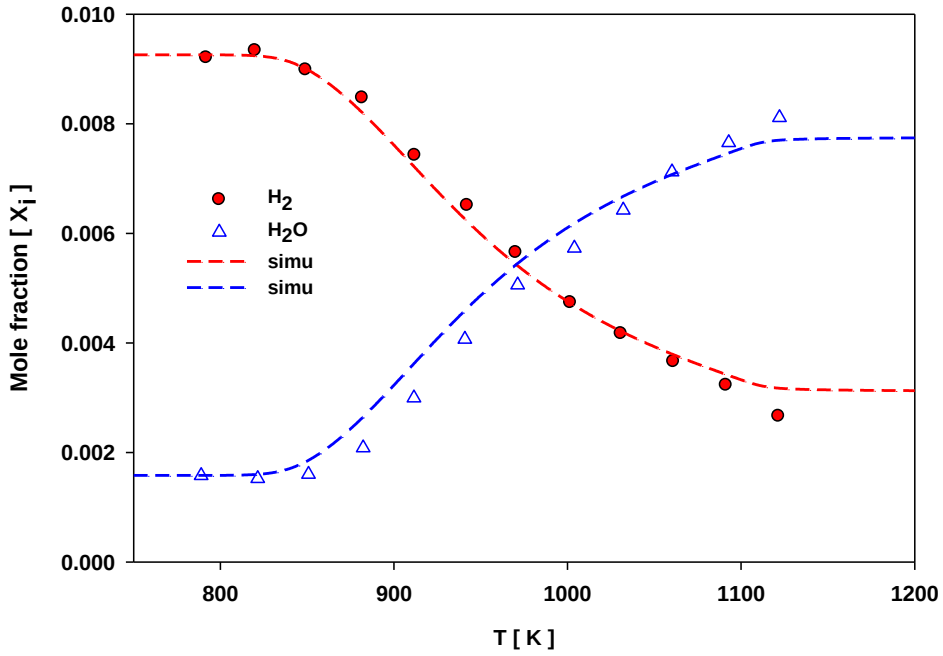

Figure S2.49: Comparison between model prediction and measurements for $H_2/O_2/N_2$ oxidation at 10atm, τ= 1.0 s and Ø=1.5. Symbols: measurements from [54]. See table V, Mixture 1 for initial condition and mixture composition.

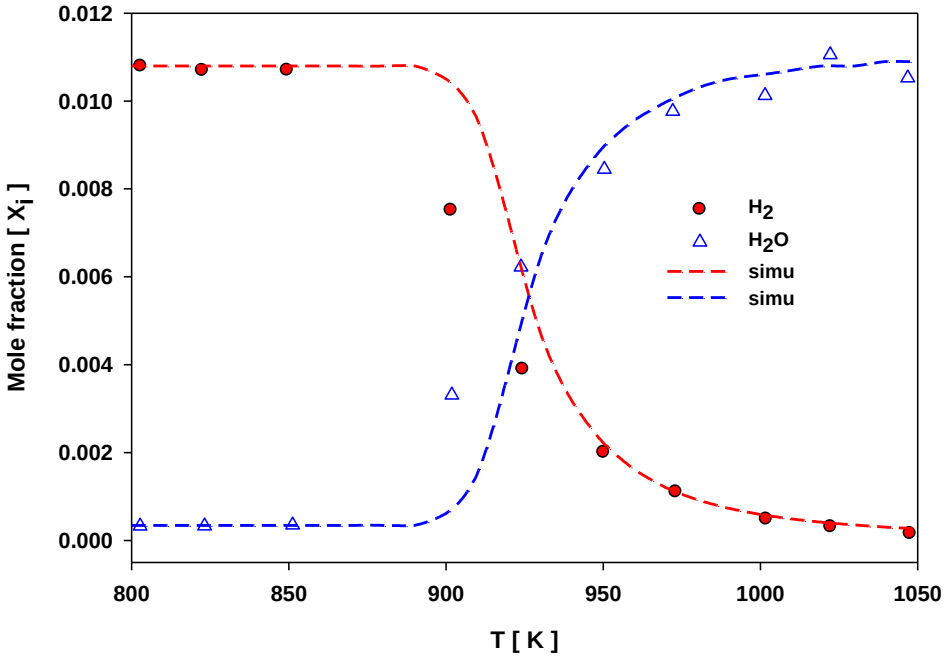

Figure S2.50: Comparison between model prediction and measurements for $H_2/O_2/N_2$ oxidation at 1atm, τ= 0.12 s and Ø=0.2. Symbols: measurements from [55]. See table V, Mixture 3 for initial condition and mixture composition.

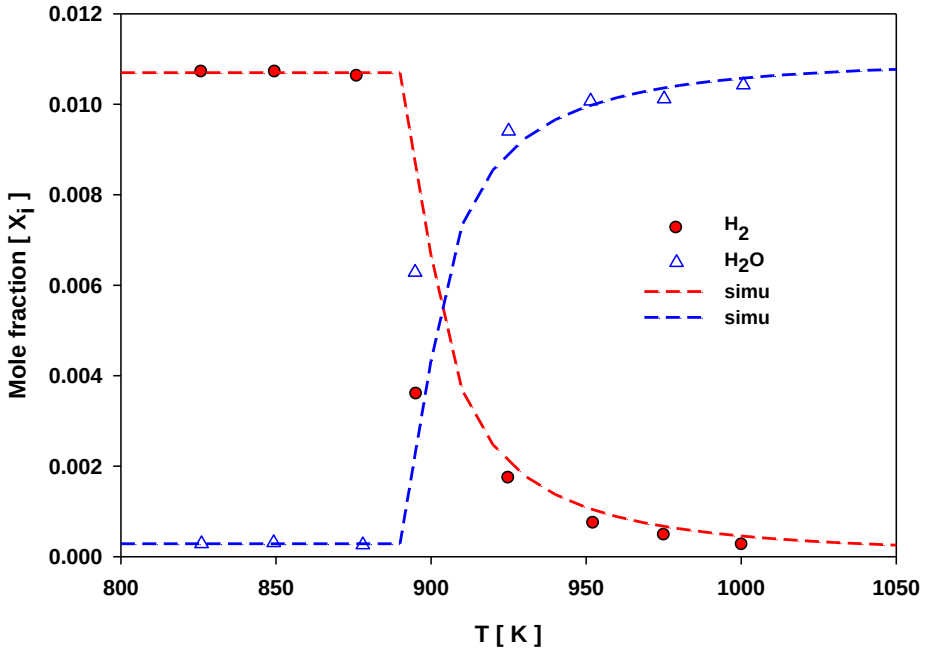

Figure S2.51: Comparison between model prediction and measurements for $H_2/O_2/N_2$ oxidation at 1atm, τ= 0.12 s and Ø=0.5. Symbols: measurements from [55]. See table V, Mixture 3 for initial condition and mixture composition.

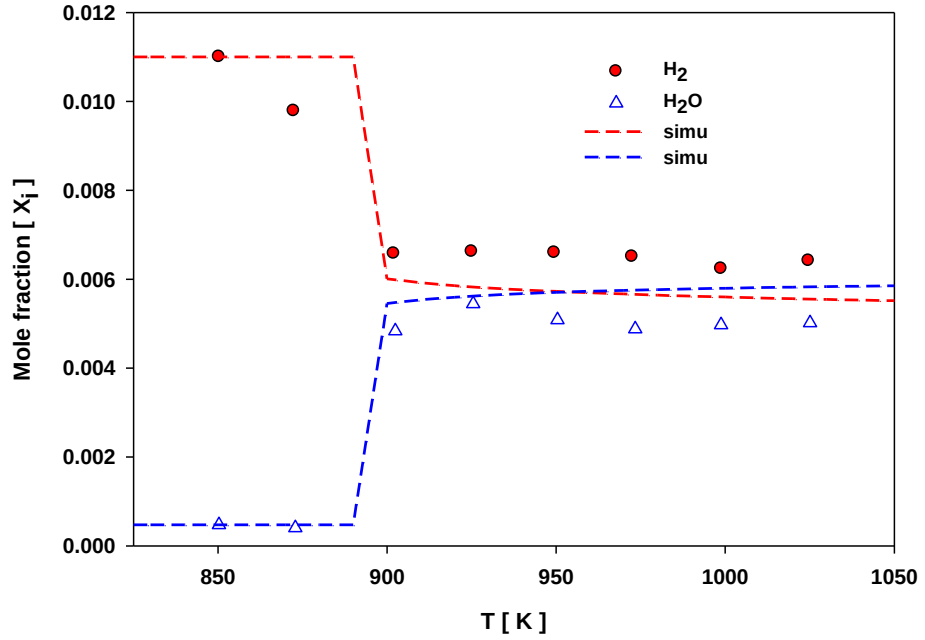

Figure S2.52: Comparison between model prediction and measurements for $H_2/O_2/N_2$ oxidation at 1atm, τ= 0.12 s and Ø=2.0. Symbols: measurements from [55]. See table V, Mixture 3 for initial condition and mixture composition.

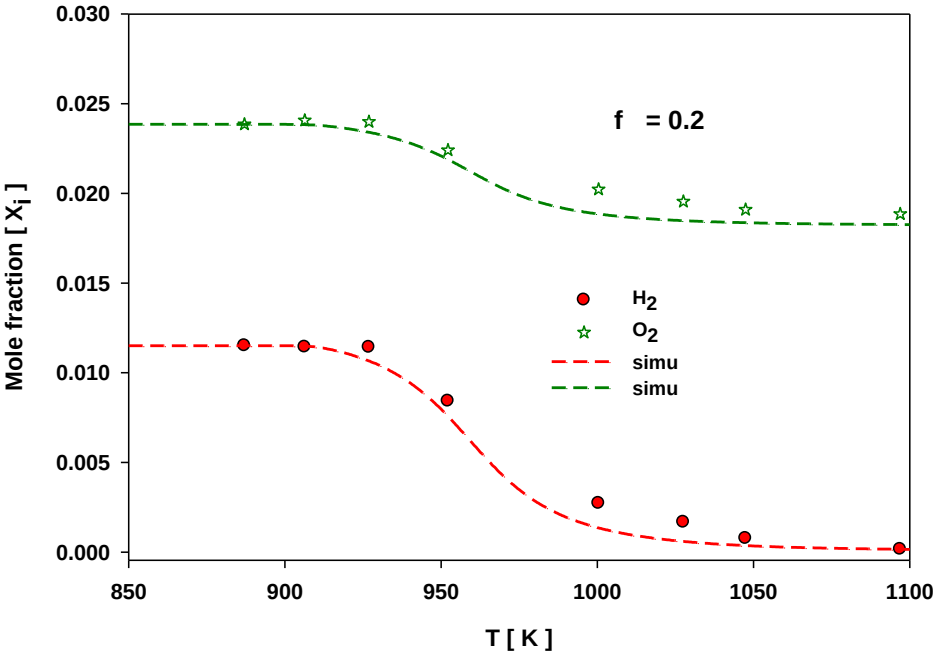

Figure S2.53: Comparison between model prediction and measurements for $H_2/H_2O/O_2/N_2$ oxidation at 1atm, τ= 0.12 s and Ø≈0.24, with 10 % H_2O dilution. Symbols: measurements from [55]. See table V, Mixture 4 for initial condition and mixture composition.

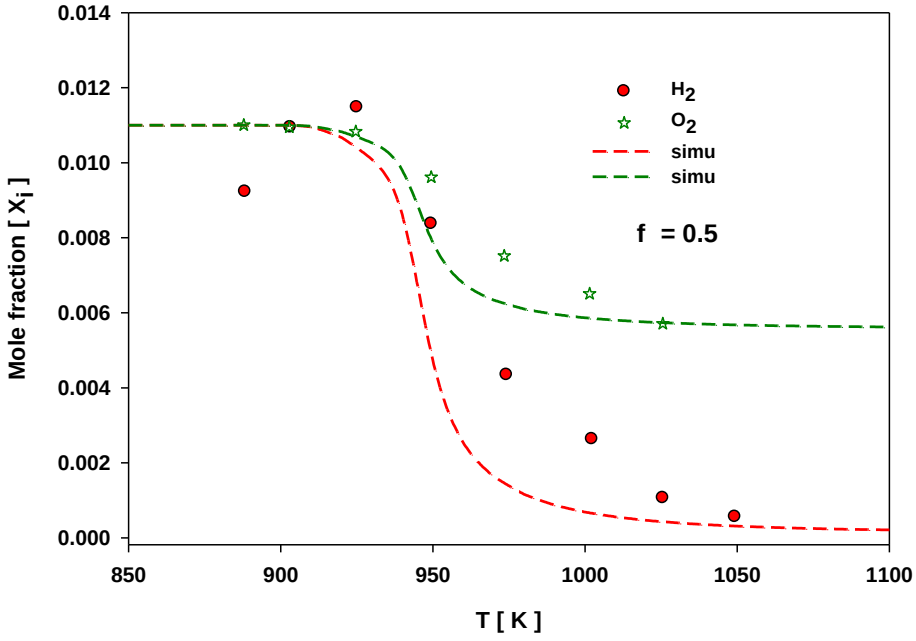

Figure S2.54: Comparison between model prediction and measurements for $H_2/H_2O/O_2/N_2$ oxidation at 1atm, τ= 0.12 s and Ø=0.5, with 10 % H_2O dilution. Symbols: measurements from [55]. See table V, Mixture 4 for initial condition and mixture composition.

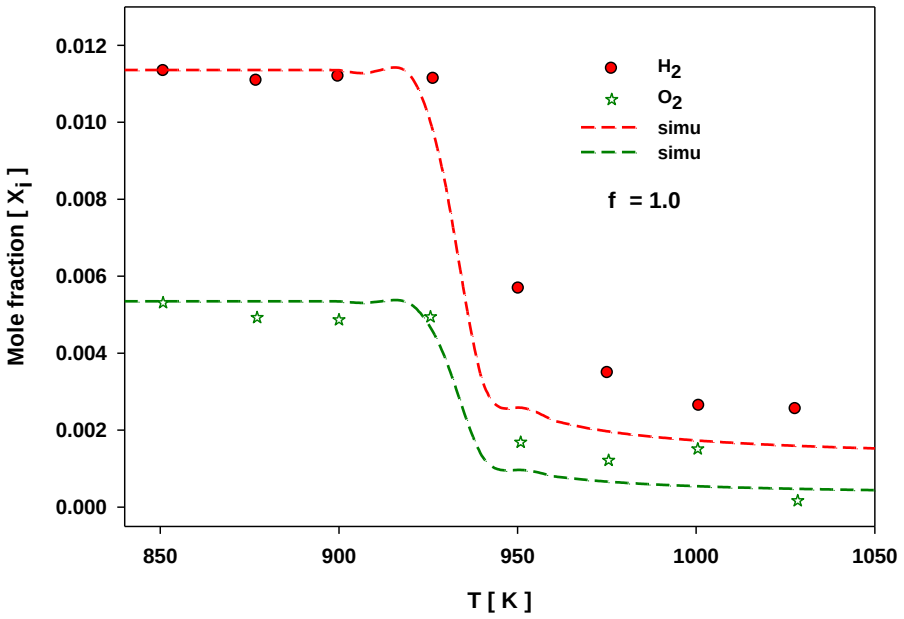

Figure S2.55: Comparison between model prediction and measurements for $H_2/H_2O/O_2/N_2$ oxidation at 1atm, τ= 0.12 s and Ø≈1.05, with 10 % H_2O dilution. Symbols: measurements from [55]. See table V, Mixture 4 for initial condition and mixture composition.

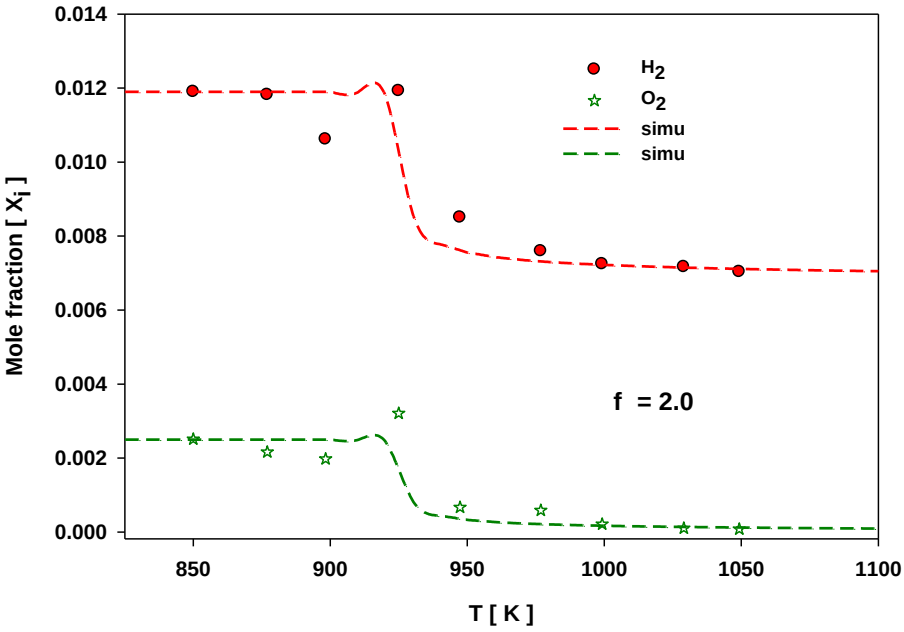

Figure S2.56: Comparison between model prediction and measurements for $H_2/H_2O/O_2/N_2$ oxidation at 1atm, τ= 0.12 s and Ø≈2.38, with 10 % H_2O dilution. Symbols: measurements from [55]. See table V, Mixture 4 for initial condition and mixture composition.

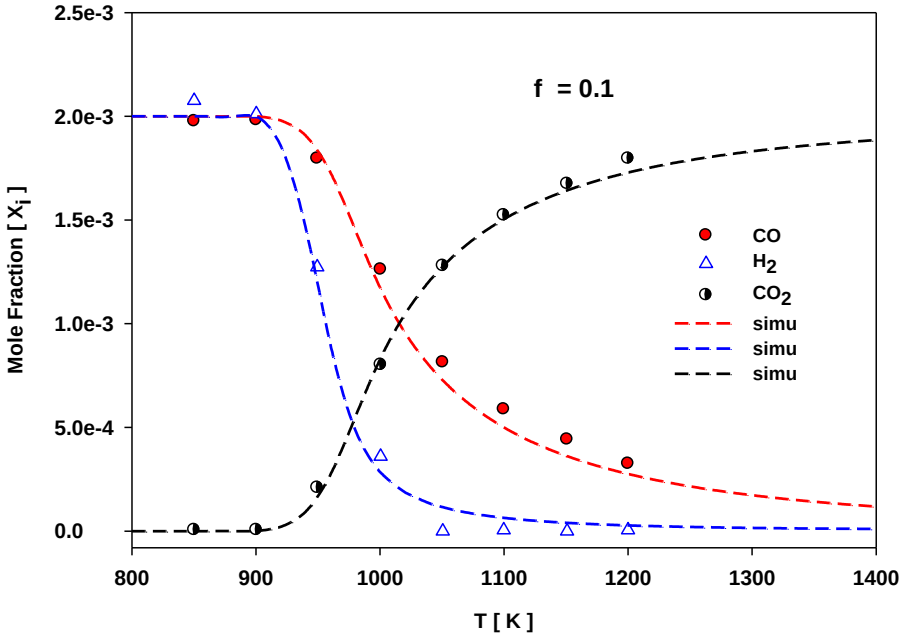

Figure S2.57: Comparison between model prediction and measurements for $CO/H_2/O_2/N_2$ oxidation at 1atm, τ= 0.12 s and Ø=0.1. Symbols: measurements from [56]. See table V, Mixture 5 for initial condition and mixture composition.

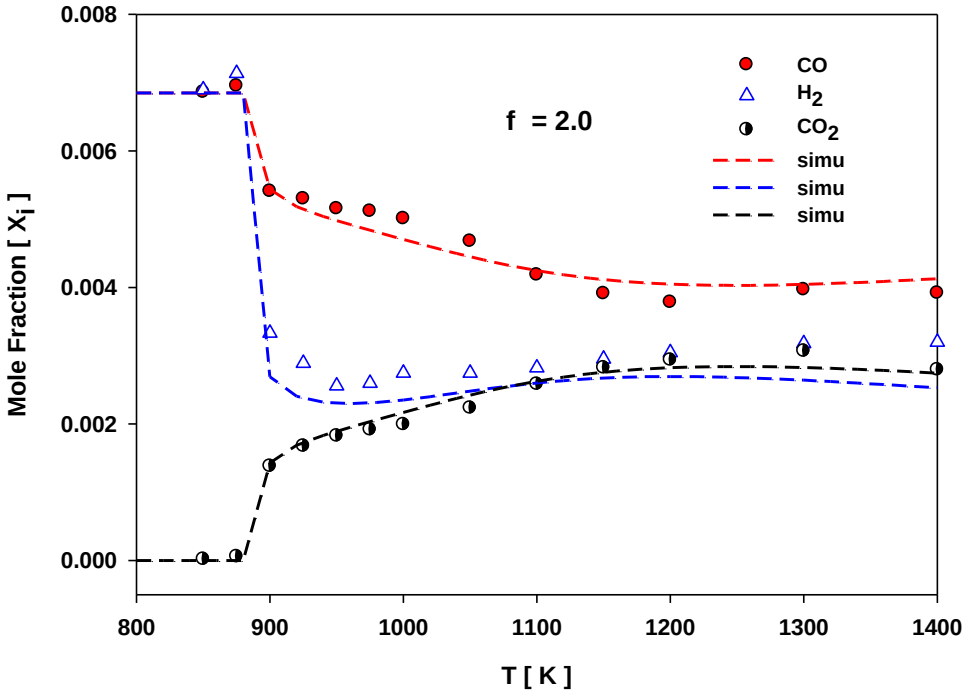

Figure S2.58: Comparison between model prediction and measurements for $CO/H_2/O_2/N_2$ oxidation at 1atm, τ= 0.12 s and Ø=2.0. Symbols: measurements from [56]. See table V, Mixture 5 for initial condition and mixture composition.

2.5 Flow Reactor

Lines represents the model prediction from this work. Symbols represents the published experimental measurements. All the experimental data for flow reactor are extracted from the plots from the original paper. The closed homogenous reactor model is used for simulation assuming the constant pressure and enthalpy except for the plots in Figure S2.68 and S2.69 where plug flow reactor model is assumed. The simulation which are performed assuming constant P-H are time shifted to match the 50 % of the initial fuel consumption to account for the mixing non idealities.

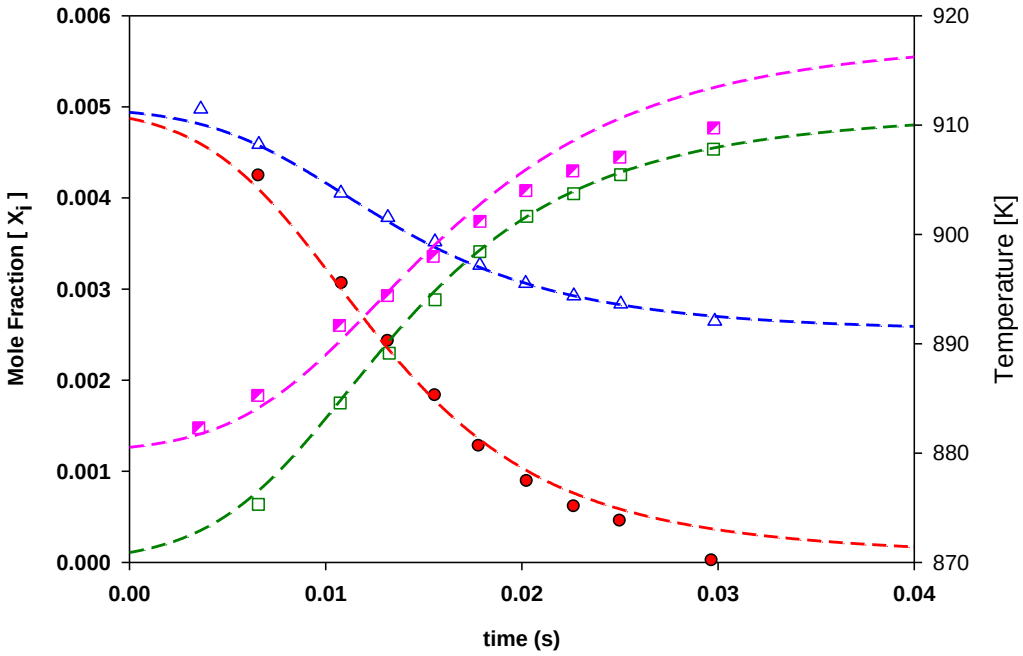

Figure S2.59: Comparison between model prediction and measurements for $H_2/O_2/N_2$ oxidation at T: 880 K, P: 0.3 atm and Ø=1.0. Symbols: measurements from [22]. See table VI, Mixture 9 for initial condition and mixture composition.

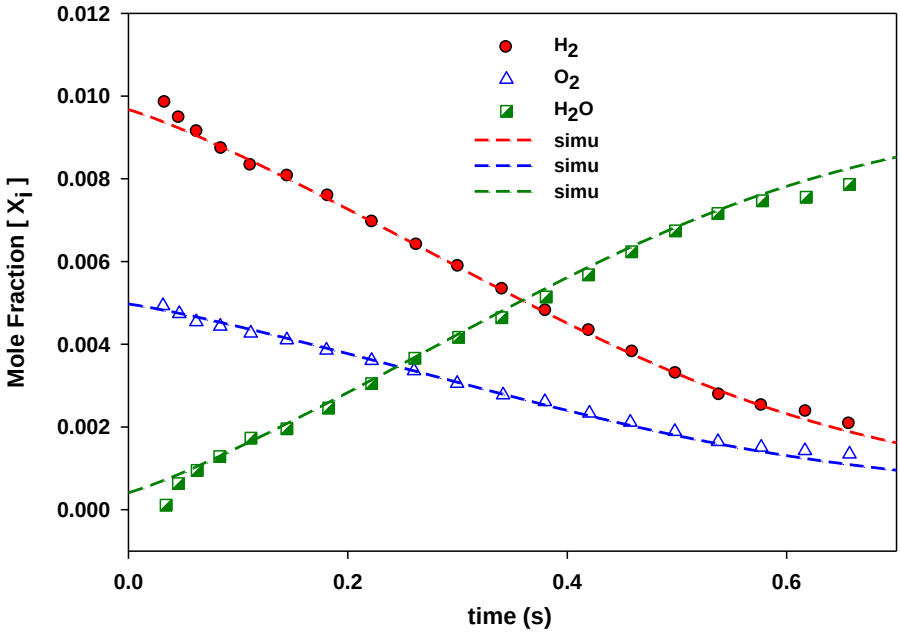

Figure S2.60: Comparison between model prediction and measurements for $H_2/O_2/N_2$ oxidation at T: 934 K, P: 6 atm. Symbols: measurements from [22]. See table VI, Mixture 8 for initial condition and mixture composition.

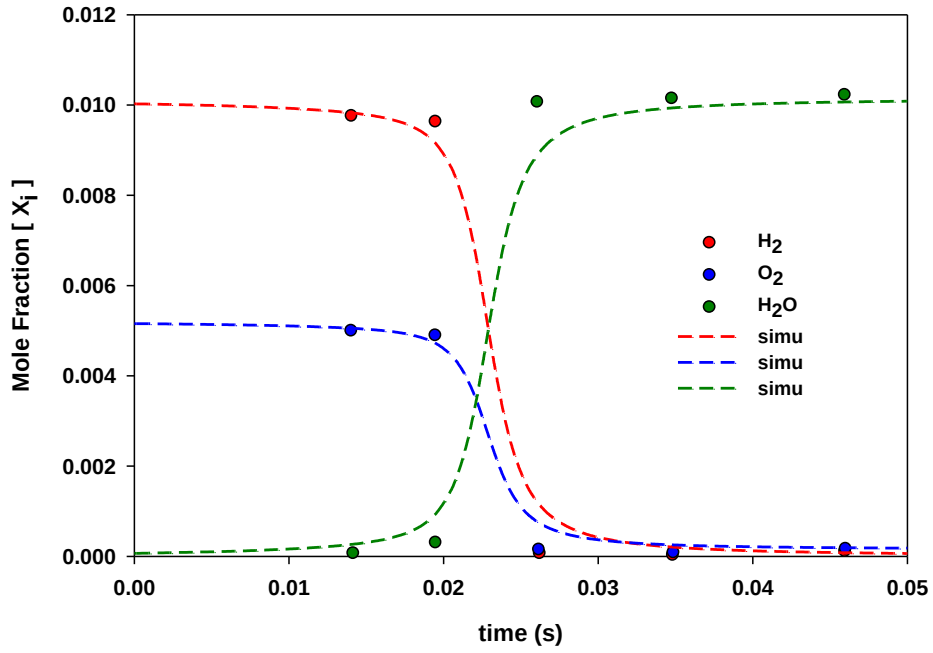

Figure S2.61: Comparison between model prediction and measurements for $H_2/O_2/N_2$ oxidation at T: 935 K, P: 2.55 atm. Symbols: measurements from [22]. See table VI, Mixture 12 for initial condition and mixture composition.

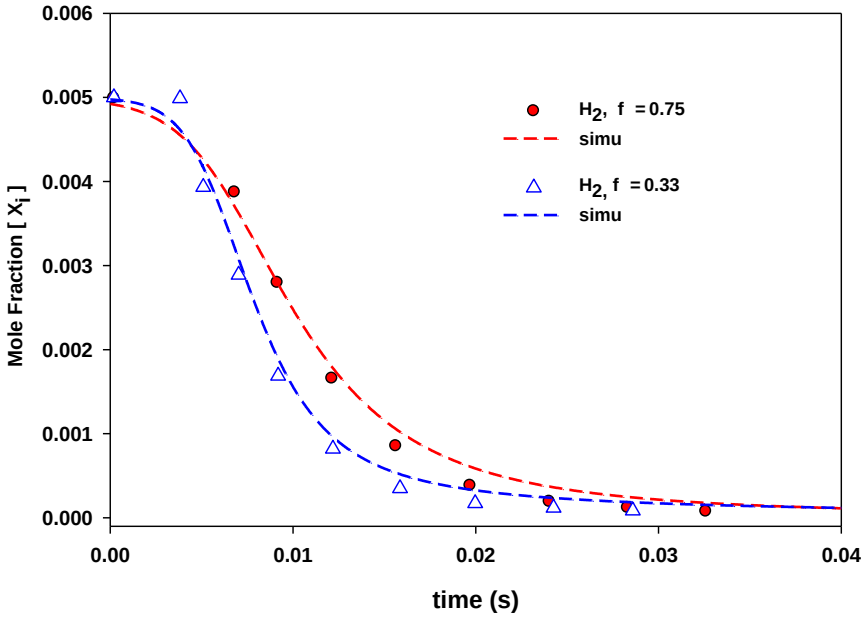

Figure S2.62: Comparison between model prediction and measurements for $H_2/O_2/N_2$ oxidation at 0.6 atm; T: 897 K, Ø=0.75 and T: 896 K, Ø=0.33. Symbols: measurements from [22]. Circle (Ø=0.75), triangle (Ø=0.33). See table VI, Mixture 10 and 11 for initial condition and mixture composition.

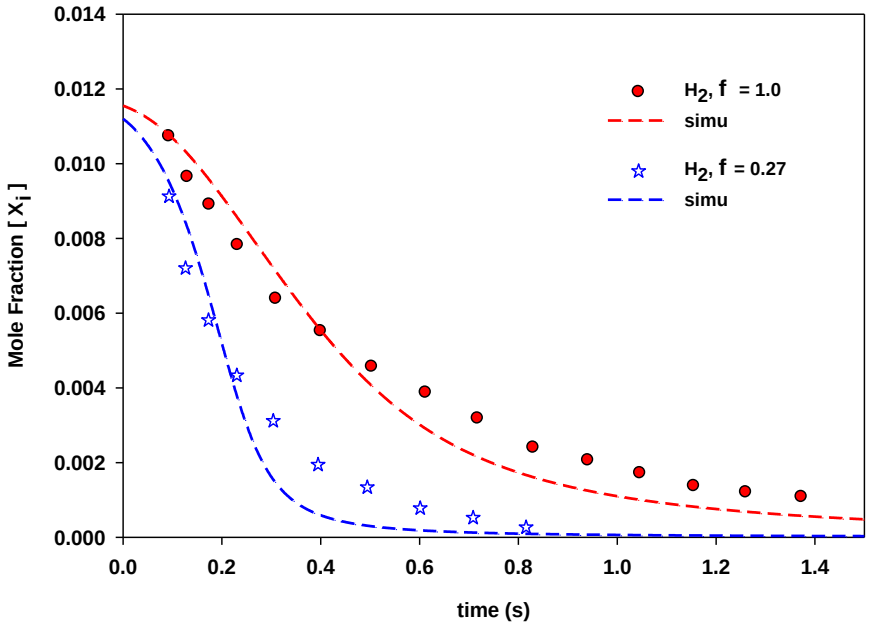

Figure S2.63: Comparison between model prediction and measurements for $H_2/O_2/N_2$ oxidation at P: 15.7 atm; T: 914 K, Ø=1.0 and 0.27. Symbols: measurements from [22]. Circle (Ø=1.0), star (Ø=0.27). See table VI, Mixture 14 and 15 for initial condition and mixture composition.

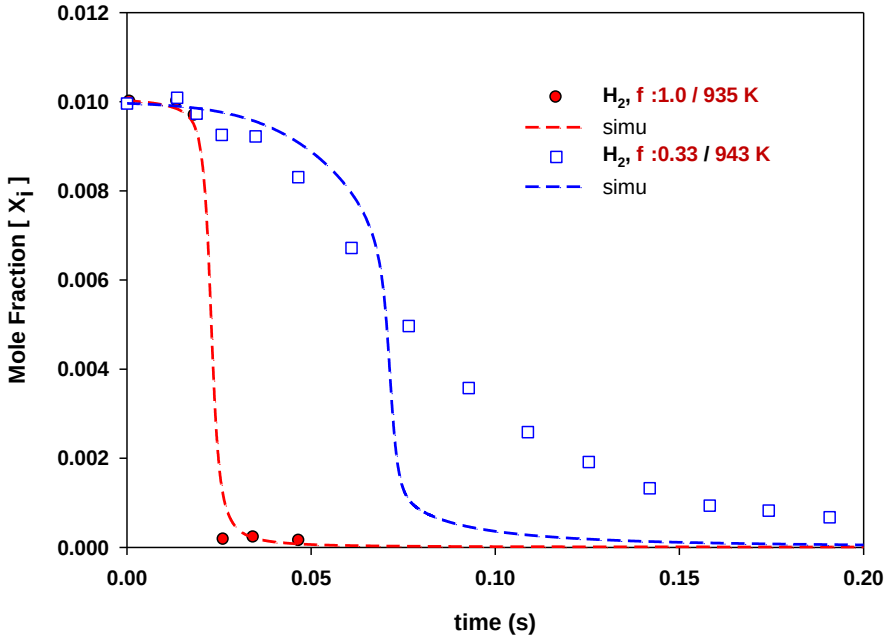

Figure S2.64: Comparison between model prediction and measurements for $H_2/O_2/N_2$ oxidation at P: 2.55 atm, T: 935 K, Ø=1.0 and P: 2.5atm, T: 943, Ø=0.33. Symbols: measurements from [22]. Circle (Ø=1.0), square (Ø=0.33). See table VI, Mixture 12 and 13 for initial condition and mixture composition.

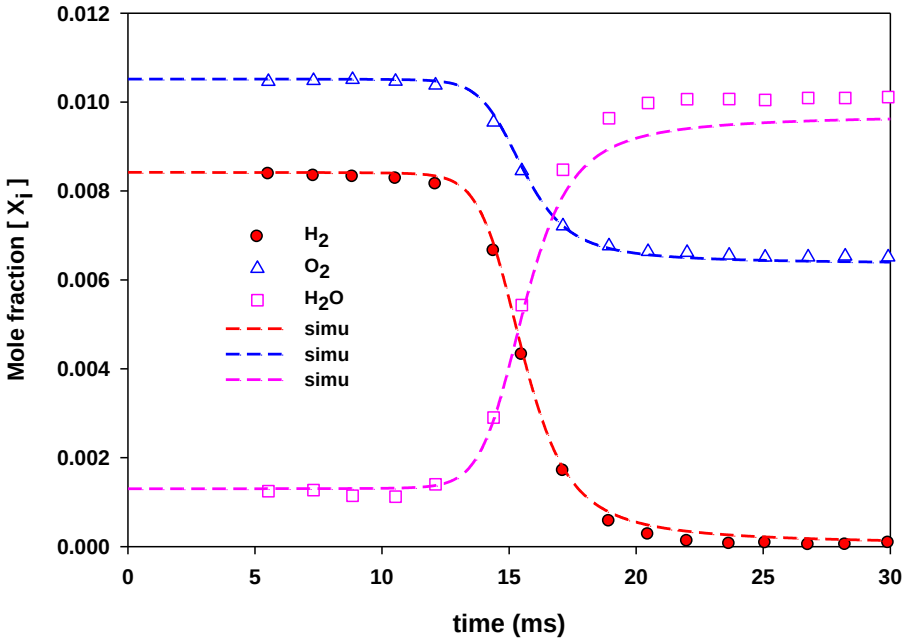

Figure S2.65: Comparison between model prediction and measurements for $H_2/O_2/N_2$ oxidation at P: 1 atm, T: 910 K, Ø=0.28. Symbols: measurements from Yetter et.al. [57]. See table VI, Mixture 1 for initial condition and mixture composition.

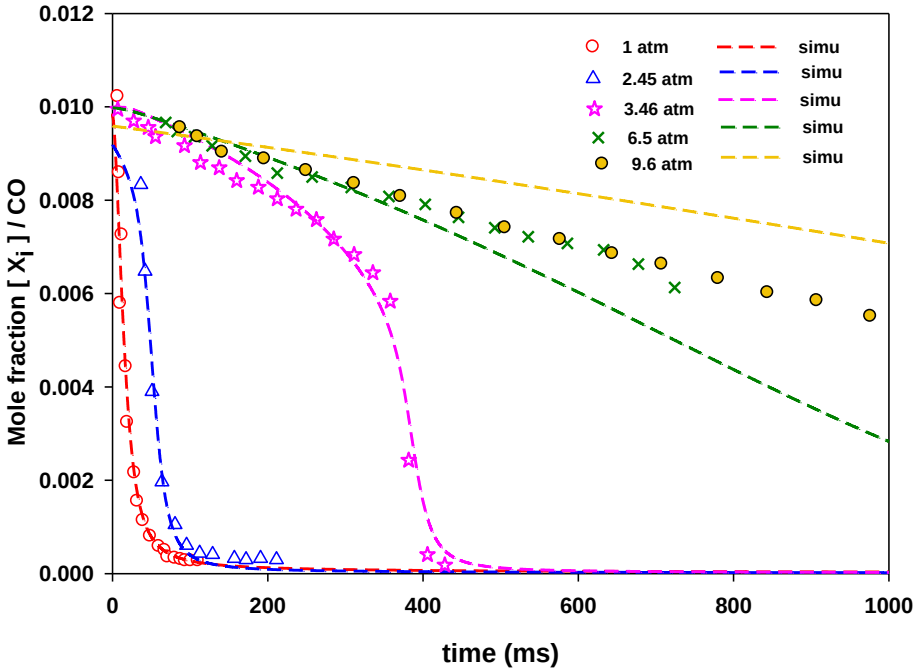

Figure S2.66: Comparison between model prediction and measurements for $CO/H_2O/O_2/N_2$ oxidation at T: 1040 K and different initial pressure. Symbols: CO concentration profile, measurements from Kim et.al. [58]. See table VI, Mixture 3 for initial condition and mixture composition.

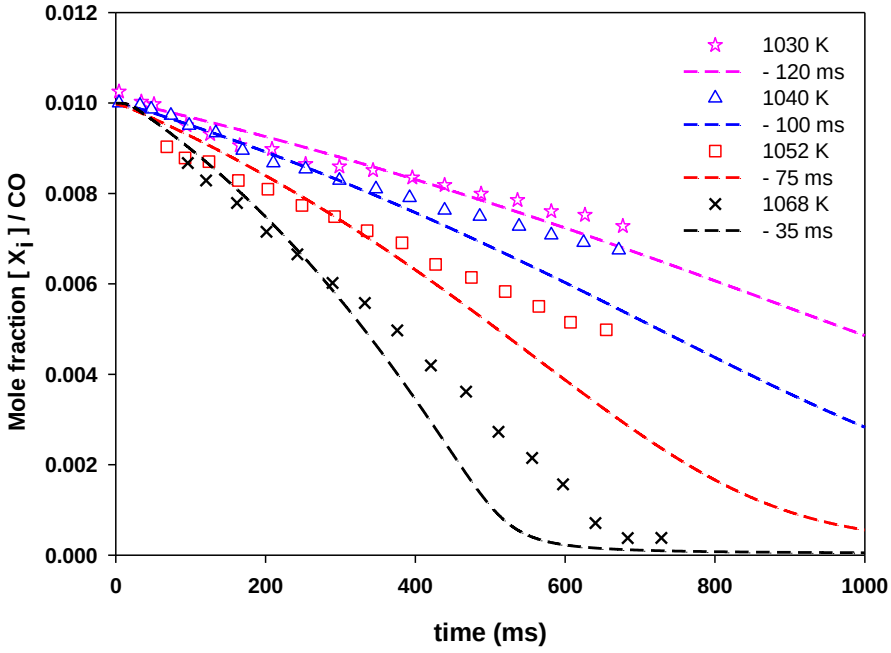

Figure S2.67: Comparison between model prediction and measurements for $CO/H_2O/O_2/N_2$ oxidation at P: 6.5 atm and different initial temperature. Symbols: CO concentration profile, measurements from Kim et.al. [58]. See table VI, Mixture 4 for initial condition and mixture composition.

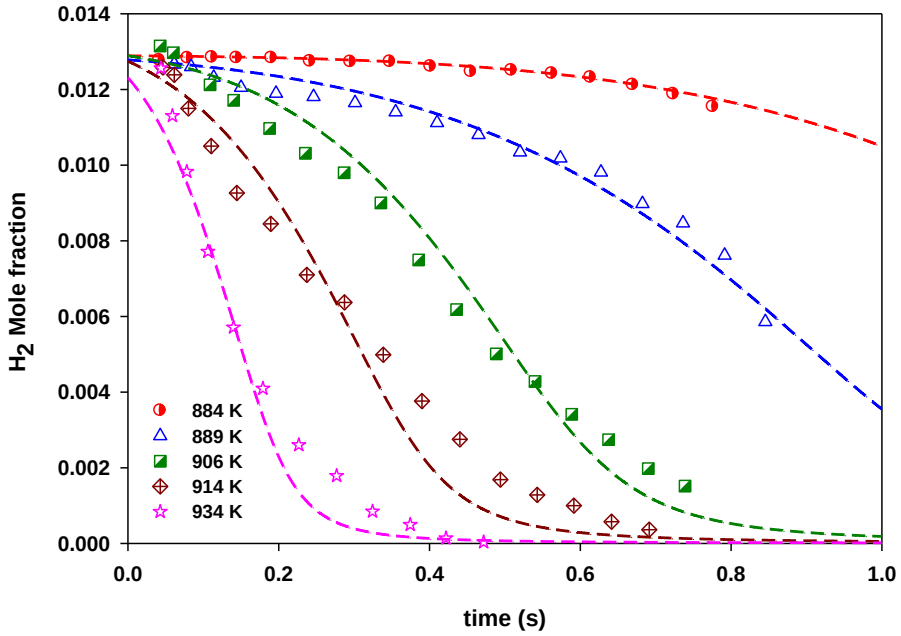

Figure S2.68: Comparison between model prediction and measurements for $H_2/O_2/N_2$ oxidation at P: 6.5 atm and different initial temperature. Symbols: H_2 concentration profile, measurements from Mueller et.al. [22]. See table VI, Mixture 16 -20 for initial condition and mixture composition.

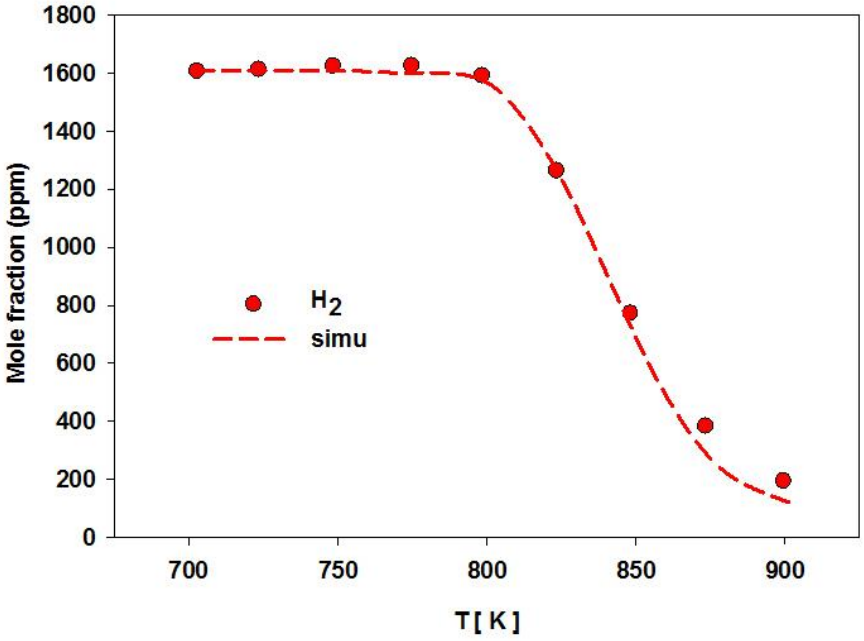

Figure S2.69: Species profile comparison between model prediction and measurements for H_2 (0.161%)/ O_2 (1.6039%) / N_2; Ø=0.05 oxidation at 50 bar. Symbols: measurements from Hashemi et.al. [59]; lines: model prediction. The simulation lines are shifted by + 5 K within the experimental uncertainty of ±

2.6 Oxidation in Shock Wave Condition

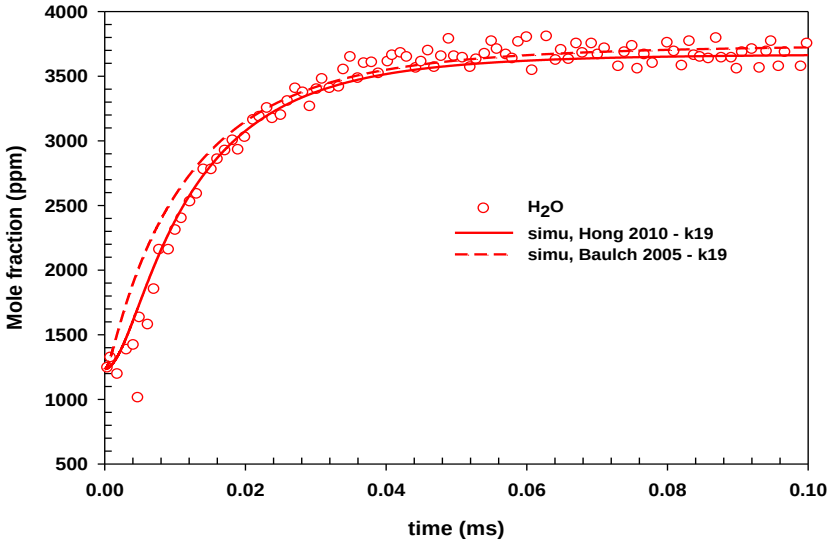

Figure S2.70: H_2O profile comparison between model prediction and measurements for H_2O_2 (2540 ppm)/ H_2O (1234 ppm)/ O_2 (617 ppm)/ Ar oxidation in shock tube at initial condition of 1.91 atm and 1398 K. Symbols measurements from Hong et.al. [25]. Lines are model prediction; solid line: prediction with this work adopting the rate constant for reaction R19 (H_2O_2+OH=HO_2+H_2O) from Hong et.al. [25], dash line: prediction when using the rate constant for R19 from Baulch et.al. [1] in this work.

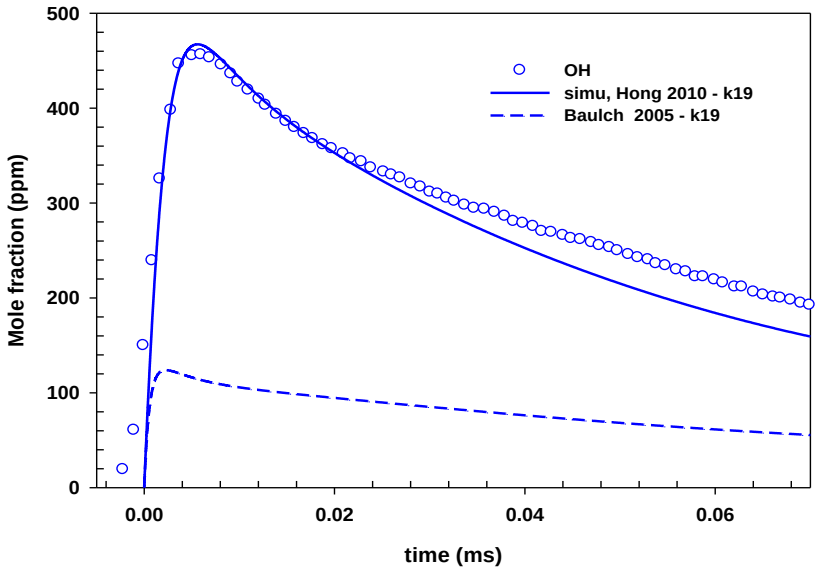

Figure S2.71: OH profile comparison between model prediction and measurements for H_2O_2 /H_2O / O_2 / Ar oxidation in shock tube. The mixture composition, initial condition and legend information are same as in Figure S2.71.

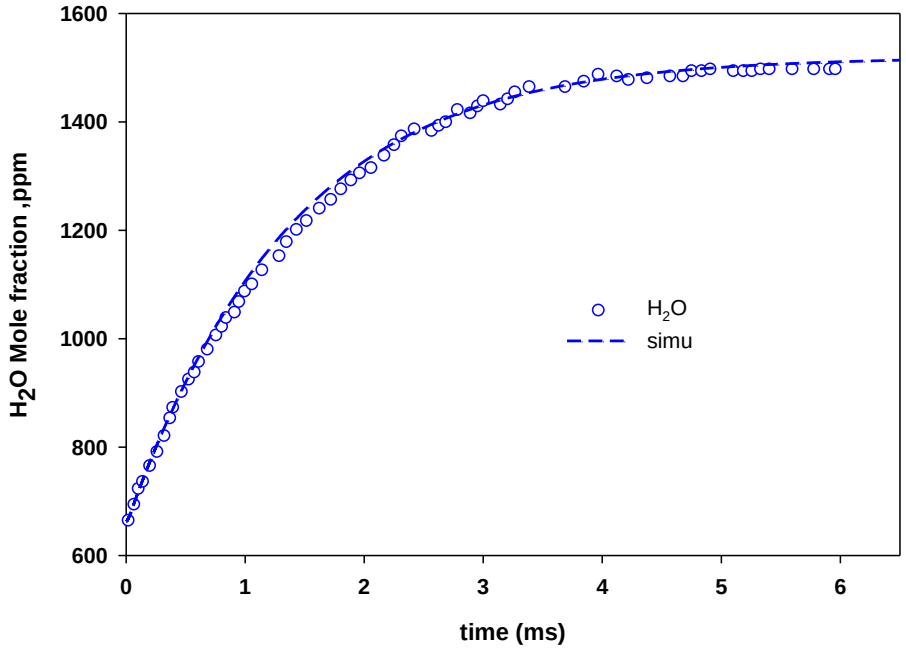

Figure S2.72: H_2O profile comparison between model prediction and measurements for H_2O_2 (860 ppm) /H_2O (663 ppm) / O_2 (332 ppm)/ Ar oxidation in shock tube at initial condition of 1.83 atm and 1057 K. Symbols measurements from Hong et.al.[60]; Line model prediction from this work.

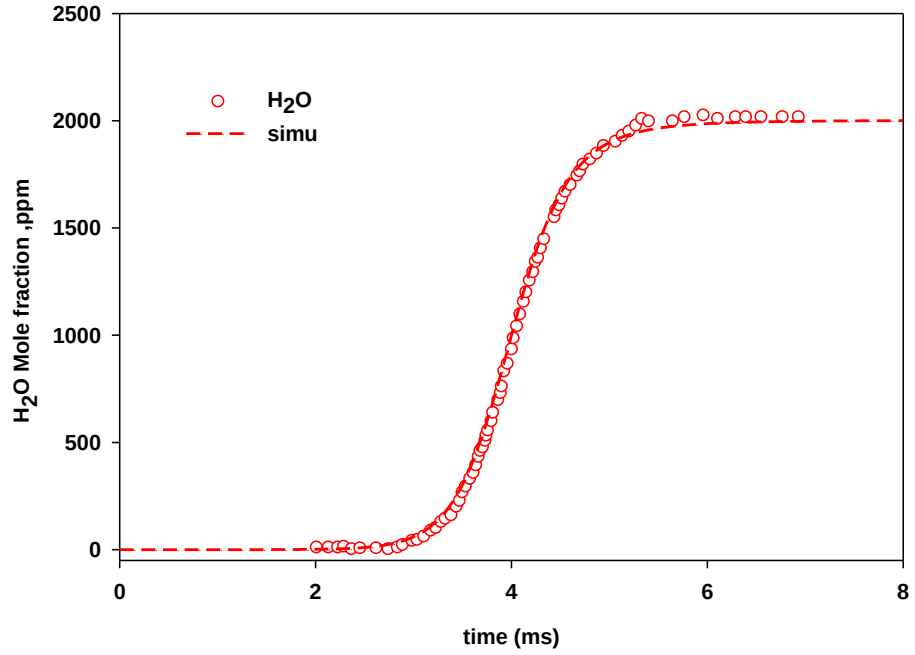

Figure S2.73: H_2O profile comparison between model prediction and measurements for H_2 (2.9 %) / O_2 (0.1%)/ Ar oxidation in shock tube at initial condition of 1.95 atm and 1100 K. Symbols measurements from Hong et.al. [61]. Line model prediction from this work.

References

[1] D.L. Baulch, C.T. Bowman, C.J. Cobos, R.A. Cox, T. Just, J.A. Kerr, M.J. Pilling, D. Stocker, J. Troe, R.W. Walker, J. Warnatz, D.L. Baulch, J. Phys. Chem. Ref. Data 34 757 (2005).

[2] J. Warnatz, U. Maas, R.W. Dibble, Combuation : Physical and Chemical Fundamentals, Modeling and Simulation, Experiments, Pollutant Formation, Springer Verlag, 2006.

[3] A. Kéromnès, W.K. Metcalfe, K.A. Heufer, N. Donohoe, A.K. Das, C. Sung, J. Herzler, C. Naumann, P. Griebel, O. Mathieu, M.C. Krejci, E.L. Petersen, W.J. Pitz, H.J. Curran, Combust. Flame 160 (2013) 995–1011.

[4] N. Peters, Lecture Notes in Physics : Part I, Springer Verlag, 1993.

[5] J.A. Manion, R.E. Huie, R.D. Levin, D.R. Burgess Jr., V.L. Orkin, W. Tsang, W.S. McGivern, J.W. Hudgens, V.D. Knyazev, D.B. Atkinson, E. Chai, A.M. Tereza, C.-Y. Lin, T.C. Allison, W.G. Mallard, F. Westley, J.T. Herron, R.F. Hampson, D.H. Frizzell, NIST Chemical Kinetics Database, NIST Standard Reference Database 17, Version 7.0 (Web Version), Release 1.6.8, Data Version 2015.12, National Institute of Standards and Technology, Gaithersburg, Maryland, 20899-8320, 2015.

[6] “Chemical-Kinetic Mechanisms for Combustion Applications”, San Diego Mechanism Web Page, Mechanical and Aerospace Engineering (Combustion Research), 2014.

[7] A.M. Starik, N.S. Titova, A.S. Sharipov, V.E. Kozlov, Combust. Explos. Shock Waves 46 (2010) 491–506.

[8] A.A. Konnov, Combust. Flame 152 (2008) 507–528.

[9] T. Varga, C. Olm, T. Nagy, I.G. Zse´ly, E. Valko, P. álv´olgyi Robert, H.J. Curran, T. Turányi, Int. J. Chem. Kinet. 48 (2016) 407–422.

[10] Z. Hong, S.S. Vasu, D.F. Davidson, R.K. Hanson, J.J.P.C. Ref, J. Phys. Chem. A 114 (2010) 5520–5525.

[11] Z. Hong, D.F. Davidson, R.K. Hanson, Combust. Flame 158 (2011) 633–644.

[12] Z. Hong, K. Lam, R. Sur, S. Wang, D.F. Davidson, R.K. Hanson, Proc. Combust. Inst. 34 (2013) 565–571.

[13] M.A. Mueller, R.A. Yetter, F.L. Dryer, Int. J. Chem. Kinet. 31 (1999) 705–724.

[14] M.P. Burke, M. Chaos, Y. Ju, F.L. Dryer, S.J. Klippenstein, Int. J. Chem. Kinet. 44 (2012) 444–474.

[15] M.P. Burke, S.J. Klippenstein, L.B. Harding, Proc. Combust. Inst. 34 (2013) 547–555.

[16] X. Li, X. You, F. Wu, C.K. Law, Proc. Combust. Inst. 35 (2015) 617–624.

[17] H. Sun, S.I. Yang, G. Jomaas, C.K. Law, Proc. Combust. Inst. 31 (2007) 439–446.

[18] J. Li, Z. Zhao, A. Kazakov, M. Chaos, F.L. Dryer, J.J. Scire, Int. J. Chem. Kinet. 39 (2007) 109–136.

[19] S.G. Davis, A. V Joshi, H. Wang, F. Egolfopoulos, Proc. Combust. Inst. 30 (2005) 1283–1292.

[20] J. Troe, Combust. Flame 158 (2011) 594–601.

[21] J. V Michael, J.W. Sutherland, L.B. Harding, A.F. Wagner, Proc. Combust. Inst. 28 (2000) 1471–

1478.

[22] M.A. Mueller, T.J. Kim, R.A. Yetter, F.L. Dryer, Int. J. Chem. Kinet. 31 (1999) 113–125.

[23] R.X. Fernandes, K. Luther, J. Troe, V.G. Ushakov, Phys. Chem. Chem. Phys. 10 (2008) 4313–4321.

[24] W. Tsang, R.F. Hampson, J. Phys. Chem. Ref. Data 15 (1986) 1087–1280.

[25] Z. Hong, R.D. Cook, D.F. Davidson, R.K. Hanson, R. V January, V. Re, M. Recei, V. April, J. Phys. Chem. A 114 (2010) 5718–5727.

[26] X. You, H. Wang, E. Goos, S.J. Klippenstein, J. Phys. Chem. A 111 (2007) 4031–4042.

[27] C.J. Jachimowski, W.M. Houghton, Combust. Flame 17 (1971) 25–30.

[28] S.P. Karkach, I. V Osherov, J. Chem. Phys. 110 (1999) 11918–11927.

[29] T. Kathrotia, M. Fikri, M. Bozkurt, M. Hartmann, U. Riedel, C. Schulz, Combust. Flame 157 (2010) 1261–1273.

[30] T. Kathrotia, Reaction Kinetics Modeling of OH*, CH*, and C2* Chemiluminescence, Universität Heidelberg, 2011.

[31] T. Kathrotia, U. Riedel, A. Seipel, K. Moshammer, A. Brockhinke, Appl. Phys. B Lasers Opt. 107 (2012) 571–584.

[32] T. Kathrotia, M. Fikri, M. Bozkurt, M. Hartmann, U. Riedel, C. Schulz, Combust. Flame 157 (2010) 1261–1273.

[33] M.C. Krejci, O. Mathieu, W.K. Metcalfe, H.J. Curran, M.C. Krejci, A.J. Vissotski, T.G. Sikes, E.L. Petersen, A. Ke, W. Metcalfe, H.J. Curran, J. Eng. Gas Turbines Power. 135 (2013) 21503-1–9.

[34] E. Hu, Z. Huang, J. He, H. Miao, Int. J. Hydrogen Energy 34 (2009) 8741–8755.

[35] M.C. Krejci, Development of a New Flame Speed Vessel to Measure the Effect of Steam Dilution on Laminar Flame Speeds of Syngas Fuel Blends at Elevated Pressures and Temperatures, Texas A&M University, 2012.

[36] S.D. Tse, D.L. Zhu, C.K. Law, Proc. Combust. Inst. 28 (2000) 1793–1800.

[37] M.I. Hassan, K.T. Aung, G.M. Faeth, J. Propuls. Power 13 (1997) 239–245.

[38] J. Natarajan, Y. Kochar, T. Lieuwen, J. Seitzman, Proc. Combust. Inst. 32 (2009) 1261–1268.

[39] M.P. Burke, Z. Chen, Y. Ju, F.L. Dryer, Combust. Flame 156 (2009) 771–779.

[40] Y. Ai, Z. Zhou, Z. Chen, W. Kong, FUEL 137 (2014) 339–345.

[41] C. Prathap, A. Ray, M.R. Ravi, Combust. Flame 155 (2008) 145–160.

[42] H.J. Burbano, J. Pareja, A. ´s A. Amell, Int. J. Hydrogen Energy 36 (2011) 3232–3242.

[43] J. Natarajan, T. Lieuwen, J. Seitzman, Combust. Flame 151 (2007) 104–119.

[44] C. Prathap, A. Ray, M.R. Ravi, Combust. Flame 159 (2012) 482–492.

[45] N. Bouvet, C. Chauveau, I.G. Gokalp, S.-Y. Lee, R.J. Santoro, Int. J. Hydrogen Energy 36 (2011)

992–1005.

[46] I.C. Mclean, D.B. Smith, S.C. Taylor, Twenty-FifthSymposium(International)on Combust. (1994) 749–757.

[47] K. Lee, B. Jeong, S. Lee, J. Mech. Sci. Technol. 29 (2015) 3005–3015.

[48] C. Dong, Q. Zhou, Q. Zhao, Y. Zhang, T. Xu, S. Hui, Fuel 88 (2009) 1858–1863.

[49] J. Vandooren, J. Bian, Proc. Combust. Inst. 23 (1990) 341–346.

[50] D.A. Knyazkov, A.M. Dmitriev, T.A. Bolshova, V.M. Shvartsberg, A.G. Shmakov, O.P. Korobeinichev, Proc. Combust. Inst. 0 (2016) 1–8.

[51] A.A. Paletskii, L. V Kuibida, T.A. Bolshova, O.P. Korobeinichev, Combust. Explos. Shock Waves 32 (1996) 245–250.

[52] E.L. Petersen, D.F. Davidson, M. Rohrig, R.K. Hanson, in:, AIAA 95-3113, 31st AIAA/ASME/SAE/ASEE Jt. Propuls. Conf. Exhib., 1995, 1–10 1–10.

[53] R. Me´vel, S. Javoy, F. Lafosse, N. Chaumeix, G. Dupre ´, C.-E. Paillard, Proc. Combust. Inst. 32 (2009) 359–366.

[54] G. Dayma, P. Dagaut, Combust. Sci. Technol. 178 (2006) 1999–2024.

[55] T. Le Cong, P. Dagaut, Energy & Fuels 23 (2009) 725–734.

[56] P. Dagaut, F. Lecomte, J. Mieritz, P. Glarborg, Int. J. Chem. Kinet. 35 (2003) 564–575.

[57] R.A. Yetter, F.L. Dryer, H. Rabitz, Combust. Sci. Technol. 79 (1991) 129–140.

[58] T.J. Kim, R.A. Yetter, F.L. Dryer, Twenty-FifthSymposium(International)on Combust. (1994) 759–766.

[59] H. Hashemi, J.M. Christensen, S. Gersen, P. Glarborg, Proc. Combust. Inst. 35 (2015) 553–560.

[60] Z. Hong, A. Farooq, E.A. Barbour, D.F. Davidson, R.K. Hanson, J. Phys. Chem. A 113 (2009) 12919–12925.

[61] Z. Hong, D.F. Davidson, E.A. Barbour, R.K. Hanson, Proc. Combust. Inst. 33 (2011) 309–316.